ABSTRACT

TANVIR, SHAMS. Modeling and Simulation of Driving Activity from an Energy Use-Emissions Perspective (Under the direction of Dr. Nagui Rouphail and Dr. Henry Frey).

Proper understanding of driving activity at the systems level is essential to implement control technologies which improve energy efficiency and reduce emissions of harmful pollutants. The research presented in this dissertation includes methods and framework development to analyze both simulated and observed driving activities. To this end, the objectives of this research are – (a) to develop methods to efficiently evaluate transportation management strategies (TMS) in terms of emissions reduction using large scale network simulator; (b) to develop enhanced methods to generate realistic synthetic trajectories from mesoscopic traffic simulators that can faithfully represent driving activity; (c) to quantify the effect of driver and vehicle performance on the observed driving activity; and (d) to develop metrics which can distinguish the effect of driving styles on energy consumption from other confounding factors.

Network and corridor wide performances of four different TMS were tested to address objective (a) within a mesoscopic simulator, DTALite. Replacing the existing fleet for a network in Raleigh, North Carolina with all 'Tier 2' regulatory class vehicles yielded more than 80% reduction in network wide NO_X, CO, and HC emissions. Peak spreading, an active demand management strategy, reduced emissions of network wide NO_X by 6%. In case of a corridor with incident, average NO_X emissions per vehicle mile on the path increased 193% from the base scenario (with 39% speed drop). Even in a scenario with 30% diversion to alternative routes from incident location, NO_X emissions increased 155% from the base scenario.

Post-processing methods for simulated trajectories were developed to achieve objective (b). A Savitzky-Golay filter with window width of 7 simulation time-steps and 10 smoothing iterations produced realistic simulated trajectories under congested conditions. Under uncongested condition, addition of different levels of white noise in different modes (idle, cruise, acceleration, and deceleration) of the speed trajectories generated realistic trajectories.

Variabilities in driving activities were quantified for different combinations of drivers and vehicles to attain objective (c). To this objective, we have gathered microscale vehicle activity measurements from 17 controlled real-world driving schedules and two years of naturalistic driving data from 5 drivers. We also developed a metric for driving style termed 'envelope deviation', which is a distribution of gaps between microscale activity (1 Hz) and fleet average envelope. We found that there is significant inter-driver heterogeneity in driving styles when controlling for vehicle performance. The choice of vehicle was found to be not significantly altering the natural driving style of a driver.

To realize objective (d), a trip based driving style metric, Fuel Efficiency Score (FES), was developed from observed microscale (1 Hz) driving activity. FES was consistent throughout 24 month period for 25 drivers. Moreover, the use of FES enabled identification of 4 significantly different classes of driving styles in terms of drivers normalized fuel efficiency. The findings capacitated the use of naturalistic driving activity information for a range of personalized eco-driving technologies in the system model.

Modeling and Simulation of Driving Activity from an Energy Use-Emissions Perspective

by
Shams Tanvir

A dissertation submitted to the Graduate Faculty of
North Carolina State University
in partial fulfillment of the
requirements for the degree of
Doctor of Philosophy

Civil Engineering

Raleigh, North Carolina

2018

APPROVED BY:

_____	_____
Dr. Nagui M. Rouphail Co-Chair of Advisory Committee	Dr. Henry Frey Co-Chair of Advisory Committee
_____	_____
Dr. Bastian Schroeder	Dr. Xuesong Zhou External Member

DEDICATION

This work is dedicated to my father Abdul Wahab Sikder for his endless love and support.

BIOGRAPHY

Shams Tanvir was born in Faridpur, Bangladesh to Rasida Begum and Abdul Wahab Sikder. After graduating from Notre Dame College in Dhaka, Bangladesh in 2004, he enrolled in Bangladesh University of Engineering and Technology (BUET) in Dhaka, Bangladesh. He received his BS in Civil Engineering in 2009 and MS in Civil Engineering with specialization in Transportation Engineering in 2013 from BUET. Before joining NC State as a Ph.D. student in August 2013, he taught undergraduate courses and lab sections as a lecturer in the Civil Engineering Department, BUET.

ACKNOWLEDGMENTS

This dissertation is the culmination of the past four years of my doctoral journey. Exploring this multi-disciplinary and evolving research front has only been possible with the help of some extraordinary people.

I would like to express my deepest gratitude to my advisor, Dr. Nagui M. Rouphail for his continuous encouragement and support to explore new research ideas. He introduced me to challenging and diverse research projects and overall taught me to be an independent researcher. I am sure that his exemplary work ethics, dedication, and management skills will benefit me immensely in my future career.

I would like to thank Dr. H. Christopher Frey for teaching me rigor in research, helping me to perfect academic writing and reviewing, and epitomizing an academician. I am grateful to Dr. Bastian Schroeder, Dr. Downey Brill, and Dr. Xuesong Zhou for their encouragement and valuable feedback on my proposal and this dissertation. I am indebted to our conversations with Dr. Sangkey Kim. Special thanks to Thomas Chase, Behzad Aghdashi, Nabaruna Karmakar, Tai-jin Song, Kwanpyo Ko, and Ishtiak Ahmed for helping me in my research. I would like to convey my gratefulness to my parents, family members, friends, and colleagues for their support. Thanks to my wife, Rahnuma Shahrin, for supporting and challenging me at the same time. She and my son, Sahir, sacrificed immensely to get me to this stage.

Finally, I would like to acknowledge the funding and support of this dissertation by US Environment Protection Agency (EPA), North Carolina Department of Transportation (NCDOT), and US Department of Energy (DOE).

TABLE OF CONTENTS

LIST OF TABLES

LIST OF FIGURES

CHAPTER 1

INTRODUCTION

Driving activity refers to the externally observable dynamics of a vehicle operated by a human driver and subjected to the physical constraints imposed by the operating condition of the driving route and vehicle performance. Examples of driving activity variables include speed, acceleration, jerk (derivative of acceleration), yaw (rotation with respect to the vertical axis), roll (rotation with respect to longitudinal axis), pitch (rotation with respect to transverse axis). Vehicle power demand is highly correlated to some of the driving activity variables such as longitudinal speed and acceleration. Since both fuel use and emissions are directly correlated to the vehicle power demand, proper understanding of related driving activity variables is necessary to control energy consumption and emissions from on-road vehicles. The research described in this dissertation has analyzed both simulated and measured driving activity to enhance this understanding.

The stimulus for this research came from two emerging techniques to tackle transportation related energy use-emissions issues, namely, dynamic network simulation and eco-driving. While dynamic network simulation has made it possible to simulate traffic states in detail and with some accuracy, simulating accurate microscopic level driving activity is still a challenge when implemented on large networks. On the other hand, eco-driving, although experimented with and tested for a number of years, is yet to be adopted widely before its benefits can come to fruition. Ubiquitous sensing and personalized signaling have opened the avenue for improved characterization of driving activity for eco-driving and simple scaling-up of the operation. This dissertation attempts to address some theoretical and practical problems in these regards.

A brief background of the problem, research needs, objectives, limitations, and research framework are discussed in this chapter.

1.1 Background

Road traffic is a major source of total energy consumption and consequent emissions of harmful pollutants (EPA, 2014). Continuous enhancements are being achieved in improving fuel efficiency and reducing emissions of vehicles through adaptation of new technologies such as electric vehicles, hybrid vehicles, and exhaust gas filters. However, driving behavior and traffic infrastructural system level inefficiencies cause substantially contribute to increased levels of fuel burned during congestion. In addition, traffic systems breakdowns during the recurrent peak period congestion, emergency evacuation, incidents, and work zones cause suboptimal operation of engines in terms of generation of harmful pollutants such as nitrogen-oxide and carbon mono-oxide. The problem is accentuated by the inability to deploy proper transportation management strategies and control mechanisms which can address system inefficiencies at sufficient spatial and temporal resolution. Traffic systems are difficult to control due to their highly stochastic nature in both the spatial and temporal domains. Lack of observability of traffic states at a disaggregate level are approached through the development of traffic simulation models. However, traffic simulation models are historically focused on operating condition, travel time, and safety relevant objectives; the propagation of effects of traffic control mechanisms towards fuel use and emissions were often unaddressed. On the other hand, significant advancements have been made in estimating emissions from microscale level vehicle parameters. There was a lack of concordance between traffic simulation and emissions estimation methods.

In recent years, much emphasis has been given to integrating traffic simulation and emissions estimation modules (Bartin, Mudigonda, & Ozbay, 2007; Ligterink & Lange, 2009; Lin, Chiu, Vallamsundar, & Bai, 2011a; Song, Yu, & Zhang, 2012; Xie, Chowdhury, Bhavsar, & Zhou, 2011). The current research is a continuation of this development. Dynamic mesoscopic simulation models have the unique capability of processing traffic in large networks in a computationally efficient manner without sacrificing the spatial and temporal resolution; the simplified vehicle specific power (VSP) based estimation modules can estimate fuel use and emissions with high level of accuracy and computational efficiency. Integration of these two state-of-the-practice technologies can help achieve traffic energy efficiency states with a range of control scenarios and answering several what-if questions. The agent based integrated models stands one step ahead in terms of added capability as those have become compatible with real-time personalized control system's architecture.

Even though integrated dynamic mesoscopic simulators and emissions estimators have addressed many challenges, there are still significant inconsistencies in representing 'true' microscale driving activity. Within the traffic simulator microscale driving activities such as speed, acceleration are generated in a post-processing stage through the use of simplified car-following models. However, simulated driving activities have inconsistencies rooted in them; removing inconsistencies would require substantial pre- and/or post-processing which can add to the computational burden. There is a gap in the literature in the identification of appropriate post-processing methods to realistically represent simulated driving activity generated through simplified car-following models. Moreover, methodological development of sophisticated microscale trajectory simulation methods has

not paid adequate attention to improve the computational performance of these methods. In order to incorporate an integrated framework in a real-time or near-real-time platform, attention has to be provided towards reducing the amount of computation performed during the simulation.

Another aspect of real-time control of driving activity is provision of information, instructions, and incentives to individual drivers to improve energy efficiency. The U.S. Department of Energy (DOE) has recently selected five teams for designing and testing new network optimization approaches using simulations, to improve energy efficiency of personal transportation. These teams are expected to design a system model (SM) that dynamically simulates a large transportation network and its energy use. Also, there is a need for a control architecture (CA) that can combine wireless signals with personalized incentives to affect real-time energy use. In order to serve as a SM with this type of CA, the integrated simulation framework must be able to mimic the heterogeneity observed in driving styles of the driver population. Traditionally heterogeneity is incorporated through the application of vehicle type and age distribution; this method, however, is incapable of identifying which set of information needed to be transmitted to which class of drivers. Fortunately, in recent years the wide use of probe vehicles has enabled the observation of a wide range of driving styles over an extended period of time. The relationship between simultaneously observed driving activity and fuel use can be used to populate heterogeneous driver classes in the SM.

A key strategy that has a significant impact on energy savings in a regional urban highway network is to induce a change in driving style, one that reduces the levels of excessive accelerations, decelerations and speeds (ref). Modest savings at the individual driver or trip level, when extrapolated to the million VMT's traveled on a daily basis in

several metropolitan areas in the US can generate significant regional energy reductions. This strategy of changing driving style, known as ‘eco-driving’, is manifested through driving activity. Moreover, driving activity can also be affected by trip attributes including operating conditions on the route and vehicle performance conditions. Drivers do not have direct control on these factors and short term strategies may not work well with long term decisions such as mode choice. Therefore, there is a need to segregate the effect of driving style from the effects of trip choice factors within the observed driving activity. Proper characterization of driving style will enable benchmarking and standardization of drivers in an eco-driving scheme.

1.2 Research Objectives

This dissertation is motivated to address the drawbacks in existing methods to characterize driving activity in both simulation and control. The following research needs are identified and addressed in the subsequent chapters:

a. Chapter 2: To develop methods to efficiently evaluate transportation management strategies (TMS) in terms of emissions reduction using large scale network simulator.
b. Chapter 3: To develop enhanced methods to generate realistic synthetic trajectories from mesoscopic traffic simulators that can faithfully represent driving activity.
c. Chapter 4: To quantify the effect of driver and vehicle performance on the observed driving activity.
d. Chapter 5: To develop metrics which can distinguish the effect of driving styles on energy consumption from other confounding factors..

1.3 Research Scope and Limitation

Addressing research objective (a) relies on the integrated mesoscopic simulation and emissions estimator platform already developed (Zhou et al., 2015). Although significant

improvements for the integrated platform is suggested in chapter 3, those improvements were not implemented to revise the findings for chapter 2. Moreover, chapter 2 focuses on testing the multi-pollutant framework of DTALite and does not explicitly focus on fuel use.

Research objective (b) was limited to establishing the post-processing method for synthetic trajectory generation. Although significant modification (pre-processing) can be made to the existing simplified car-following model, concentration will be focused only on post-processing results from an existing model. This researcher acknowledges an active body of research in developing improved car-following models; however, those works are beyond the scope of this research. Moreover, objective (b) is limited to the operating mode bin structure of driving activity data. In addition, post-processing increases the computational burden on the trajectory generator as there is always an accuracy – computational cost tradeoff involved in simulation. Computational burden was not explicitly considered in the optimization framework. No directly observed fuel use was used for this evaluation.

Objective (c) was limited to a defined driving style metric. Objective (d) was accomplished through observation of probe vehicle fleet data using on-board diagnostic sensors and global positing systems. Incorporation of new technologies and wide shift in driver behavior can question validity of the developed insights.

1.4 Thesis Organization

The research in this dissertation is documented in four chapters. Each chapter introduces the problem, motivates the work through a detailed literature review, delineates the methods, discusses the results, and concludes on the defined research questions. Chapter 2 motivates the broader significance of this dissertation by adding a detailed description of the problem

and state-of-the-art method. The overall organization of this research and the flow of work can be visualized through Figure 1.1.

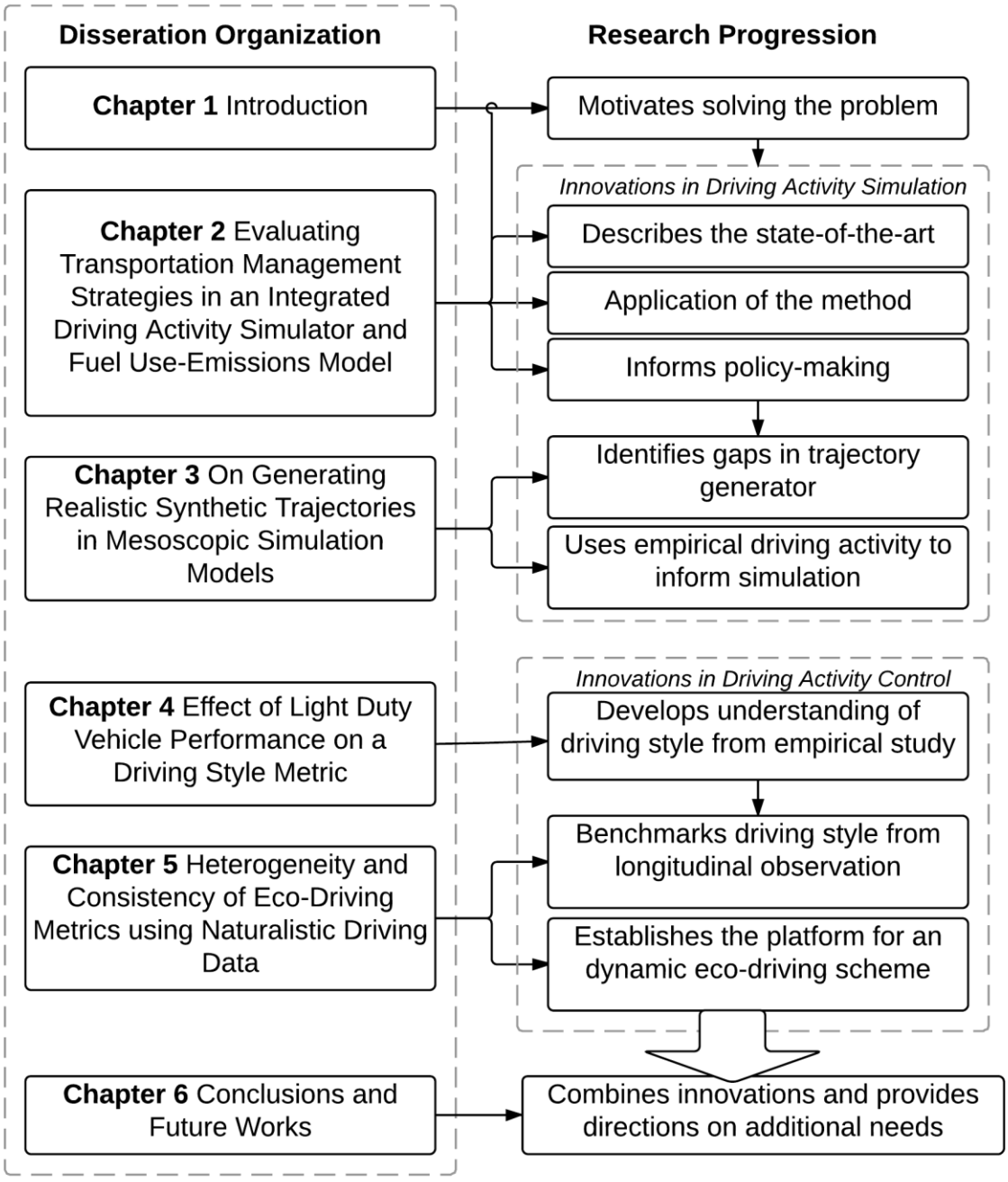

Figure 1.1. Dissertation organization and research framework

CHAPTER 2

EVALUATING TRANSPORTATION MANAGEMENT STRATEGIES IN AN INTEGRAGRATED DRIVING ACTIVITY SIMULATOR AND FUEL USE-EMISSIONS MODEL[*]

2.1 Introduction

Road traffic is a major contributor to emissions of deleterious pollutants. There is a need for high spatially and temporally disaggregated emissions information to assess the impacts of potential interventions on a large scale regional network (Samaranayake et al., 2014). However, few studies have been attempted in this area due to lack of efficient algorithms and tools to achieve the necessary level of disaggregation. A recent implementation (Zhou et al., 2015) of a reduced-form vehicle emissions model within the framework of a mesoscopic dynamic traffic assignment simulation model has addressed some of these issues. However, the capability of the coupled framework in evaluating both network and path level operational improvement options is not properly perceived.

This chapter provides a motivational foundation for the remainder of this dissertation by reviewing the literature to understand the extent of the problem under consideration. In addition, state-of-the-art method in integrated driving activity simulator and fuel use-emissions model are described in detail. Finally, policy relevant applications of the integrated platform are designed, implemented, and evaluated.

[*] Part of this chapter published as Zhou, X., Tanvir, S., Lei, H., Taylor, J., Liu, B., Rouphail, N. M., & Frey, H. C. (2015). Integrating a simplified emission estimation model and mesoscopic dynamic traffic simulator to efficiently evaluate emission impacts of traffic management strategies. *Transportation Research Part D: Transport and Environment*, *37*, 123-136.

2.1.1 Fuel use and emissions from road traffic

Road transportation is a major consumer of energy and contributor to emissions of deleterious pollutants. Motorized vehicles are the second highest source of CO_2 emissions in the United States. Transportation sources are causing 28% of total CO_2 emissions in 2012 and 84% of that is from onroad traffic (EPA, 2014). Emissions from anthropogenic sources, particularly burning of fossil fuels, is attributed as a key factor in increase in atmospheric CO_2 concentration in recent years (Etheridge et al., 1996). In 2013, the United States consumed 97.1 quadrillion BTUs (Quads) of energy; 26.7 Quads (more than 25% of the total energy supply) were used in transportation sector. In doing so 173,493 million gallons of motor fuel was used including both gasoline and diesel (BTS, 2015). All major urban areas are experiencing widespread congestion due to increased demand of vehicular traffic (D. L. Schrank & Lomax, 2007). Yearly delay per commuter has increased to 42 hours in 2014 compared to 18 hours in 1982 resulting in a congestion cost of $160 billion (D. Schrank, Eisele, Lomax, & Bak, 2015). Increased demand for travel has caused increase in number of motorized vehicles, resulting in increased congestion on roadways. Drivers are facing frequent flow disruption and increased waiting time at intersections. These factors can lead to increased emission of deleterious pollutants such as carbon dioxide (CO_2), carbon mono-oxide (CO), nitrogen oxides (NO_x), hydrocarbons (HCs) (Oduyemi & Davidson, 1998). Oversaturation is the main contributor to predicted total emissions for CO and HC (Smit, 2006). Increased emission from congestion may be a result of more idling time, and more acceleration and deceleration events associated with stop and go conditions.

2.1.2 Detrimental effects of emissions

Epidemiological studies show that vehicular emission causes elevated risks of non-allergic respiratory morbidity, cardiovascular morbidity, cancer, allergic illnesses, adverse pregnancy and birth outcomes, and diminished male fertility for drivers, commuters and individuals living near roadways (Krzyzanowski, Kuna-Dibbert, & Schneider, 2005). Congestion resulting in increased travel delay creates higher exposure to deleterious pollutants; a 30 min./day travel delay accounts for 21±12% of the total daily benzene exposure (a component of total HC) and 14±8% of $PM_{2.5}$ exposure (Zhang & Batterman, 2009). Emissions of CO, HC and NO_x per unit of distance traveled were found to be increasing respectively 4-fold, 3-fold and 2-fold at a congested condition with average speed of 13 mph compared to uncongested condition (38-44 mph) (Sjodin, Persson, Andreasson, Arlander, & Galle, 1998). Another study concluded that increase of emissions with congestion depends on the type of vehicles and roadway type and indicated 10% increase of emissions per unit time for CO, HC, and fuel consumption; 20% increase of NO_x emissions per unit time at congested conditions compared to an uncongested state (De Vlieger, De Keukeleere, & Kretzschmar, 2000). CO, HC and NO were found to be increased by 50% due to congestion based on in-use measurement (Frey, Rouphail, Unal, & Colyar, 2001).

Increased exposure to surface transportation-induced emissions can cause significant potential negative health impacts such as premature mortality, exacerbation of preexisting respiratory health conditions, asthma, and poor cardiovascular health (Health Effects Institute. Panel on the Health Effects of Traffic-Related Air Pollution, 2010). NO_x and CO are two of the six principal pollutants regulated under National Ambient Air Quality Standard (NAAQS) for their harmful effects on public health. Short term NO_2 exposure is

associated with increased airway responsiveness, often accompanied by respiratory symptoms, particularly in children and asthmatics (EPA, 2008). Increased CO concentration reduces the oxygen carrying capacity of human blood, thereby reducing oxygen supply to important body organ and tissues (EPA, 2010). HC is mostly a byproduct of incomplete combustion and evaporation of fuel, which along with NO_x plays a vital role in production of ground level ozone, which is another pollutant regulated under the NAAQS (Twigg, 2007). Sixteen out of 189 listed hazardous air pollutants or air toxics are hydrocarbons including benzene, which is a well-established human carcinogenic.

2.1.3 Techniques for reducing fuel use and emissions from road traffic

There has been many improvements in prevention and control of mobile source emissions in recent years such as modifying fuel, vehicle operation, engine design, behavior, regular maintenance, and most commonly by exhaust gas treatment. Improvements such as low sulfur fuels, computerized fuel metering, electronic ignition, air injection, exhaust gas recirculation, and 3-way catalytic converters have substantially reduced emissions on an individual vehicle basis (Faiz, Weaver, & Walsh, 1996). During hard acceleration events emissions of HC and CO can increase as vehicle engines operate in a fuel rich mode (Alkidas, 2007). Emissions of PM and HC can increase under deceleration due to the presence of unburned fuel (Cappiello, 2002). A common emissions mitigation measure considered by transportation planners is to enhance the capacity of the roadways. But the effect of capacity augmentation on reduction of emissions is not well quantified; such augmentation may increase induced travel resulting in quick decrease of initial emission reduction benefits (Noland & Quddus, 2006).

Many transportation planning and operations strategies are planned and being implemented to reduce this problem (Eliasson, Hultkrantz, Nerhagen, & Rosqvist, 2009; Tonne, Beevers, Armstrong, Kelly, & Wilkinson, 2008). Changing intersection design, traffic signal design, freeway metering technologies are some examples of operational strategies that are practiced (Greene & Plotkin, 2011). The United States Environmental Protection Agency (USEPA) is implementing 'Tier 3 Motor Vehicle Emissions and Fuel Standard' from 2017; which is going to be an important shift in standards for 'regulatory classes' that follows EPA's adoption of 'Tier 2' program in 2000. By the year 2030, 'Tier 3' class of vehicles are expected to reduce onroad NO_X, VOC, CO, SO_2, Benzene emissions by 25%, 16%, 24%, 56%, 26% respectively. Furthermore, the phasing in of more stringent vehicle emission regulations, and fleet turnover to lower emitting vehicles, can be a factor in reducing on-road emissions of regulated pollutants such as CO, NO_x, and HC.

In contrast to all the above mentioned techniques, an alternative and complementary approach could be the use of technologies to target the behavioral and system factors to improve the overall energy efficiency without altering the mechanical efficiency of each mode (car, bus, truck). Passenger vehicles run with 60% unutilized capacity (BTS, 2015); improving occupancy can make a big difference in total travel demand. Online taxi and ride sharing services such as Waze, Uber, RubyRide, Zipcar, Lyft has provided travelers with unique flexibility in terms of mode choice. Inefficient driving styles cause loss of 45% of the optimal fuel economy (Sivak & Schoettle, 2012). Emergence of communication technologies such as cellular and internet networks and social networks such as Facebook, Twitter has made it possible to influence travel behavior of individuals. Moreover, congestion arising from suboptimal route choice and oversaturation increases transportation energy use up to

33% (Roughgarden, 2012). Informed travel mode, route, and departure time choice is possible through real time travel information services such as google map, INRIX and personalized navigation systems. A practical framework with real time response capability for monitoring, communicating, incentivizing, and controlling trip making and driving behavior attributes can make energy efficiency an integral part of the optimized transportation network.

2.1.4 Traffic simulation to assess energy use and emissions

Controlling energy use and emissions from road transportation requires an understanding of the prevailing conditions and identification of specific individual and system behaviors which can be influenced through different strategies. The Clean Air Act Amendments (CAAA) of 1990 classified transportation control measures in five broad categories: regulatory (employer trip reduction, speed limit, maximum parking ratio), mobility improvements (HOV, transit, bicycle, pedestrian, land use management), traffic operations and flow improvements, travel demand management and market based mechanisms (Cambridge Systematics, 1996). All these types of control measures involve changing system properties at regional or corridor wide network levels that can have implications at various spatial and temporal scales. Therefore, comprehensive impact assessment or measures of effectiveness for these TMSs are required to be performed at a network level. Moreover, there is a need for high spatially and temporally disaggregated emissions information to assess impacts of potential interventions on a large scale network (Samaranayake et al., 2014).

2.1.5 Integrated traffic simulation and energy use-emissions estimation

Traffic simulation models at different levels of complexity and scales have been and are being developed for assessing energy use-emissions impact. To conduct project-level traffic environmental impact studies, microscopic emissions models are often adopted in transportation evaluation projects (Ahn, Rakha, Trani, & Van Aerde, 2002; Nam, Brazil, & Sutulo, 2002; Stathopoulos & Noland, 2003). Microscopic traffic simulation tools have been widely used to generate vehicle emissions estimates by evaluating driving speed and acceleration characteristics/profiles on a vehicle-by-vehicle and second-by-second basis. Although a high-fidelity traffic simulator is desirable for analyzing individual movement delays and facilities with complex geometric configurations, microscopic simulation can be computationally intensive and typically requires a wide range of detailed geometric data and driving behavior parameters, which can be difficult to calibrate, especially for the purpose of producing high fidelity emissions estimates. This has limited their applicability to small- and medium-scale corridors.

Alternatively, many organizations have utilized post-processing techniques for estimating vehicle emissions from their travel demand model results. Large scale air pollution maps are generally produced by using static estimates of average traffic and weather conditions. Most of the existing research for regional or city level emission assessment have used historic O-D matrices (Gualtieri & Tartaglia, 1998), land use transport models (Lautso & Toivanen, 1999), travel demand models (Karppinen et al., 2000), traffic assignment modules (Namdeo, Mitchell, & Dixon, 2002). These estimates lack the sensitivity of dynamic vehicular travel demand and cannot reflect temporal fluctuations of road conditions.

Recognizing that conventional static traffic assignment models are not sensitive to the dynamic interaction of vehicular travel demand and time-dependent road conditions, planning practitioners have increasingly recognized the capabilities of mesoscopic Dynamic Traffic Assignment (DTA) models. However, many planners and engineers are still concerned that DTA tools, typically based on fine-grained network representations, are computationally intensive and lack model components/details necessary for accurately representing high-fidelity traffic dynamics. Differences in resolution between traffic simulation and emissions estimation models is a barrier to integrating them into one framework. In recent years, a multi-resolution modeling approach has been exploited by many practitioners. Typically, this approach aims to integrate many existing simulation tools in a loosely coupled software platform that can provide multiple levels of modeling detail regarding network dynamics and traveler/driver choices. For example, in a subarea study, one can simply extract vehicle path data from a (macroscopic/mesoscopic) DTA tool for use in a microscopic simulation model (e.g. VISSIM, Paramics, TRANSIMS) to generate second-by-second vehicle speed and acceleration outputs for microscopic emissions or mobility-related analysis.

Estimation of emissions is dependent on the simulated driving activity such as instantaneous speeds and accelerations. Therefore, the accuracy of fuel use and emissions estimation hinge on the accuracy of traffic simulation. Traditional traffic simulations are focused on the mobility and safety aspects of the network. In contrast, traffic simulations to assess fuel use and emissions are focused on the capability of the model to emulate driving activity parameters properly. In addition to the fundamental difference in simulation purpose, a few functionality and compatibility issues are equally important in energy use and

emissions estimation. The simulator framework can be visualized as Figure 2.1 has two different modules namely a traffic simulation module and an emissions estimation module. Data flow between these two modules should be consistent and uninterrupted in ideal conditions.

There have been many efforts in the past to couple an emission model with a traffic simulator either manually or directly. AIMSUN has been used with a European modal emissions model, VERSIT+ (Ligterink & Lange, 2009). MOBILE6 emissions model has been coupled with EMME/2 and PARAMICS (Bartin et al., 2007). MOVES emission model has been used with PARAMICS, DynusT, and VISSIM (Lin, Chiu, Vallamsundar, & Bai, 2011b; Song et al., 2012; Xie et al., 2011). Dynamic linkage of traffic and emissions models is challenging and can lead to significantly longer run times. Evaluation for a large-scale network is a trade-off between estimation accuracy and computational tractability. Therefore, it is a challenge to properly estimate emissions related impacts that is greatly exceeded by the imprecision and/or inaccuracy of the estimate.

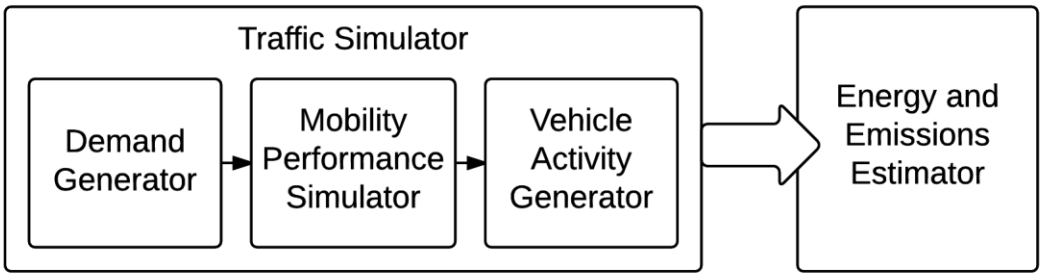

Figure 2.1. Modules of integrated traffic simulation and emission estimation

Multi-resolution modeling system such as a mesoscopic DTA has a relatively low simulation resolution (e.g. 6 second update interval), while microscopic traffic simulators

typically use 0.1 seconds as the simulation interval. To ensure theoretical convergence of the integrated models, it is necessary to use multiple iterations between different simulation/assignment components to determine the mobility and emission impact of high-level demand and traveler behaviors. However, internal discrepancies between different modeling resolutions make tight interconnections and consistent modeling extremely challenging.

2.1.6 Energy use and emissions estimation

Effective tools to estimate emissions for different scenarios are required to assess the effect of these strategies at different spatial and temporal resolution. There are several emissions models available that can estimate vehicle emissions for the prediction and management of air pollution levels near roadways. These models use information on weather, fuel type, fleet composition, vehicle type, and activity schedule as input.

For planning purposes, average speed and flow based models have been used for a long time. However, these models cannot adequately represent the dynamic effects of driving styles. Average speed based models use predetermined speed trajectories upon which relationships between cycle or link-based average-speed and average emission rates are estimated (e.g. MOBILE (USEPA, 2007), EMFAC (CARB, 2002), COPERT (Ntziachristos et al., 2000)). US Environmental Protection Agency (EPA) have developed MOVES that can take into account a second-by-second vehicle speed trajectory (Chamberlin, Swanson, Talbot, Dumont, & Pesci, 2011). There are other models, such as CMEM (An, Barth, Norbeck, & Ross, 1997), that also consider operating modes in estimating emissions. Thus, MOVES is attractive in being able to represent a wide range of driving cycles for any user specified speed trajectory.

Vehicle specific power (VSP) based estimation

VSP is a well-evaluated and widely used quantitative indicator of engine power demand that is an excellent predictor of vehicle fuel use and that is also highly correlated with vehicle tailpipe exhaust emissions for a wide range of pollutants (Jimenez-Palacios, 1998). VSP is a function of vehicle speed, road grade, and acceleration which accounts for kinetic energy, rolling resistance, aerodynamic drag, and gravity (Zhai, Frey, Rouphail, Goncalves, & Farias, 2009). It is usually reported as power required per mass of the vehicle (for example: kilowatts per ton). Calculated VSP is categorized into different operating mode bins by speed and VSP ranges to estimate emissions factor for vehicles. Therefore, VSP is a parameter with important practical application. But accurate determination of VSP depends on proper quantification of measured vehicle operating characteristics, such as speed, acceleration, road grade etc. Microscopic traffic characteristics e.g. speed, acceleration, headway etc. are highly dependent on the roadway, traffic, driver behavior characteristics.

VSP is usually estimated using developed equations for different classes of vehicles. According to MOVES the equation to calculate VSP is expressed as

$$VSP = \left(\frac{A}{M}\right)v + \left(\frac{B}{M}\right)v^2 + \left(\frac{C}{M}\right)v^3 + (a + \sin(\Phi))v$$

Where: A, B and C refer to the rolling term, rotating term and the drag term respectively. M is the vehicle mass, is the vehicle speed, *a* is vehicle acceleration and Φ is road grade. The parameters are different for each vehicle type.

MOVES provides default coefficients for different group of vehicles. Derivation of these coefficients is based on chassis dynamometer tests. The VSP formulation for light-weight vehicles provided by MOVES is

$$VSP = (A * v + B * v^2 + C * v^3 + m * v * a)/m$$

VSP = vehicle specific power, kW/ton

v= speed at time t, m/s ; a = acceleration at time t, m/s^2

A= rolling resistance coefficient = 0.1565 kW-sec/m

B= rotational resistance coefficient = 2.002X10-3 $kW\text{-}sec^2/m^2$

C= aerodynamic drag coefficient = 4.926X10-4 $kW\text{-}sec^3/m^3$

m = vehicle mass = 1.479 ton.

EPA MOVES model

On March 2, 2010, USEPA announced the official release of the Motor Vehicle Emissions Simulator (MOVES2010) for use in state implementation plan (SIP) submissions to EPA and regional emission analysis for transportation conformity (Koupal, Cumberworth, Michaels, Beardsley, & Brzezinski, 2002). It replaced MOBILE 6.2 model where vehicle emissions rates represent averages over a driving schedule with defined average speed. MOVES2010 considers the relative time spent and emissions rate in vehicle speed and vehicle specific power bins (Fujita et al., 2012). Except for braking and idling, these OpMode bins are stratified by 21 speed ranges (<25 mph, 25 to 50 mph, and >50 mph) and by Vehicle Specific Power (VSP) (Koupal, Michaels, Cumberworth, Bailey, & Brzezinski, 2002; Vallamsundar & Lin, 2011). The main purpose of this tool is to quantitatively predict emissions from mobile sources for a wide range of user-defined parameters e.g. vehicle type, time periods, geographical areas, pollutants, vehicle operating characteristics and road type (EPA, 2012). Therefore, MOVES is a significant improvement in the state-of-art for emissions estimation. The inputs from traffic simulation software can be linked to MOVES in three different formats:

a) Average speeds for the links of the network (similar to MOBILE)

b) Link driving schedule (LDS) for each link of the network. LDS is a time dependent speed profile for a particular link. Generally LDS is selected for a representative vehicle or by sampling.
c) Operating mode distribution of vehicles of the link.

However, MOVES is computationally intensive. Some investigators have attempted to use traffic simulation output for vehicle speed trajectories as input to MOVES, leading to time consuming computations for evaluation of different traffic management strategy scenarios.

Simplified emissions estimator – MOVESLite

As an alternative approach, a reduced form version of MOVES, referred to as MOVES Lite, has been recently developed (Frey & Liu, 2013). MOVES Lite is based on the same computational structure as MOVES with respect to Op Mode bins and, therefore, is capable of estimating emissions for any specified speed trajectory. MOVES Lite is less computational intensive than MOVES because it is calibrated to a base cycle and employs a cycle correction factor to adjust for differences in emission rates between any cycle of interest and the base cycle. MOVES Lite is based on a more limited set of vehicle types and pollutants than MOVES. Since traffic simulations are often for periods of a few hours, MOVES Lite does not take into account variations in factors such as fuel properties, inspection and maintenance programs, and ambient conditions that do not change substantially or at all during such short periods of time. MOVES Lite is 3,000 times faster and can produce emissions estimates within ±5% deviation compared to MOVES.

Because many factors where MOVES is sensitive are approximately constant during the time period of a typical simulation, there is no need to run MOVES in its entirety for every link in a network. Furthermore, because MOVES estimates emission factors based on

weighted combinations of OpMode bins, a similar approach can be used as part of a simplified model that can be directly coded as part of a traffic simulation model. MOVESLite harnesses these benefits to develop a less computationally intensive vehicle emission estimation module. The conceptual model of MOVESLite is based on (a) base emission rate for site-specific characteristics (b) a cycle correction factor for speed trajectories and OpMode bin emission rates. The cycle correction factor is calculated using the following equation

$$CCF_{p,c,a,v} = \left(\frac{(\sum_m f_m^c \times ER_{p,a,v,m})}{(\sum_m f_m^b \times ER_{p,a,v,m})} \right) \left(\frac{V^b}{V^c} \right)$$

Where,

$ER_{p,a,v,m}$ = default emission rate for pollutant p, age a, vehicle type v, in operating mode bin m, gram/hour

$f_m{}^c$ = fraction of time in OpMode bin m in cycle c

$f_m{}^b$ = fraction of time in OpMode bin m for base cycle b

V^c = cycle average speed for cycle c, mph

V^b = cycle average speed for base cycle b, mph

The base emissions rate is then corrected for the simulated cycle using the following equation

$$CE_{p,c} = \sum_v \left\{ \left[\sum_a (EF_{p,b,a,v} \times CCF_{p,c,a,v} \times f_{a,v}) \right] \times f_v \right\}$$

Where,

$CE_{p,c,}$ = cycle average emission factor for any arbitrary driving cycle c, for pollutant p, for a fleet of vehicles with mixed types and ages, gram/mi

$ER_{p,b,a,v}$ = base emission rate for base cycle b, age a, vehicle type v, and pollutant p, gram/mi

$CCF_{p,c,a,v}$ = cycle correction factor for driving cycle c, age a, vehicle type v, and pollutant p

$f_{a,v}$ = age fraction for age a and vehicle type v

f_v = vehicle type fraction for vehicle type v

c = cycle c

b = base cycle

p = pollutant

Comparison of the 2 models across similar criteria shown in Table 2.1 and Table 2.2.

Table 2.1. Performance of MOVES across different functional criteria

Criterion	**MOVES**
Accuracy	Accurate comparing with empirical emission factors.
Runtime	Relatively slow.
Requirement for Input	Substantial input data requirements.
Requirement for Platform	Need to install MOVES package, JAVA, and MySQL.
Connection with TDM and TSM	Difficult to be coupled into TDM or TSM.
Usability	Errors, warnings arise frequently, especially for beginning users.
Time consuming procedures	Adjust fuel property, temperature, humidity, air conditioning use, and I/M program for each link in the network.
Vehicle dynamic data	Second by second data, or OpMode distribution
Vehicle Types	13 Vehicle types: Passenger Car, Passenger Truck, Refuse Truck, Single-Unit Short-Haul, Truck Single-Unit Long-Haul Truck, Motor Home, Intercity Bus, Transit Bus, School Bus, Combination Short-Haul Truck , Combination Long-Haul Truck, Motorcycle
Adjusted emission rate map (reflecting vehicle distribution and climate)	Yes, took vehicle distribution and weather condition (temperature and humidity) into account.

Table 2.2. Performance of MOVES lite across different performance criteria

Criterion	MOVES lite
Accuracy	Within ±5% errors comparing with MOVES.
Runtime	3000 times faster than MOVES.
Requirement for Input	Limited input data requirements.
Requirement for Platform	Can be run in MS EXCEL or MATLAB. It has a computational algorithm.
Connection with TDM and TSM	Can be integrated into TDM or TSM easily.
Usability	User-friendly.
Time consuming procedures	Set fuel property, temperature, humidity, air conditioning use, and I/M program constant by link in the network.
Vehicle dynamic data	Same as MOVES
Vehicle Types	For U.S. based model: Five vehicle types that comprise of more than 95% of the fleet: Passenger Cars, Passenger Trucks, Light Commercial Trucks, Single Unit Short Haul Trucks, and Combination Long Haul Trucks.
Adjusted emission rate map (reflecting vehicle distribution and climate)	Yes, took vehicle distribution into account.

2.1.7 Characterization of TMS impacts on emissions

Modeling both supply- and demand-side TMS requires proper characterization and behavioral realism of the agents involved. Few studies, however, have related TMS induced changes in travel behavior and driving activity to emissions. TDMs have generally involved policy decisions and regulatory changes. For example, network demand or capacity increases as a result of building new roads and adding vehicles onto the network was estimated to increase emissions of Nitrogen-Dioxide (NO_2); city wide road pricing was estimated to decreases traffic emissions of NO_2 and particulate matter (PM_{10}); and the use of alternative fuels was estimated to produce minor and statistically insignificant improvements of city-wide air quality (Mitchell, Namdeo, Lockyer, & May, 2002). However, a challenge in such estimates is the lack of comprehensive emissions rate inventory and granularity in driving activity estimation.

Mode shift (MS) is a popular TDM technique that is intended to reduce the number of vehicle trips. MS involves combination of different mix of strategies to promote HOVs by improving HOV lanes, ridesharing and reducing single occupancy vehicles (SOV) through parking regulation and congestion pricing. A TDM program in an area wide level of application can reduce vehicle miles traveled by 4%-8% (Meyer, 1999). Situations for which MS may be most effective include congested urban areas; a reduction of VMT is expected to improve traffic operations and consequently reduce emissions. However, for a relatively unsaturated network, MS is not expected to bring significant improvement and may even increase emissions.

Fleet replacement (FR) is a regulatory intervention to promote the deployment of newer (cleaner) vehicles in the fleet. Over time older vehicles leave the fleet, and newer vehicles enter the fleet. Improvements such as low sulfur fuels, computerized fuel metering, electronic ignition, air injection, exhaust gas recirculation, and 3-way catalytic converters have substantially reduced emissions on an individual vehicle basis (Faiz et al., 1996). Thus, over time, the fleet average emission rate is lowered. The actual effectiveness of fleet turn-over with regard to emissions reduction depends on a variety of factors, such as whether older vehicles actually leave the fleet, the deterioration rate of emissions for vehicles in the fleet, fuel properties, the effectiveness of inspection and maintenance programs in preventing tampering that might increase emission rates. The Environmental Protection Agency (U.S. EPA) implemented 'Tier 2 Motor Vehicle Emissions and Fuel Standard' from 2002, which was an important shift in standards for 'regulatory classes'. By 2030 those standards are expected to lower total vehicular Nitrogen Oxide (NO_x) emissions by 74% and total emissions by 3 million tons annually (EPA, 1999). An agent based framework is most

suitable to assess emissions impacts of FR on a regional network. Even though a few previous studies assessed effects of vehicle turnover on emissions (Frey, Zhai, & Rouphail, 2009), comparable effectiveness of FR as a TMS was never assessed that can provide balanced insight regarding what combination of approaches may be effective in reducing emissions.

Cycle average emission rates when plotted against cycle average speed typically exhibit a parabolic shape, with high emissions rates at both ends and low emissions rates at moderate speeds of around 40 to 60 mph (Barth & Boriboonsomsin, 2009), depending on the pollutant. This relationship has motivated the consideration of congestion mitigation, speed management, and traffic smoothing strategies. Related TMS include variable speed limits, dynamic intelligent speed adaptation (ISA), congestion pricing, among others. Peak spreading (PS) is a traffic smoothing strategy is aimed at decreasing the frequency and intensity of acceleration and deceleration events due to congestion. PS can be achieved by altering the trip departure time choices of individuals by providing network congestion information. It can also increase network capacity significantly (Mahmassani & Liu, 1999). However, signs of PS implementation are only found in smaller cities where potential for urban sprawl and decentralization is much more limited (Gordon, Kumar, & Richardson, 1990).

Incidents, such as car accidents that disrupt traffic flow, are a major component of non-recurring congestion. Proper incident management programs have been shown to significantly improve network throughput (Lomax et al., 1997). The effects of incidents and incident response strategies on traffic operations are typically assessed using microscopic simulations since it is difficult to simulate a single incident in a macroscopic model. For this

reason, the majority of the previous literature was limited to a single corridor or a small or medium size network. However, advanced traveler information systems (ATIS) such as variable message sign (VMS) and radio broadcasts can have network wide influence on traveler choice, and thus can be used in response to incidents to encourage changes in trip departure time or diversions.

2.2 Research Questions

The two key research questions are addressed in this chapter – (1) how can emissions impacts from a large-scale network be assessed? and (2) how do different TMS interventions on the network impact travel behavior, driving activity, and emissions at a regional and corridor level?

2.3 Existing Methodology of Integrated DTALite and MOVES Lite Framework

Incorporation of the traffic simulation model DTALite with the simplified microscopic emission estimation model MOVES Lite is illustrated in Figure 2.2. Starting with the traffic simulation model, typical data sources for simulation-based dynamic traffic assignment in the integrated model include 1) link-node network data, 2) origin-destination demand table (with optional departure time profile), and 3) different traffic mitigation strategies such as signal optimization, ramp metering and road pricing. In the driving activity simulation phase, there is a need to incorporate a number of microscopic emission estimation model attributes, so these additional vehicle attributes are assigned to vehicles during the vehicle generation process at the beginning of the DTA simulation. Following the execution of the traffic assignment, a vehicle trajectory reconstruction module is utilized to recover microscopic speed and acceleration profiles from individual vehicles. The data are then passed along to

the emission model, which calculates the distribution of trip time in each VSP- and speed-based operating mode bin, calculates emissions based on operating model bin emission rate tables (e.g., Table 2.3), and makes corrections based upon base cycle rates and vehicle attributes. In general, the procedure can be described in four steps; described in some detail next.

1) Vehicle Generation
2) Traffic Assignment
3) Vehicle Trajectory Reconstruction
4) Microscopic Emissions Estimation

Table 2.3. Selected Average Emission Rate for Zero-Age Passenger Cars (Frey, Yazdani-Boroujeni, Hu, Liu, & Jiao, 2013)

Operating Mode	**Energy (KJ/h)**	**CO2 (g/h)**	**NOX (g/h)**	**CO (g/h)**	**HC (g/h)**
0	49206	3536	0.05	2.37	0.04
1	45521	3271	0.01	4.06	0.00
…	…	…	…	…	…
40	641649	46113	14.34	407.60	2.73

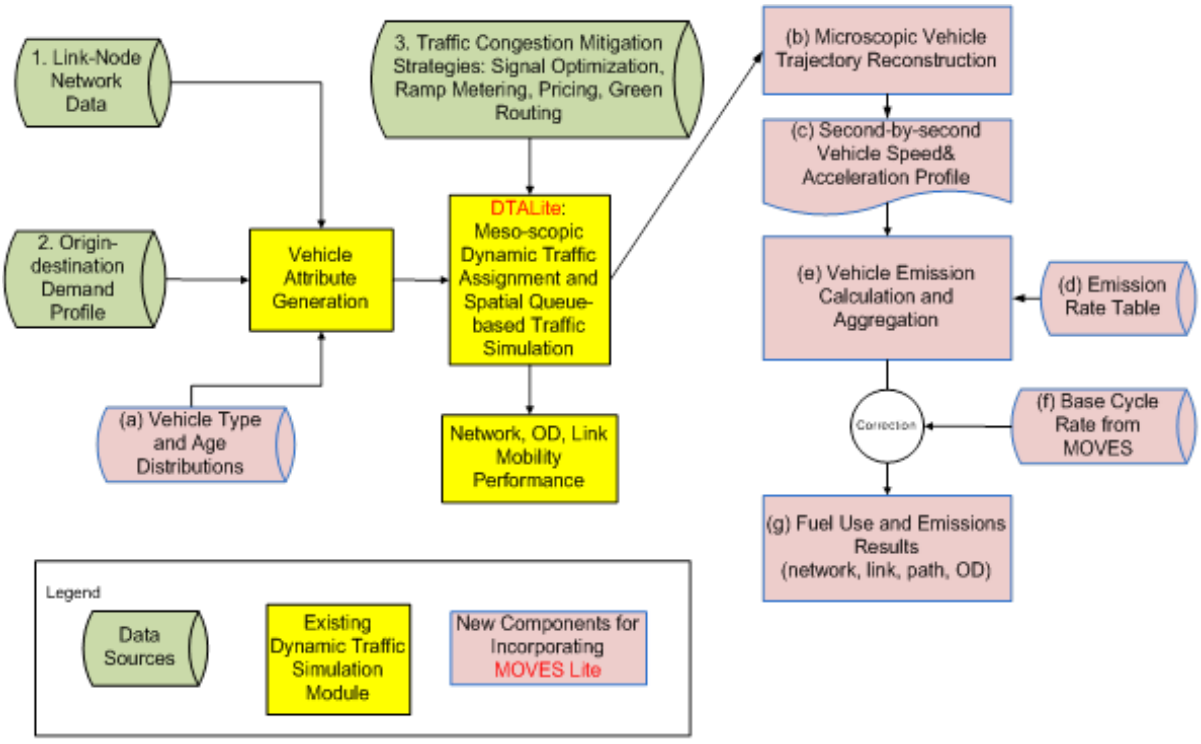

Figure 2.2. Systems framework of DTALite and MOVES Lite

Step 1: Vehicle generation (with type and age distribution)

A typical traffic demand database describes the number of vehicles traveling between each origin and destination pair in the network, and the demand type associated with the vehicles, such as LOV (low occupancy passenger vehicle), HOV (high occupancy passenger vehicle) and trucks. Demand type classes are typically used to study different road tolling rules and different values of time in traffic demand management applications. The challenge is how to reasonably generate the detailed vehicle type and age distribution required for emission estimation. First, a table similar to Table 2.4 is used to distribute vehicles in each demand type to different vehicle types. Then a table similar to Table 2.5 is used to further disaggregate vehicles in each vehicle type to different age groups based on a simple probability distribution of the fleet makeup. The values in Table 2.4 and Table 2.5 should be

calibrated using state-wide or local regional data sources (Bureau of Transportation Statistics, 2013).

Table 2.4. Example Sample Distribution for Mapping from Demand Type to Vehicle Type

Demand Type	Vehicle Type				
	Passenger Car	**Passenger Truck**	**Light Commercial Truck**	**Single Unit Short-haul Truck**	**Combination Long-haul Truck**
Single occupancy passenger vehicle (SOV)	80%	20%	0%	0%	0%
High occupancy passenger vehicle (HOV)	80%	20%	0%	0%	0%
Truck	0%	0%	72%	22%	6%

Table 2.5. Vehicle Age Distribution by Type and Age (Frey et al., 2013)

Vehicle Type	Name	Vehicle Age Distribution			
		Age 0	**Age 5**	**Age 10**	**Age 15**
1	Passenger Car	6%	48%	28%	18%
2	Passenger Truck	3%	43%	26%	28%
3	Light Commercial Truck	3%	44%	26%	27%
4	Single Unit Short-haul Truck	4%	52%	23%	21%
5	Combination Long-haul Truck	4%	52%	23%	21%

Based on the number of vehicles traveling from each origin to each destination, the departure time profile, and the mapping information from demand type to vehicle type and age distribution, the vehicle generator then creates vehicles to be simulated in the DTA model. Each vehicle in the simulation is characterized by the origin and destination node, the departure time at the origin node, vehicle type and vehicle age.

Step 2: Traffic assignment and simulation modules to achieve user equilibrium

Using network data, generated vehicles, and traffic control measures, the mesoscopic DTA model typically performs the following steps at each iteration.

a. Shortest Path Calculation: Calculates the time-dependent least-cost or least-time path for each vehicle based on its origin, destination and departure time.
b. Traffic Simulation: Perform traffic simulation to move the vehicles from their origins to their destinations, subject to link and node capacity constraints. Update the time-dependent link travel times for next shortest path calculation.
c. Vehicular Flow Assignment: The assignment module assigns a certain percentage of vehicles to newly-computed least-cost or least-time path.
d. Convergence Checking: The assignment and simulation steps are repeated until the equilibrium is achieved. Typically, 20-40 iterations are required to reach a desirable relative user equilibrium gap value (e.g., 1%).

DTALite is a simulation-based dynamic network loading model used to move vehicles through the network. Based on a triangular flow-density relation shown in Figure 2.1, there are two closely related finite-difference-based numerical solution schemes to solve the traffic simulation problem as the first order kinematic wave problem: (i) Newell's simplified model (Newell, 1993) that keeps track of shock wave and queue propagation using cumulative flow counts on links, and (ii) Daganzo's cell transmission model (Daganzo, 2006) that adopts a "supply-demand" or "sending-receiving" framework to model flow dynamics between discretized cells. Newell's kinematic wave (KW) model is used in DTALite's implementation to represent bottlenecks and capture shockwave propagation.

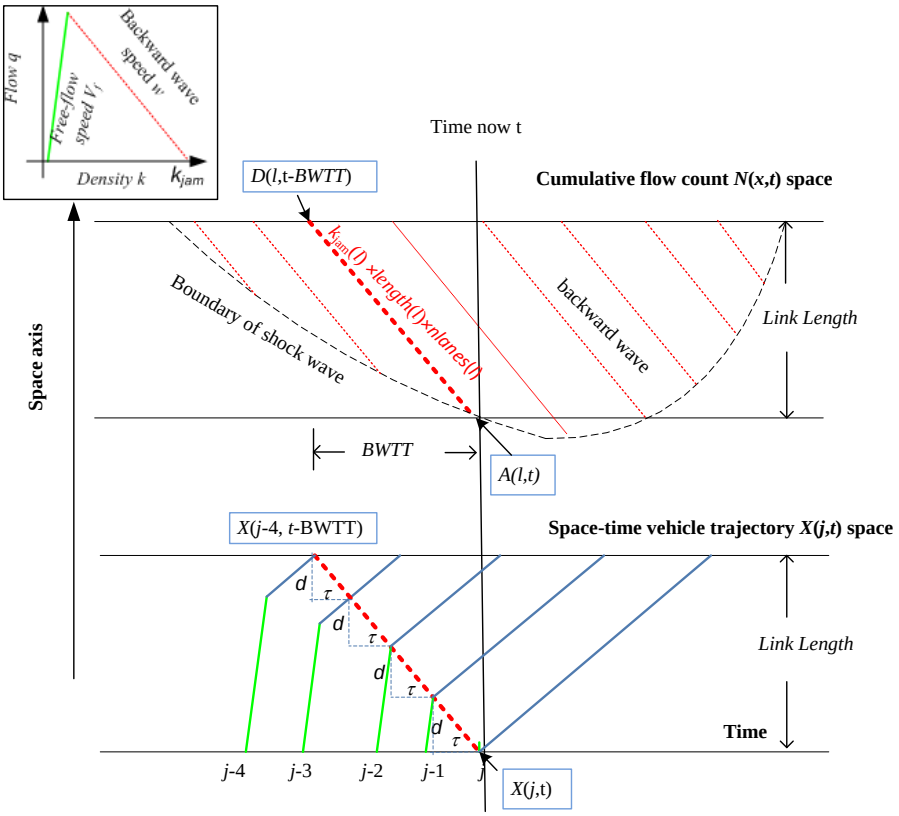

Figure 2.3. Consistent representation of backward wave propagation in both Newell's kinematic wave and simplified linear car following models (Zhou et al., 2015)

By explicitly using the cumulative arrival and departure curves, Newell's flow model provides an effective means to realistically represent traffic dynamics and capture (forward and backward) shockwaves as the result of bottleneck capacities. In addition, compared to other cell-based models that need to subdivide a long link into segments with short lengths, Newell's model can handle reasonably long links with homogeneous road capacity. Its simple traffic flow model and computational efficiency make it particularly appealing in establishing theoretically sound and practically operational DTA models for large-scale networks. There are a number of related studies on Newell's kinematic model, to name a few, model calibration research by Hurdle and Son (Hurdle & Son, 2000), extensions to node merge and diverge cases (Ni, Leonard, & Williams, 2006; Yperman, 2007).

DTALite adopted Hurdle and Son's framework (Hurdle & Son, 2000) to illustrate how Newell's approach can model backward waves using cumulative flow counts. Let *x* denote the location along the corridor. A wave w(q, x) represents the propagation of a change in flow *q* and density *k* along the roadway,

$$w(q,x) = \frac{dx}{dt}. \quad (1)$$

Let us focus on the change of *N* curves along a characteristic line (wave) at links; that is,

$$dN(x,t) = \frac{\partial N}{\partial x}dx + \frac{\partial N}{\partial t}dt = qdt - kdx \quad (2)$$

where $N(x, t)$ is the actual cumulative count of vehicles that pass location *x* from time 0 to time *t*. Along the movement of a wave, the definition of *w* in equation (1) leads to $dt = \frac{dx}{w}$ and simplifies equation (2) as

$$dN(x,t) = qdt - kdx = \left(-k + \frac{q}{v}\right)dx. \quad (3)$$

In the triangular-shaped flow-density relation, the values of (forward and backward) waves are constant. In the case of backward wave propagation, the congested region of the triangular shaped flow-density model gives $-k + \frac{q}{w_b} = -k_{jam}$. (4)

Thus, $dN = \left(-k + \frac{q}{wb}\right)dx = k_{jam}(l) \times length(l) \times nlanes(l)$ (5)

The cumulative flow count, $N(x,t)$, space in the upper part of Figure 2.3 illustrates the backward waves in capturing queue spillback phenomenon from cumulative departure count at time t-BWTT $D(l, t - BWTT)$ to cumulative departure time count $A(l, t)$. In this example, the downstream end of link *l* is a temporary bottleneck, and a queue builds up from the downstream node and spills back to the upstream node. Exactly at time *t*, the tail of the queue propagates to its upstream node, when the backward wave is able to propagate through the congested time-space "mass" of the link with $k_{jam}(l) \times length(l) \times nlanes(l)$ vehicles.

Step 3: Vehicle trajectory construction module

DTALite outputs the link arrival and departure times for each vehicle, which can be used to construct cumulative vehicle arrival and departure counts on each link. Given the arrival and departure time of the individual vehicle on a link, we adapt Newell's simplified linear car following (LCF) (Newell, 2002) model to reconstruct the vehicle trajectory in the link. Then the detailed second-by-second vehicle speed and acceleration are derived from the reconstructed vehicle trajectory. It is not necessary to construct the vehicle trajectory for each iteration of the DTA simulation. To save computational time, one can convert only the cumulative flow counts from the last iteration of the DTA process to generate second-by-second speed profiles and corresponding emission results.

The main idea of Newell's car following model is that a (following) vehicle *n* maintains a minimum space and time gap between it and the preceding vehicle *n-1*. When the lead vehicle *n-1* changes its speed, the following vehicle *n* changes its speed along the backward wave w. The car following trajectory is illustrated in Figure 2.4 .

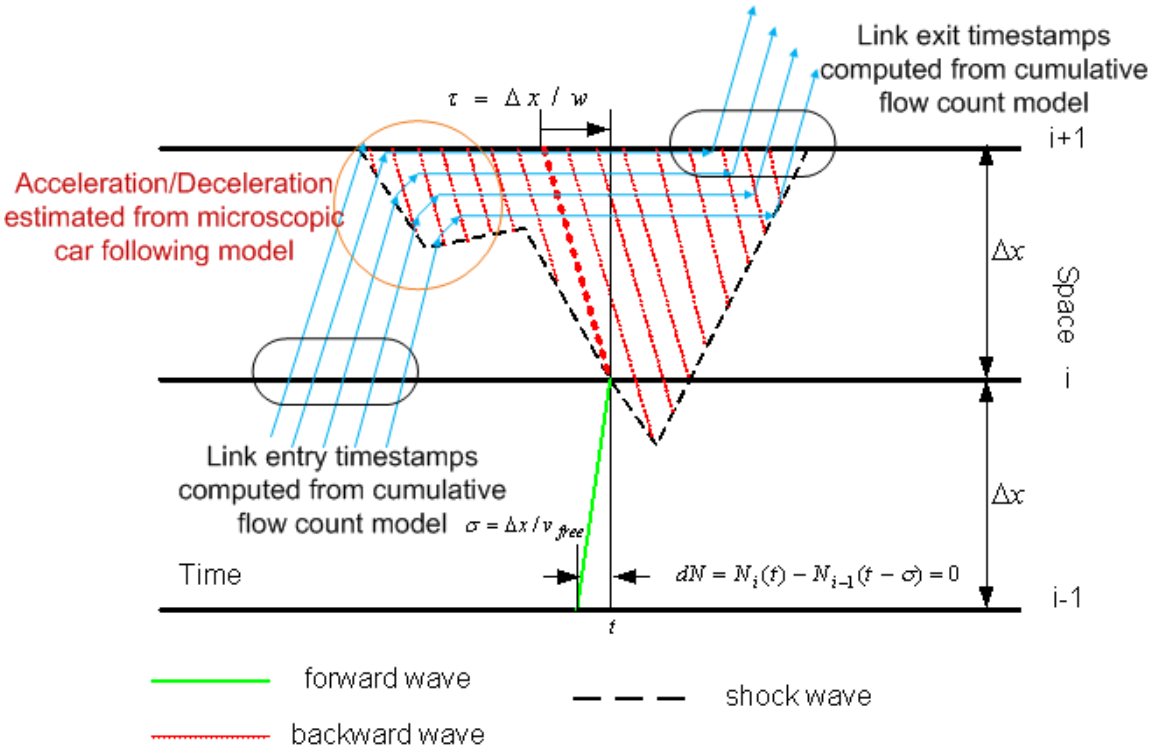

Figure 2.4. Constructing microscopic vehicle trajectory from mesoscopic simulation results (Zhou et al., 2015)

Mathematically, Newell's car following model states that the vehicle trajectory relationship between the following vehicle *n* and the lead vehicle *n-1* is defined as:

$$x_n\left(t+\tau_n\right)=x_{n-1}\left(t\right)-d_n \tag{6}$$

where $x_{n-1}\left(t\right)$ is the position of the lead vehicle at time *t*, $x_n\left(t+\tau_n\right)$ is the position of the following vehicle at time $t+\tau_n$; τ_n and d_n are the appropriate time and space gaps, respectively. Given the vehicles' arrival and departure times on the link from a macroscopic dynamic traffic assignment and simulation model such as DTALite, the procedure for calculating the vehicle trajectories along this link is described below.

Input:

L: the length of the link;

v_f : the free flow speed on the link;

d : the minimum space gap;

τ : the minimum time gap;

$Arr(n)$: the arrival time of vehicle n at the upstream node of the link;

$Dep(n)$: the departure time of vehicle n at the downstream node of the link;

ΔT : the time step increment (e.g. 0.1 seconds);

Variables:

$X(n,t)$: the position of vehicle n at time t;

For each vehicle $n = 1, \mathrm{K}, N$

Initialize the starting position of a link $X(n, Arrival(n))$=0;

For each time interval *t* = $Arr(n)$ to $Dep(n)$

Calculate free-flow driving position:

$$X^F(n,t+\Delta T) = \min\left\{X(n,t) + v_f \times \Delta T, L\right\};$$

If *n* is the first vehicle, where $n == 0$

$$X(n,t+\Delta T) = X^F(n,t+\Delta T)$$

Else

Calculate position determined by backward wave propagation from the leader *n-1*:

$$X^B(n,t+\Delta T) = X(n-1,t+\Delta T-\tau) - d;$$

Calculate the final feasible position:

$$X(n,t+\Delta T) = \min\left\{X^F(n,t+\Delta T), X^B(n,t+\Delta T)\right\};$$

End If

$t = t + \Delta T$;

End For

End For

A recent paper by Dr. Daganzo in UC Berkeley (Daganzo, 2006) has shown that, by assuming a triangular flow-density diagram, vehicle trajectories constructed from a simplified kinematic wave model are equivalent to those generated by Newell's simple linear car-following model and two types of cellular automata (CA) models within a certain approximation range. In a calibration and validation study for a number of well-known car following models, Newell's simplified LCF model showed reasonable performance with limited calibration efforts.

Step 4: Microscopic emissions module

MOVES Lite first calculates the second-by-second VSPs based on the corresponding vehicle operating parameters. Using a combination of calculated VSPs and the vehicle speed, the calculation process then finds the appropriate operating modes from the operating mode bin table (e.g., Table 2.3). This is followed by another table lookup (Table 2.4, Table 2.5) with the vehicle emission rate table based on operating mode, vehicle type and age. The emission and fuel consumption are accumulated and corrected with base cycle emission rates calibrated previously using MOVES. Additional reporting mechanisms are applied to generate the final emission reports.

2.4 Methodology for Evaluation of Transportation Management Strategies (TMS)

The integration of MOVES Lite with mesoscopic simulator DTALite in a multi-resolution platform provided a unique opportunity to assess emissions impacts of network interventions in a consistent and efficient manner (Frey & Liu, 2013). The methodology discussed in this chapter attempts to organize these different components as a system framework, depicted in Figure 2.5. The system relies on two parallel processes: attribution of emissions estimation module, MOVES Lite (shown in grey boxes) and functioning of DTALite in simulation of TMS scenarios. The left box in Figure 2.5 shows the input requirements for the framework. MOVES Lite depends on site-specific vehicular, regulatory, and weather information to establish assumptions regarding simplification of MOVES database. Network and traffic related input data are converted, corrected and verified to assemble the baseline network. Proper characterization of TMS is supported through regulatory, policy, economic, and technological evaluation of these interventions (shown in clouds at the bottom). TMS's can then be implemented in the calibrated baseline model and the estimation of emissions can be done through the integrated DTALite-MOVES Lite interface.

2.4.1 Data preparation

Preparation of network data

Networks represented by links, nodes and zones are generally characterized in a GIS shape file format. Regional and city planning authorities maintain this file, which also contain demand data that is periodically updated. These data needs to be converted into the hourly-decomposed DTA consistent format. A large amount of network information regarding volume, speed, and travel time are required to calibrate and validate the model. Potential data sources are volume and speeds from fixed sensors, or probe based travel time information for

major road segments (example: Traffic.com, INRIX). Supplementary data sources could include video surveillance and floating car sensing information.

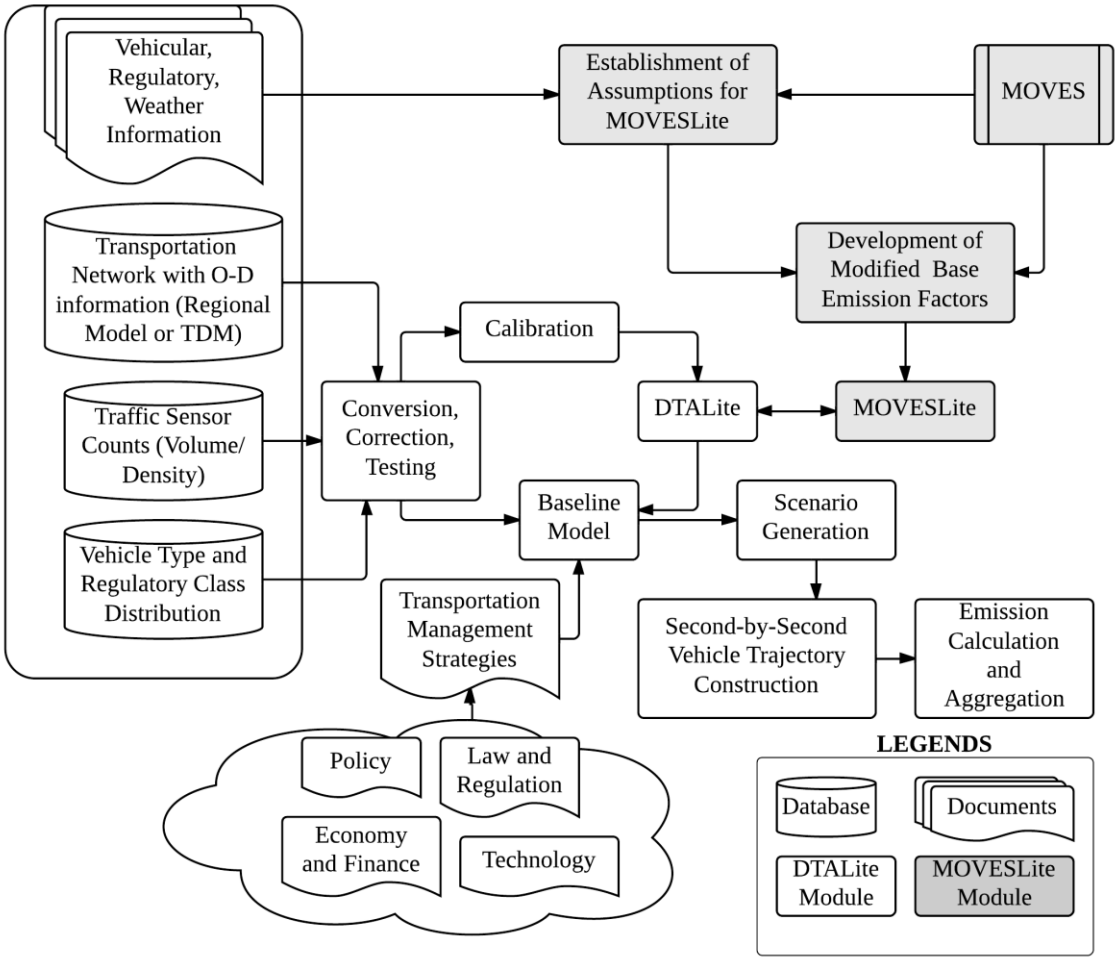

Figure 2.5. System framework and data-flow for assessing emissions impacts of Transportation Management Strategies

Preparation of emissions data

MOVES Lite is implemented as an inbuilt capability of DTALite. The MOVES Lite to DTALite interface is maintained through four input files: base cycle emissions factor different pollutants by different vehicle type and age, fraction of time that different vehicle types remain in different OpMode, vehicle emissions rates by different vehicle types, ages

and OpMode, and vehicle type and age distribution. Agent based DTALite stores type and age characteristics of each vehicles and serves as the reverse interface. Trajectories are generated in terms of 1 Hz speed and acceleration for each modeled vehicle. The trajectories are used to calculate vehicle specific power (VSP) and the fraction of time spent in each OpMode for a given cycle. Therefore, a cycle correction factor (CCF) for link based driving cycle can be generated for each vehicle type. The base cycle emission factors can then be corrected and aggregated over a link for each vehicle type to produce the desired link emissions estimates. Thus, the spatial resolution of the estimate is the link. However, the estimation of emissions will depend on a proper characterization of speed trajectory in DTALite. For validation purposes, the LCF generated trajectories are compared to real world measurement of driving activity. The result have shown some unrealistic acceleration and deceleration events, and a lack of diversity between simulated trajectories. A potential remedy to this problem is to separate the cycle profile in segments and match them with real-world micro-trips; matched profile segments that can then be combined to reconstruct the vehicle trajectory (Zhou et al., 2015). In spite of this model limitation, the method provided a practical way to bridge data requirements between a mesoscopic traffic model and microscopic emissions estimation model.

2.4.2 Experimental design for evaluation of TMS

Preparation of baseline network

The baseline network represents characteristics and conditions of the present 'without intervention' scenario. It is essential that the baseline model emulate field observed volumes, speeds and travel times. This process is called calibration; it alters the historic and default network parameters to match field conditions. O-D estimation techniques are built into

mesoscopic simulation tools that modify the O-D matrices in such a way to reduce the gap between field-measured and modeled link properties.

Scenario generation and modeling

The TMS scenarios implemented in this work come from different generic classes, have different data needs and require individual modeling needs. Mode shift (MS) depends on a policy decision about the desired fraction of vehicle-trips to be reduced. DTALite implements four vehicle classes namely, SOV, HOV, trucks, and transit, each having different person trips and occupancy parameters. If a certain percentage of person trips is transferred to a higher occupancy ratio mode (SOV and HOV are modeled as having occupancy ratios of 1 and 2 respectively), there will be a resultant reduction in overall vehicle trips. MS scenario is implemented by changing the person trip distribution across modes, while keeping the total number of *person trips* the same as the baseline network. After implementation the model is iterated few times to achieve equilibrium.

The fleet replacement (FR) scenario is intended to alter the vehicle age distribution considered in the model. Two vehicle classes are considered under the demand classes described above: passenger car (PC) and passenger truck (PT). The baseline model uses the age distribution for these vehicle classes based on statistics from the North Carolina Department for Environment and natural Resources (NCDENR). FR as a regulatory decision can be used to change the age distribution of these vehicle classes and assess its impact on emissions.

Peak spreading (PS) scenario was modeled as a shift in trip departure times. The operational improvements resulting from peak-spreading strategies occur by reducing peak demand, and enabling a more uniform distribution of demand over time. In the model, hourly demand tables are adjusted to match a desired level of peak spreading.

Incident (INC) scenario was modeled at the link level by specifying the event start time, end time, and its impact on link capacity. All those parameters depend on the type and severity of the simulated incident. If no warning information is provided via VMS, vehicles traveling through the incident location will not alter their route despite the capacity reduction. Under the VMS scenario, advanced information to the vehicles traveling on the path will prompt diversion to alternate paths away from the incident site.

Method for performance evaluation

Validation of the mesoscopic model performance measures must be carried out at multiple stages; first to validate whether mobility related outputs such as volume and speed correspond to the scenario being simulated. Subsequently, the analyst must validate whether the simulated emissions correspond to the condition being modeled. Validation of the mobility parameters have been discussed in a previous paper (Tanvir, Karmakar, Rouphail, & Schroeder, 2016). The accuracy of link level simulated emissions depends on two factors – accurate simulation of driving activity through the car-following model and accuracy of the corresponding emissions rates provided by MOVES Lite. The former was found to be reasonable when the speed-acceleration envelopes of simulated and empirical trajectories were compared (Zhou et al., 2015). Simulated link emissions are assumed to be inherently valid as MOVES Lite provides a very faithful implementation of MOVES (Frey & Liu, 2013) and there is no established method to observe link level emissions.

Alterations in emissions over space and time should be assessed as there is both spatial and temporal consequences to implementation of a TMS. Mode shifts (MS), fleet replacement (FR), and peak spreading (PS) strategies are policy level decisions and their impacts are considered to be network-wide. But there will be observable dynamics with time.

For this reason, change of network-wide emissions rate or emissions profiles can provide insights for comparative assessment. A 15-minute aggregation interval is selected as demand dynamics varies at this temporal resolution. The percentage change in network-wide pollutants across the various pollutants, when compared to the baseline model values can serve as an overall performance measure for those three strategies.

For the incident (INC) scenario with and without VMS, those effects are concentrated on a small portion of the total network. Though there might be region wide effects of capacity reduction for a key section on the network, the effect in our case study was not significant enough to address. For this reason, INC and VMS are best assessed at the corridor level. Path based average emissions estimate per vehicle mile traveled is used to capture the corridor wide impact.

2.5 Case Study

2.5.1 Description of test network

The methodology described above has been implemented for a large scale regional network combining three cities in North Carolina, namely Raleigh, Durham, and Chapel Hill. The network is converted to a DTALite format from a TRANSCAD based Triangle Regional Model (TRM) for the specific area. TRM contains 9,528 nodes, 20,258 links and 7,193 origin-destination zones. A schematic of the network is shown in FIGURE 2. The baseline model has services nearly a million vehicle trip for a period of 5-hours. The baseline model only considered two demand classes: SOV and HOV; two types of vehicles were modeled under these demand classes: PC and PT.

The baseline model (BASE) was calibrated with sensor based volume data provided by Traffic.com on the major freeways and arterials for the modeled time period. Calibration

was done at a 15-minute resolution. The calibrated network is able to match the baseline traffic flows, with a R^2 value of 0.82. The baseline model mode split for passenger trips was 85% SOV's and 15% HOV's. To implement MS for the case study, 15% of the passenger trips from SOV were converted to HOV trips. This resulted in a 7.5% reduction in total vehicle trips in MS compared to the BASE scenario. The age distribution for PC and PT for BASE model was extracted from the vehicle registration inventory in the study area. The model considered 30 age groups at 1 year interval, with the newest vehicle representing vehicle model for year 2012. To assess the upper bound on the possible effectiveness of FR, 100% of the vehicles were modeled as age 0 year. Finally, PS scenario for the case study is implemented by applying a hypothetical uniform demand profile distribution across the 5 hours of simulation. The model is then iterated to reach equilibrium.

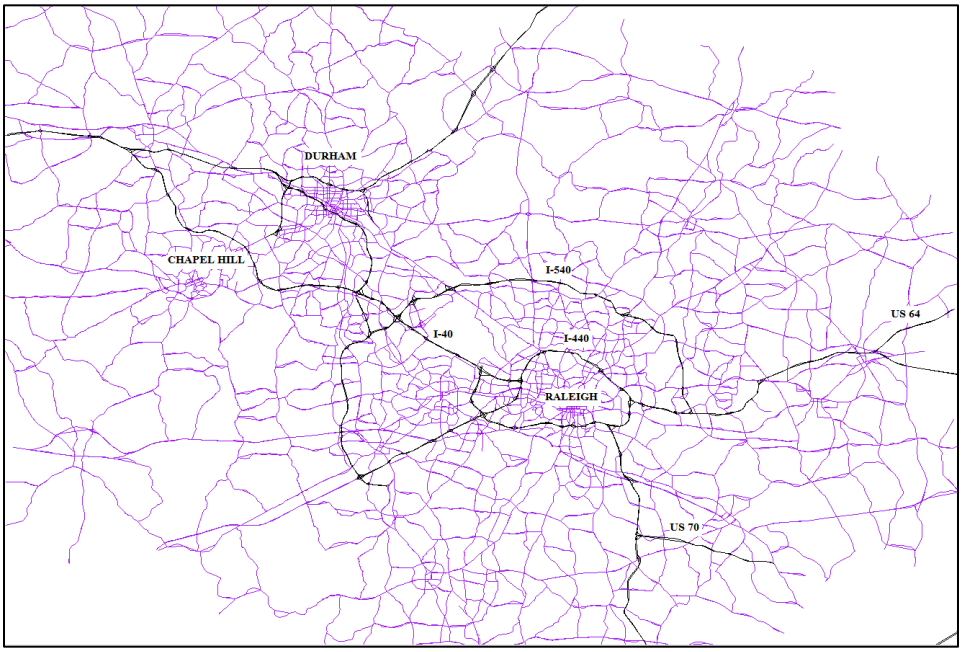

Figure 2.6. Schematic of the model network

At the corridor level, INC is implemented on a selected link on the I-540 freeway. The incident lasted for the entire simulation time, had a 50% capacity reduction and reduced the speed limit to 30 mph. Three dynamic message signs were posted upstream of the incident location to implement VMS.

2.6 Results and discussions

Network wide profiles and total mobility and emission changes comparing BASE, MS, FR and PS scenarios are presented in Figure 2.7 and Table 2.6 respectively. No speed change for implementation of FR was evident, as it is a regulatory intervention that does not impact traffic flow characteristics. MS and PS yielded a 1% and 3% speed gain respectively, indicating an improvement in network operations. Fleet replacement reduced the emissions of nitrogen oxides (NO_X), carbon monoxide (CO) and hydrocarbons (HC) by a margin of 80% to 90%, but has insignificant effect on carbon dioxide (CO_2) emissions. This is probably due to the fact that the Tier 2 standard for newer vehicles does not have a stricter regulation on CO_2 emissions compared to NO_x, CO, and HC. The MS strategy yielded a relatively high reduction in CO compared to NO_X, CO_2, and HC. PS yielded a higher reduction in NO_X compared to other pollutants. It shows evidence of higher sensitivity to NO_X emissions of traffic operational characteristics such as frequent stopping and acceleration.

The peak spreading scenario essentially did not alter traffic or traffic composition. The 1% increase in total network traffic in PS may be due to increased operational efficiency of the network; therefore allowing more demand to be loaded onto the network. Even though the network average speed increased only by 3%, emissions of NO_x were reduced significantly (6%). In Figure 2.7, all four pollutants have similar diurnal patterns in terms of emissions reduction for peak spreading and the reduction is at its highest when the baseline

peaks were occurring. Therefore, peak spreading has the effect of significantly lowering overall network wide emissions during the peak period in addition to decreasing overall emissions. Shifting of demand towards the off-peak direction also does not degrade conditions during those periods. It is to be noted that effect of peak spreading would be different for links at different operating conditions. Links that already had frequent flow disruptions and queuing will benefit from the improvement in operational condition the most. On the other hand, significant improvement in speed may cause vehicles to be operated at higher power demands and therefore may cause increase in link emissions. The benefit of a large-scale modeling framework lies in the fact that city managers can adjust the extent of a peak spreading scheme.

Table 2.6. Network wide change for Mode Switch (MS), Fleet Replacement (FR), and Peak Spreading (PS) strategies compared to Baseline (BASE)

Parameters	**% of change compared to BASE**		
	MS	**FR**	**PS**
Cumulative vehicle count	-8%	0%	1%
Average speed	1%	0%	3%
Total CO_2	-5%	-1%	-2%
Total NO_X	-2%	-81%	-6%
Total CO	-9%	-78%	-2%
Total HC	-6%	-91%	-3%

Table 2.7. I-540 Path wide changes for Incident (INC) and corresponding variable message sign (VMS) strategy compared to Baseline (BASE)

Parameters	**% of change compared to BASE**	
	INC	**VMS**
Cumulative vehicle count	-8%	-30%
Average speed	-39%	6%
Average CO_2 per vehicle-mile	62%	36%
Average NO_X per vehicle-mile	193%	155%
Average CO per vehicle-mile	4%	-13%
Average HC per vehicle-mile	47%	12%

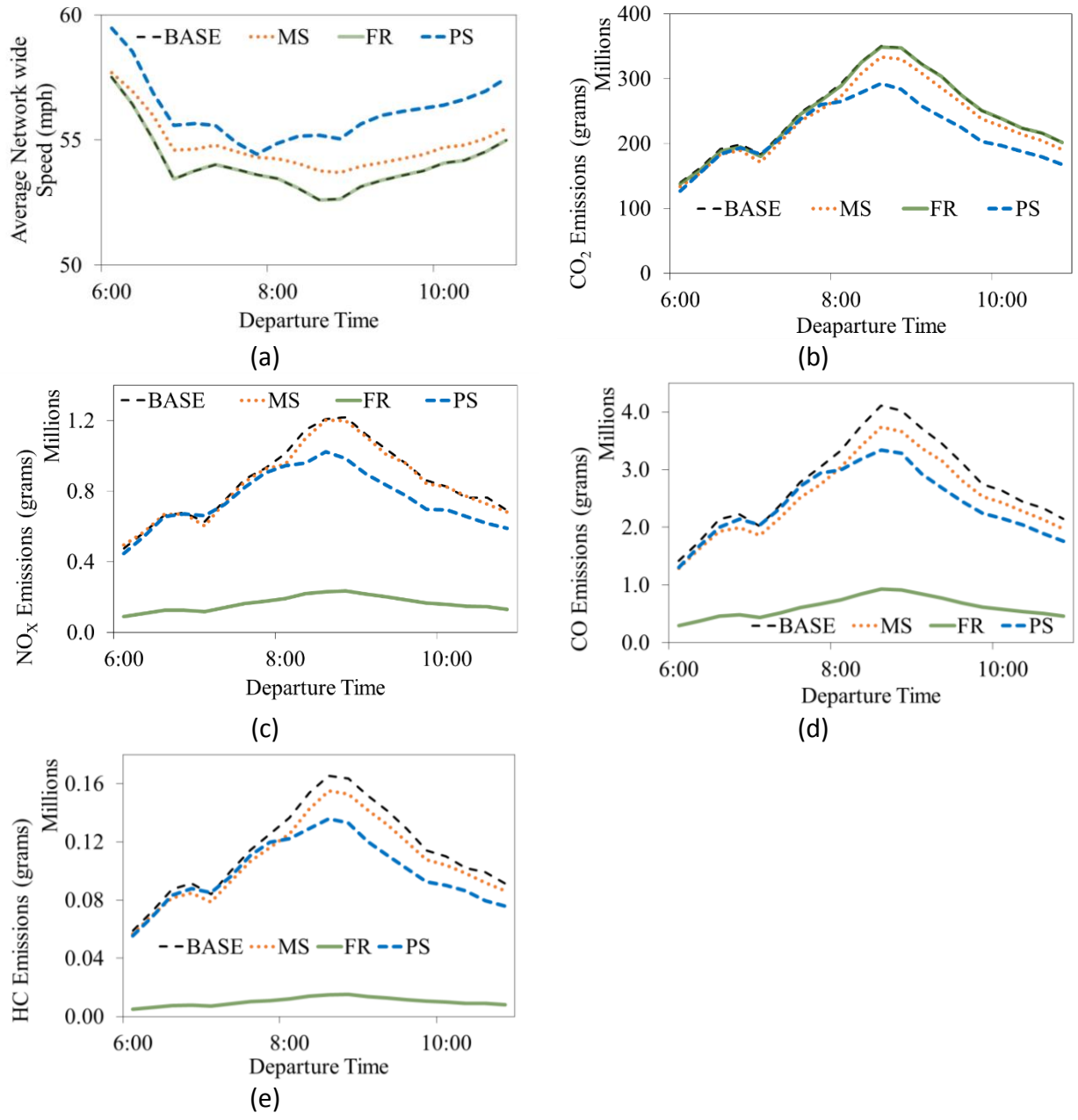

Figure 2.7. Network wide profile (a) average network speed (mph) (b) CO_2 emissions (grams) (c) NO_X emissions (grams) (d) CO emissions (grams) (e) HC emissions (grams). [BASE = Baseline, MS = Mode Shift, FR = Fleet Replacement, PS = Peak Spreading]

Path based emissions profiles and average emissions statistics are presented in Figure 2.9 and Table 2.7 respectively. VMS scenario yielded a much higher level of diversion (30%) compared to INC (8%) on the affected path.

The corridor performance due to simulated incident and successive VMS implementation is shown in Figure 2.8. Though there is still some presence of a bottleneck, operational condition under the VMS scenario is even more improved than the BASE for the corridor. However, the presence of the bottleneck in VMS increased NO_X emissions by 155% compared to the BASE. VMS was found lower CO emissions by 13%. Finally, approximately a 31% reduction in HC, 25% reduction in NO_x, and 20% reduction in CO_2 was associated with VMS implementation, when compared to INC.

In general, and as expected, the 15 minute aggregated quantities have higher levels of variability. Thus, the plots in Figure 2.8 need to be interpreted carefully. Variation in vehicle-mile average NO_x, CO, and HC increases with INC and VMS scenarios. This is due to sudden degradation or improvements in simulated operating conditions. With VMS in place, and as the peak period approaches, fewer vehicles choose to divert because the operational conditions of the diverted paths would also be degraded during the same period.

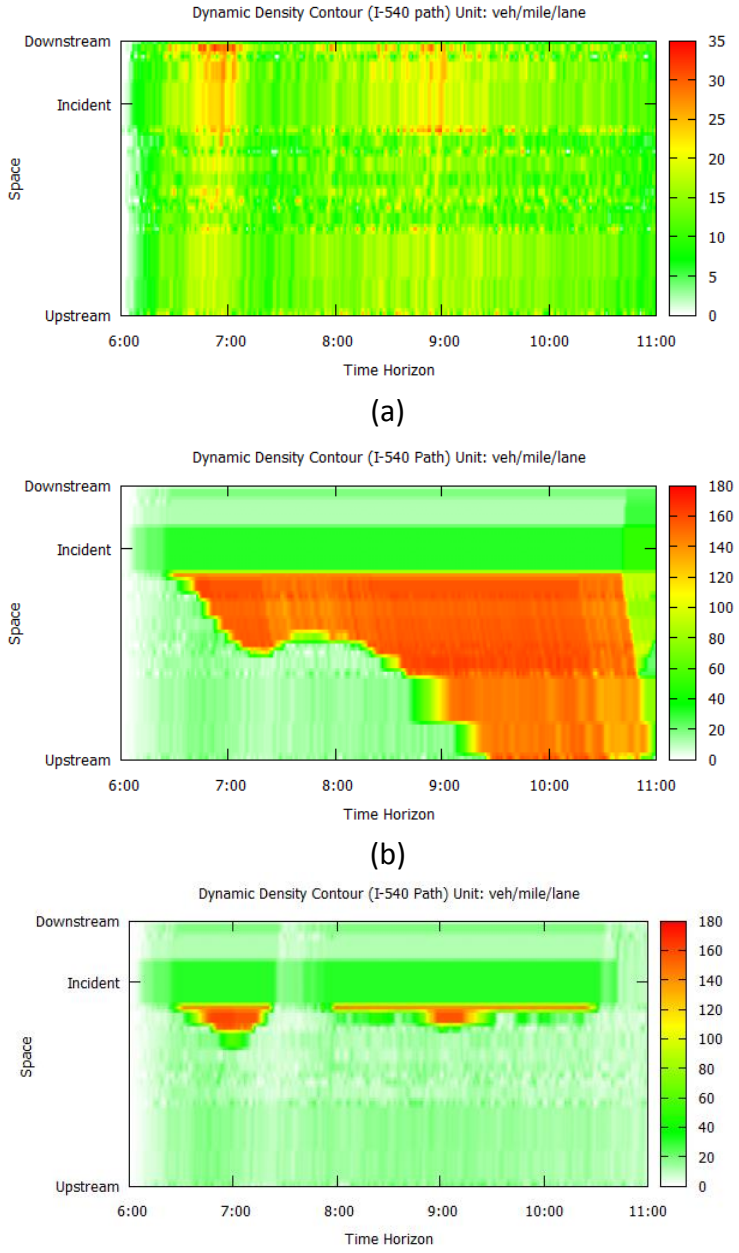

Figure 2.8. Dynamic density contour on the I-540 path for (a) Baseline (BASE) (b) Incident only (INC) (c) Incident with variable message sign (VMS) scenarios.

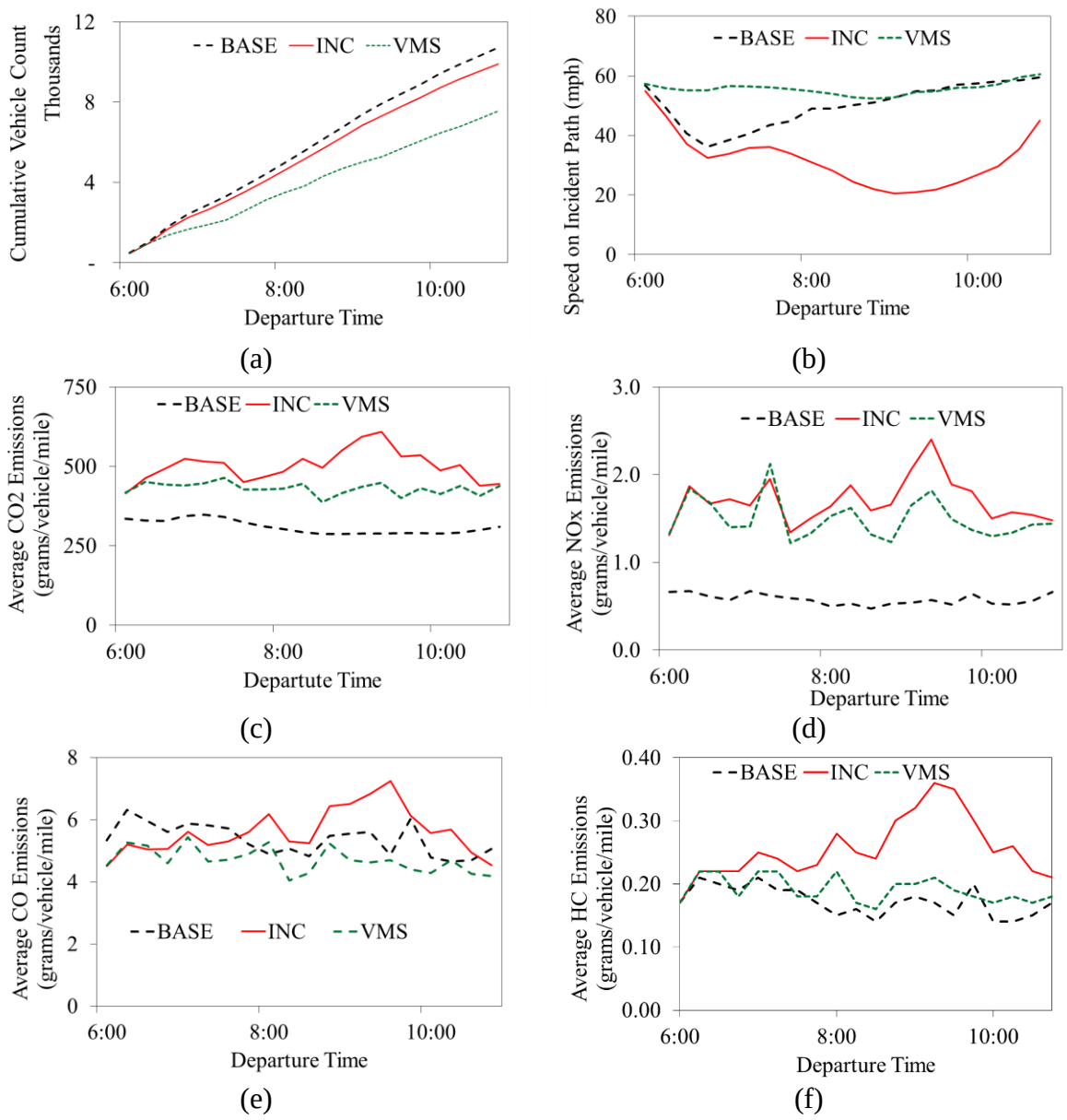

Figure 2.9. Path based profile on selected I-540 path (a) cumulative vehicle count(b) average speed (mph) (c) average CO_2 emissions (grams per vehicle per mile) (c) average NO_X emissions (grams per vehicle per mile) (d) average CO emissions (grams per vehicle per mile) (e) average HC emissions (grams per vehicle per mile). [BASE = Baseline, INC = Incident only, VMS = Incident with variable message sign]

2.7 Conclusions

A new framework was developed to quantify network level mobility and emissions impacts of Transportation Management Strategies (TMS) when applied to a regional network at a

mesoscopic modeling scale. An integrated application of a simplified adaptation of the EPA MOVES model, called MOVES Lite, paired with a dynamic traffic assignment model DTALite, enabled a network analysis to be more consistent, reasonably realistic and computationally tractable. Regarding the impact of TMS on emissions, that effect depended on the particular strategy and its attributes.

A Mode Shift (MS) strategy from SOV to HOV travel essentially reduces total vehicle trips demand on the network. MS generally reduces total emissions. But emissions per VMT may increase for some pollutants because at an existing uncongested network reduction of demand may provide stimulation for speeding and consequently higher emissions. Regulatory rules such as fleet replacement (FR) can provide marked reduction of emissions for pollutants whose ambient level is regulated and for others due to improvement in vehicular and fuel technology. In the bounding case involving total replacement of the fleet to 'Tier 2' regulatory classes on a regional network in North Carolina, reductions of 81%, 78%, and 91% in NO_X, CO and HC levels respectively were estimated. CO_2 reduction is insignificant (1%) as there is not much difference between the EPA 'Tier 1' and 'Tier 2' standards for this pollutant. However, this regulatory decision does not affect traffic flow characteristics such as speed or travel time.

Implementation of peak spreading (PS) strategy depends on the degree of peaking and congestion level on the existing network. The literature verified that PS was found not to produce emissions improvement at a significant level. However, when testing a bounding case with uniform demand across the peak period, not only emissions per VMT were reduced, but also the peak emission level dropped. By lowering the ambient concentration

and adjusting the temporal distribution of emissions, one can reduce the exposure level and generation of secondary pollutants such as Ozone.

Evaluation of emissions at a corridor level is presented to demonstrate the capability of the developed framework in handling multiple spatial resolutions. Assessment of an incident and implementation of a variable message sign or VMS can only be observed at a path or corridor level. Network level benefits of such interventions are considered to be insignificant. Incident without VMS assistance or INC simulates bottlenecking of a network point without providing any related information to trip makers, causes adherence to the historic route choice decisions for the majority of the travelers. However, due to queue spillback and longer duration of the incident, some (8%) of the traffic is diverted to alternative routes even without VMS. In the INC case, however, there is a marked increase in pollutants especially NO_x.

VMS involves information provision to reduce congestion at the incident bottleneck. In the case study, nearly 30% of the trips through the incident location were diverted to alternative routes. The implementation even estimated an increase in the average speed of the corridor compared to the baseline case. However, vehicles on the incident path still have to negotiate the bottlenecks and those travelers experienced an increase in NO_x emission of 155% (average VMT basis).

The comparison of TMS scenarios with regard to emissions can help policy makers make informed decision regarding the combination, intensity and timing of responses. The modeling approach demonstrated here for developing link-based data could be extended to support estimation of near road air quality, exposure, and health effects. The model is based on an open source software platform that enables future augmentation of additional

components. For example, near road air quality measurements can be augmented with this modeling approach; adopted MOVES based emissions rates can be calculated from road side concentration measurements through inverse modeling or adding a dispersion model to the existing framework near road pollutant concentrations can be simulated and compared with observations.

The core of this multi-resolution interfacing framework is the generation of synthetic trajectories from link-based traffic characteristics. Future research should be directed towards matching the modeled trajectory with real world observations for more accurate emissions estimation. The research methodology can be applied to a larger metropolitan area with more severe air pollution problems. Proper dynamic demand profiling and calibration of the baseline network is vital to the accuracy of estimation. There is also a need to develop faster and precise O-D estimation and calibration procedure by assimilating sensing data from multiple sources. Therefore, systematic implementation of this framework would involve synchronization of the model network backed by a well maintained network data collection protocol.

2.8 Acknowledgments and Disclaimer

The research described in the article has been funded wholly or in part by the U.S. Environmental Protection Agency's STAR program through grant RD-83455001. The work described herein has not been subjected to any EPA review and therefore does not necessarily reflect the views of the Agency, and no official endorsement should be inferred.

2.9 References

Ahn, K., Rakha, H., Trani, A., & Van Aerde, M. (2002). Estimating vehicle fuel consumption and emissions based on instantaneous speed and acceleration levels. *Journal of Transportation Engineering, 128*(2), 182-190.

Alkidas, A. C. (2007). Combustion advancements in gasoline engines. *Energy Conversion and Management, 48*(11), 2751-2761.

An, F., Barth, M., Norbeck, J., & Ross, M. (1997). Development of comprehensive modal emissions model: Operating under hot-stabilized conditions. *Transportation Research Record: Journal of the Transportation Research Board, 1587*(1), 52-62.

Barth, M., & Boriboonsomsin, K. (2009). Traffic congestion and greenhouse gases. *ACCESS Magazine, 1*(35)

Bartin, B., Mudigonda, S., & Ozbay, K. (2007). Impact of electronic toll collection on air pollution levels: Estimation using microscopic simulation model of large-scale transportation network. *Transportation Research Record: Journal of the Transportation Research Board, 2011*(1), 68-77.

BTS. (2015). *State transportation statistics 2015*. Washington DC: US Department of Transportation, Bureau of Transportation Statistics.

Bureau of Transportation Statistics. (2013). National transportation statistics (table 1-11: Number of U.S. aircraft, vehicles, vessels, and other conveyances). Retrieved from http://www.bts.gov/publications/national_transportation_statistics/html/table_01_11.html

Cambridge Systematics. (1996). *Quantifying air quality and other benefits and costs of transportation control measures.* (No. Task 1 Report. Project 8-33.). Washington D.C: National Cooperative Highway Research, Transportation Research Board.

Cappiello, A. (2002). *Modeling traffic flow emissions* (MS Thesis).

CARB. (2002). *EMFAC 2002, california air resources board's emission inventory* . (No. Series, September).California Air Resource Board.

Chamberlin, R., Swanson, B., Talbot, E., Dumont, J., & Pesci, S. (2011). Analysis of MOVES and CMEM for evaluating the emissions impact of an intersection control change. Paper presented at the *Transportation Research Board 90th Annual Meeting*, (11-0673)

Daganzo, C. F. (2006). In traffic flow, cellular automata = kinematic waves. *Transportation Research Part B: Methodological, 40*(5), 396-403. doi://dx.doi.org.prox.lib.ncsu.edu/10.1016/j.trb.2005.05.004

De Vlieger, I., De Keukeleere, D., & Kretzschmar, J. G. (2000). Environmental effects of driving behaviour and congestion related to passenger cars. *Atmospheric Environment, 34*(27), 4649-4655.

Eliasson, J., Hultkrantz, L., Nerhagen, L., & Rosqvist, L. S. (2009). The stockholm congestion–charging trial 2006: Overview of effects. *Transportation Research Part A: Policy and Practice, 43*(3), 240-250.

EPA. (1999). *Regulatory announcements*. Ann Arbor, MI: United States Environmental Protection Agency.

EPA. (2008). *Integrated science assessment for oxides of nitrogen - health criteria (final report).* (No. EPA/600/R-08/071). Washington D.C.: U.S. Environmental Protection Agency.

EPA. (2010). *Integrated science assessment for carbon monoxide (final report).* (No. EPA/600/R-09/019F). Washington D.C.: U.S. Environmental Protection Agency.

EPA. (2012). *User guide for MOVES2010b.* (No. EPA-420-B-12-001b).United State Environmental Protection Agency.

EPA. (2014). *Inventory of U.S. greenhouse gas emissions and sinks: 1990-2012.* (No. EPA 430-R-14-003). Washington D.C.: U.S. EPA.

Etheridge, D. M., Steele, L. P., Langenfelds, R. L., Francey, R. J., Barnola, J., & Morgan, V. I. (1996). Natural and anthropogenic changes in atmospheric CO2 over the last 1000 years from air in antarctic ice and firn. *Journal of Geophysical Research: Atmospheres (1984–2012), 101*(D2), 4115-4128.

Faiz, A., Weaver, C. S., & Walsh, M. P. (1996). *Air pollutation from motor vehicles: Standards and technologies for controlling emissions* World Bank-free PDF.

Frey, H. C., Zhai, H., & Rouphail, N. M. (2009). Regional on-road vehicle running emissions modeling and evaluation for conventional and alternative vehicle technologies. *Environmental Science & Technology, 43*(21), 8449-8455. doi:10.1021/es900535s; 10.1021/es900535s

Frey, H. C., & Liu, B. (2014). Development and evaluation of a simplified version of MOVES for coupling with a traffic simulation model. *Proceedings, 91st Annual Meeting of the Transportation Research Board,*

Frey, H. C., Rouphail, N. M., Unal, A., & Colyar, J. D. (2001). No title. *Emissions Reduction through Better Traffic Management: An Empirical Evaluation Based upon on-Road Measurements,*

Frey, H. C., Yazdani-Boroujeni, B., Hu, J., Liu, B., & Jiao, W. (2013). Field measurements of 1996 to 2013 model year light duty gasoline vehicles. Paper presented at the *Proceedings, 106th Annual Conference, Air & Waste Management Association, Chicago, IL,*

Fujita, E. M., Campbell, D. E., Zielinska, B., Chow, J. C., Lindhjem, C. E., DenBleyker, A., . . . Lawson, D. R. (2012). Comparison of the MOVES2010a, MOBILE6. 2, and EMFAC2007 mobile source emission models with on-road traffic tunnel and remote sensing measurements. *Journal of the Air & Waste Management Association, 62*(10), 1134-1149.

Gordon, P., Kumar, A., & Richardson, H. W. (1990). Peak-spreading: How much? *Transportation Research Part A: General, 24*(3), 165-175.

Greene, D. L., & Plotkin, S. E. (2011). Reducing greenhouse gas emission from US transportation. *Arlington: Pew Center on Global Climate Change,*

Gualtieri, G., & Tartaglia, M. (1998). Predicting urban traffic air pollution: A GIS framework. *Transportation Research Part D: Transport and Environment, 3*(5), 329-336.

Health Effects Institute. Panel on the Health Effects of Traffic-Related Air Pollution. (2010). *Traffic-related air pollution: A critical review of the literature on emissions, exposure, and health effects* Health Effects Institute.

Hurdle, V. F., & Son, B. (2000). Road test of a freeway model. *Transportation Research Part A: Policy and Practice, 34*(7), 537-564. doi://dx.doi.org.prox.lib.ncsu.edu/10.1016/S0965-8564(99)00031-2

Jimenez-Palacios, J. L. (1998). *Understanding and quantifying motor vehicle emissions with vehicle specific power and TILDAS remote sensing*

Karppinen, A., Kukkonen, J., Elolähde, T., Konttinen, M., Koskentalo, T., & Rantakrans, E. (2000). A modelling system for predicting urban air pollution: Model description and applications in the helsinki metropolitan area. *Atmospheric Environment, 34*(22), 3723-3733.

Koupal, J., Cumberworth, M., Michaels, H., Beardsley, M., & Brzezinski, D. (2002). Design and implementation of MOVES: EPA‘s new generation mobile source emission model. *Ann Arbor, 1001*, 48105.

Koupal, J., Michaels, H., Cumberworth, M., Bailey, C., & Brzezinski, D. (2002). (2002). EPA's plan for MOVES: A comprehensive mobile source emissions model. Paper presented at the *Proceedings of the 12th CRC on-Road Vehicle Emissions Workshop, San Diego, CA,*

Krzyzanowski, M., Kuna-Dibbert, B., & Schneider, J. (2005). *Health effects of transport-related air pollution* World Health Organization Copenhagen.

Lautso, K., & Toivanen, S. (1999). SPARTACUS system for analyzing urban sustainability. *Transportation Research Record: Journal of the Transportation Research Board, 1670*(1), 35-46.

Ligterink, N. E., & Lange, R. d. (2009). Refined vehicle and driving-behaviour dependencies in the VERSIT emission model. Paper presented at the *ETAPP Symposium*,

Lin, J., Chiu, Y., Vallamsundar, S., & Bai, S. (2011a). Integration of MOVES and dynamic traffic assignment models for fine-grained transportation and air quality analyses. Paper presented at the *Integrated and Sustainable Transportation System (FISTS), 2011 IEEE Forum On*, 176-181.

Lin, J., Chiu, Y., Vallamsundar, S., & Bai, S. (2011b). Integration of MOVES and dynamic traffic assignment models for fine-grained transportation and air quality analyses. Paper presented at the *Integrated and Sustainable Transportation System (FISTS), 2011 IEEE Forum On*, 176-181.

Lomax, T., Turner, S., Shunk, G., Levinson, H. S., Pratt, R. H., Bay, P. N., & Douglas, G. B. (1997). NCHRP report 398: Quantifying congestion. *Transportation Research Board, National Research Council, Washington, DC*,

Mahmassani, H. S., & Liu, Y. (1999). Dynamics of commuting decision behaviour under advanced traveller information systems. *Transportation Research Part C: Emerging Technologies, 7*(2), 91-107.

Meyer, M. D. (1999). Demand management as an element of transportation policy: Using carrots and sticks to influence travel behavior. *Transportation Research Part A: Policy and Practice, 33*(7), 575-599.

Mitchell, G., Namdeo, A., Lockyer, J., & May, A. D. (2002). The impact of road pricing and other strategic road transport initiatives on urban air quality. Paper presented at the *Proceedings of the 8th International Conference on Urban Transport and the Environment in the 21st Century*, 481-490.

Nam, E. K., Brazil, H., & Sutulo, S. (2002) The integration of a fuel rate based modal emissions model (CMEM modified) into the VISSIM microscopic traffic model – inventory comparison with MOBILE6 in southfield michigan. . *Proceedings of the 12th CRC on-Road Vehicle Emissions Workshop,*

Namdeo, A., Mitchell, G., & Dixon, R. (2002). TEMMS: An integrated package for modelling and mapping urban traffic emissions and air quality. *Environmental Modelling & Software, 17*(2), 177-188.

Newell, G. F. (1993). A simplified theory of kinematic waves in highway traffic: (I) general theory; (ii) queuing at freeway bottlenecks; (iii) multi-dimensional flows . *Transportation Research Part B: Methodological, 27*(4), 281-313.

Newell, G. F. (2002). A simplified car-following theory: A lower order model. *Transportation Research Part B: Methodological, 36*(3), 195-205.

Ni, D., Leonard, J. D., & Williams, B. M. (2006). The network kinematic waves model: A simplified approach to network traffic. *Journal of Intelligent Transportation Systems, 10*(1), 1-14.

Noland, R. B., & Quddus, M. A. (2006). Flow improvements and vehicle emissions: Effects of trip generation and emission control technology. *Transportation Research Part D: Transport and Environment, 11*(1), 1-14.

Ntziachristos, L., Samaras, Z., Eggleston, S., Gorissen, N., Hassel, D., & Hickman, A. J. (2000). Copert iii. *Computer Programme to Calculate Emissions from Road Transport, Methodology and Emission Factors (Version 2.1), European Energy Agency (EEA), Copenhagen,*

Oduyemi, K., & Davidson, B. (1998). The impacts of road traffic management on urban air quality. *Science of the Total Environment, 218*(1), 59-66.

Roughgarden, T. (2012). The price of anarchy in games of incomplete information. Paper presented at the *Proceedings of the 13th ACM Conference on Electronic Commerce,* 862-879.

Samaranayake, S., Glaser, S., Holstius, D., Monteil, J., Tracton, K., Seto, E., & Bayen, A. (2014). Real-Time estimation of pollution emissions and dispersion from highway traffic. *Computer-Aided Civil and Infrastructure Engineering, 29*(7), 546-558.

Schrank, D. L., & Lomax, T. J. (2007). *The 2007 urban mobility report* Texas Transportation Institute, Texas A & M University.

Schrank, D., Eisele, B., Lomax, T., & Bak, J. (2015). *2015 urban mobility scorecard*. Texas: Texas A&M Transportation Institute and INRIX, Inc.

Sivak, M., & Schoettle, B. (2012). Eco-driving: Strategic, tactical, and operational decisions of the driver that influence vehicle fuel economy. *Transport Policy, 22*, 96-99.

Sjodin, A., Persson, K., Andreasson, K., Arlander, B., & Galle, B. (1998). On-road emission factors derived from measurements in a traffic tunnel. *International Journal of Vehicle Design, 20*(1), 147-158.

Smit, R. (2006). *An examination of congestion in road traffic emission models and their application to urban road networks*

Song, G., Yu, L., & Zhang, Y. (2012). Applicability of traffic microsimulation models in vehicle emissions estimates. *Transportation Research Record: Journal of the Transportation Research Board, 2270*(1), 132-141.

Stathopoulos, F. G., & Noland, R. B. (2003). Induced travel and emissions from traffic flow improvement projects. *Transportation Research Record: Journal of the Transportation Research Board, 1842*(1), 57-63.

Tanvir, S., Karmakar, N., Rouphail, N. M., & Schroeder, B. J. (2016). Modeling freeway work zones with mesoscopic dynamic traffic simulator: Validation, gaps, and guidance. *Transportation Research Record: Journal of the Transportation Research Board,* (2567), 122-130.

Tonne, C., Beevers, S., Armstrong, B., Kelly, F., & Wilkinson, P. (2008). Air pollution and mortality benefits of the london congestion charge: Spatial and socioeconomic inequalities. *Occupational and Environmental Medicine, 65*(9), 620-627.

Twigg, M. V. (2007). Progress and future challenges in controlling automotive exhaust gas emissions. *Applied Catalysis B: Environmental, 70*(1), 2-15.

USEPA. (2007). *MOBILE 6 vehicle emission modelling software and documentation.* (). Washington, DC: US Environmental Protection Agency.

Vallamsundar, S., & Lin, J. (. (2011). MOVES versus MOBILE. *Transportation Research Record: Journal of the Transportation Research Board, 2233*(1), 27-35.

Xie, Y., Chowdhury, M. A., Bhavsar, P., & Zhou, Y. (2011). An integrated tool for modeling the impact of alternative fueled vehicles on traffic emissions: A case study of greenville, south carolina. Paper presented at the *Transportation Research Board 90th Annual Meeting,* (11-3880)

Yperman, I. (2007). *The link transmission model for dynamic network loading* (Ph.D. Thesis).

Zhai, H., Frey, H. C., Rouphail, N. M., Goncalves, G. A., & Farias, T. L. (2009). Comparison of flexible fuel vehicle and life-cycle fuel consumption and emissions of selected pollutants and greenhouse gases for ethanol 85 versus gasoline. *Journal of the Air & Waste Management Association (1995), 59*(8), 912-924.

Zhang, K., & Batterman, S. A. (2009). Time allocation shifts and pollutant exposure due to traffic congestion: An analysis using the national human activity pattern survey. *Science of the Total Environment, 407*(21), 5493-5500.

Zhou, X., Tanvir, S., Lei, H., Taylor, J., Liu, B., Rouphail, N. M., & Christopher Frey, H. (2015). Integrating a simplified emission estimation model and mesoscopic dynamic traffic simulator to efficiently evaluate emission impacts of traffic management strategies. *Transportation Research Part D: Transport and Environment, 37*, 123-136. doi://dx.doi.org/10.1016/j.trd.2015.04.013

CHAPTER 3

ON GENERATING REALISTIC SYNTHETIC TRAJECTORIES IN MESOSCOPIC SIMULATORS

3.1 Introduction

Integrated transportation simulation and emissions estimation models have enabled a seamless mechanism to answer critical policy relevant questions related to sustainable transportation planning and operations. In particular, integrated mesoscopic traffic simulation and emissions estimation models have added a new dimension to the existing simulation platforms. Agent based mesoscopic traffic simulators can simulate traffic states with sufficient accuracy and within limited computational resources for dynamic supply and demand conditions in a large-scale network. Until recently, traffic state outputs from macroscopic and mesoscopic models such as link average speed and link traffic volume were used to estimate fuel consumption and emissions. In 2015, researchers at Arizona State University and North Carolina State University (Zhou et al., 2015) proposed an integrated mesoscopic traffic simulator and emissions estimator based on synthetic trajectories derived from simulated mesoscopic traffic states. This simplified trajectory generator provides synthetic trajectories which are similar to the high temporal resolution (=> 1 Hz) trajectories generated in microscopic traffic simulators. However, the synthetic trajectories have some unrealistic features such as high levels of acceleration and deceleration, and lack of speed variation, among others. The effect and methods to correct these unrealistic features is not properly understood. Moreover, the suitability of existing fuel use-emissions estimation models in regards to the synthetic trajectories were not studied before.

This chapter is organized to review existing literature to identify the research needs, to describe a methodology to address the gaps, and to discuss the results.

3.1.1 Simulation of vehicle activity in mesoscopic traffic simulators

Mesoscopic traffic simulators are inherently different from microscopic simulators in the way they generate vehicle activity information within the links of a network. In microscopic simulation individual vehicle activities are modeled and network or corridor performances arise from the complex interaction rules among the vehicles. On the other hand, mesoscopic simulators generate link mobility performance first and then reconstructs individual vehicle activity within each link (Figure 3.1). Therefore, microscopic simulators can handle relatively small number of vehicles in a smaller network covering a narrower time period compared to mesoscopic simulators.

DTALite is a lightweight mesoscopic traffic model that can simulate the dynamic interaction of vehicular travel demand and time dependent road condition (Zhou, Taylor, & Pratico, 2014). Therefore, it is an appropriate traffic simulation tool to capture the effect of traffic management strategies at a fine spatial and temporal resolution, while providing faster model run time. The method of generating link-based mesoscopic simulation outputs is described in section 2.3. To accommodate integration of microscopic emissions model into DTALite framework link-based simulation results are post processed to generate second-by-second detailed vehicle trajectories based on a simple linear car-following model (LCF).

3.1.2 Benefits of simplified trajectory generation

A simplified trajectory generation procedure used inside a dynamic mesoscopic simulator is essentially a microsimulation post processor. The trajectory generation submodule uses the outputs of the link performance generation submodule and provide detailed vehicle activity

with reasonable accuracy and computational time. The simplest of the trajectory reconstruction algorithms are car-following models. Car following models use a small set of parameters and a simple set of interaction rules between the leader and follower vehicles. The simplest of the car following models is the Newell model (Newell, 2002). It requires two parameters in congestion: the wave speed *w* and the jam spacing *s* (Figure 3.1).

The position $x_j(t + \Delta t)$ of vehicle *j* at time $t + \Delta t$ can be derived from its position $x_j(t)$ and that of its leader $x_{j-1}(t)$ at time t:

$$x_j(t + \Delta t) = \left(1 - \alpha_j\right)x_j(t) + \alpha_j x_{j-1}(t) - w_j \Delta t \qquad \text{with } \alpha_j = w_j s_j \Delta \leq t$$

The Newell model was proven to be equivalent to macroscopic LWR model (Lighthill & Whitham, 1955). The calibration of Newell mode is performed for each vehicle pair to find out the optimal values of w_j, s_j for all vehicles.

The problem with the use of microsimulation to derive driving cycles is that the whole approach must be validated, but at present, the accuracy of the trajectories drawn from the model remains untested for such an application. Simplified driving cycles classically provided by traffic simulators introduce bias when calculating fuel consumption and emissions. Fortunately, such errors remain relatively low for a given cycle and vanish when multiple cycles are aggregatd to determine the fuel consumption or emissions.

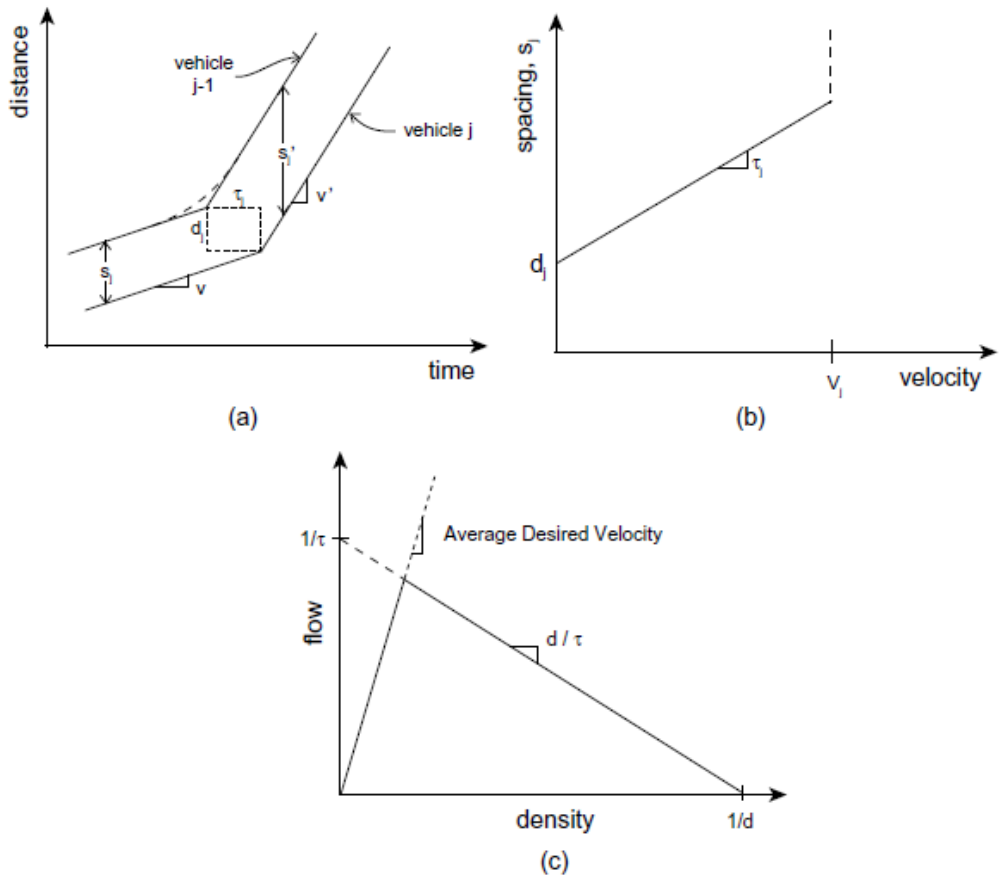

Figure 3.1. (a) Piecewise linear vehicle trajectories (adopted from (Newell, 2002)), (b) relationship between velocity and spacing for an individual driver, (c) density-flow curve for Newell's theory comparable to macroscopic LWR fundamental diagram.

3.1.3 Limitations of simplified trajectory generation

In DTALite, emissions are estimated in the post-processing stage after trajectories are simulated using Newell's car-following model. The accuracy of estimated emissions is, therefore, dependent on the accuracy of simulated vehicle activities. To be more specific, the VSP-based (Jimenez-Palacios, 1998) emissions calculations are derived from two major vehicle activity parameters: speed and acceleration. The limitations of Newell's car following theory in describing traffic with heavy lane changing and geometric inhomogeneity have been studied earlier (Ahn, Cassidy, & Laval, 2004). It is possible to construct vehicle trajectories that theoretically represent the underlying traffic dynamics,

especially backward wave propagation using Newell's car following model. A recent paper compared simulated trajectories from Newell's car following model with real-world trajectories and concluded that Newell's model provide more accurate emissions prediction for a stream of traffic than Gipps' model (da Rocha et al., 2015).

However, there are two major limitations of the model. The first of these limitations is unrealistic acceleration at the transition points (Figure 3.2). For example, the very first vehicle loaded onto a link can experience speed changes from zero to the free-flow speed of the link within a second. The second limitation is the lack of speed variation in the trajectories when the vehicle reaches a constant desired speed.

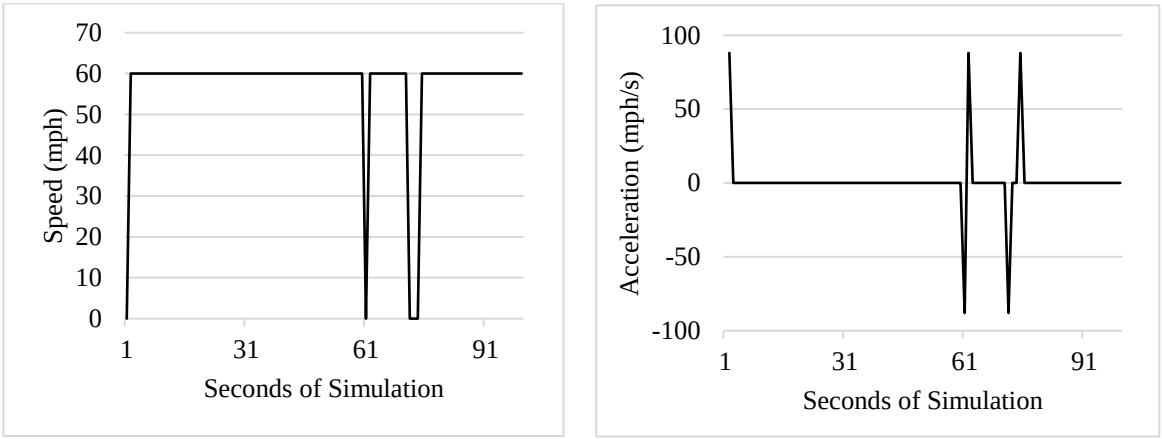

(a) (b)

Figure 3.2. Simulated trajectory for a single vehicle in DTALite (a) speed (b) acceleration

In field-measured trajectories, we can observe speed fluctuations even when the operating condition of the roadway does not change (Figure 3.3, Figure 3.4). The model estimates zero acceleration at these conditions where there are small accelerations present.

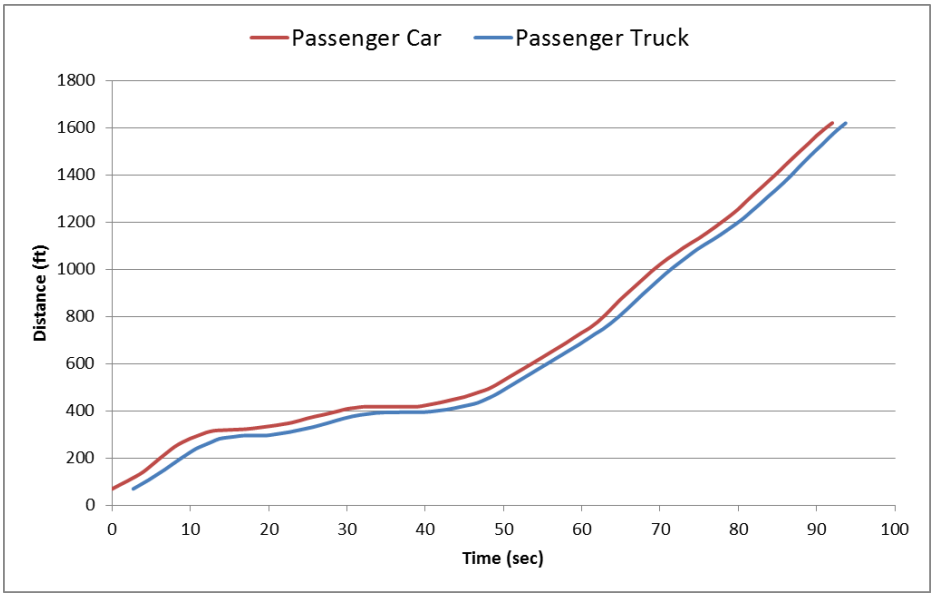

Figure 3.3. Real world vehicle trajectories from Next Generation Simulation (NGSIM) data (FHWA, 2015)

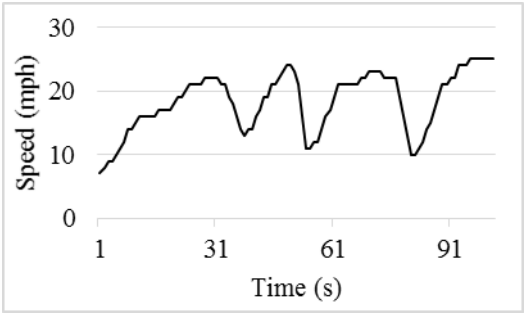

(a) Speed of Passenger Car

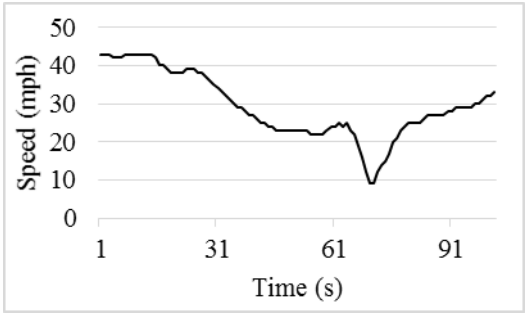

(b) Speed of Passenger Truck

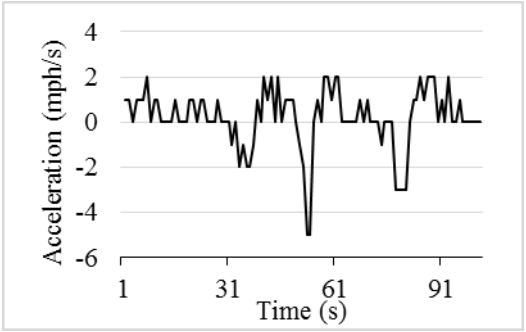

(c) Accleration of Passenger Car

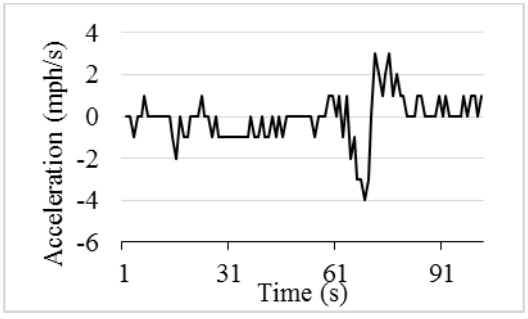

(d) Acceleration of Passenger Truck

Figure 3.4. Speed and accelerations for real-world trajectories

In addition, Newell's model ignores driver specific (inter-driver) and time-varying (intra-driver) heterogeneity in generating trajectories. Intra-driver variability accounts for a significant proportion of deviations between simulated and empirical trajectories (Kesting & Treiber, 2009). The enhanced Dynamic Time Warping (DTW) algorithm was used for calibrating synthetic trajectories from Newell's car following model that can reflect intra-driver heterogeneity (Taylor, Zhou, Rouphail, & Porter, 2015). Similar methods along with clustering have been used successfully to generate link driving schedules compatible for use with MOVES2010 (Aziz & Ukkusuri, 2015). Although limitations are present in the constructed trajectories by Newell's car following model, this simplified model holds the potential to provide a theoretically consistent and computationally efficient way to bridge the data requirements between the macroscopic traffic model and the microscopic emission estimation model.

In the light of benefits and limitations of the simplified trajectory generation process, the rest chapter is organized according to Figure 3.5

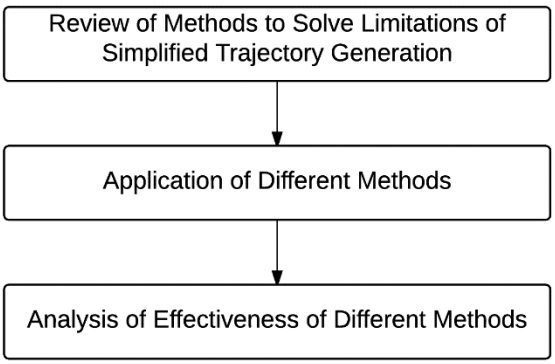

Figure 3.5. Adopted approach to solve the limitations of simplified trajectory generation

3.1.4 Solving limitations of simplified trajectory generation

The challenge of reconstructing close-to-reality vehicle trajectories from simplified simulated trajectories to provide robust emissions estimation is still open. Significant effort have been expended in trajectory reconstruction from empirical observation due to the fact that empirical trajectory extraction process is noisy in nature (Montanino & Punzo, 2015). Previous analyses showed that errors in microscopic measurements affect calibration results (to a limited extent) in the car-following model. These results, though significant, do not clarify what the impact of a calibration error on the results of a traffic simulation is. In the same way as real traffic results from the stochastic interaction of heterogeneous vehicles, traffic micro-simulation outputs are the result of the unpredictable concatenation of events simulated by the individual driver models. Therefore, performances of such models calibrated against disaggregate data are not informative on the performances of such models when they interact in a traffic simulation environment.

In order to compare observed and simulated traffic, a ‘‘trace-driven’’ simulation approach is necessary, also refereed as ‘‘correlated-inspection’’ simulation (Kleijnen, Cheng, & Bettonvil, 2000). It is grounded on the principle that the comparison of outputs from real and simulated systems is reliable only if both systems are observed under similar conditions. The rigorous condition to strictly satisfy this principle is the measurability of all inputs and outputs of the real system. In this case, measured inputs can be fed into the model in the same historical order as in the real system. Hence, simulated and measured outputs can be fairly compared as resulting from the same (measured) inputs.

The trace-driven simulation approach is relatively new in the literature of microscopic simulation validation. The problem is accentuated by the lack of empirical observations.

Even though the calibration is performed correctly to estimate the car following model parameters, unrealistic simulation outputs are inevitable as mentioned in the previous section. The usual response to correct these inconsistencies is applying filtering or smoothing on the simulated output or applying additional constraints (similar to adding new parameters) in the car-following model. It is to be noted that, choice of a simplified microsimulation model was derived from the need of a sufficiently accurate but fast approach to simulate vehicle activity. Thus, application of additional elaborate steps to correct simplified trajectories goes against the merit of the procedure.

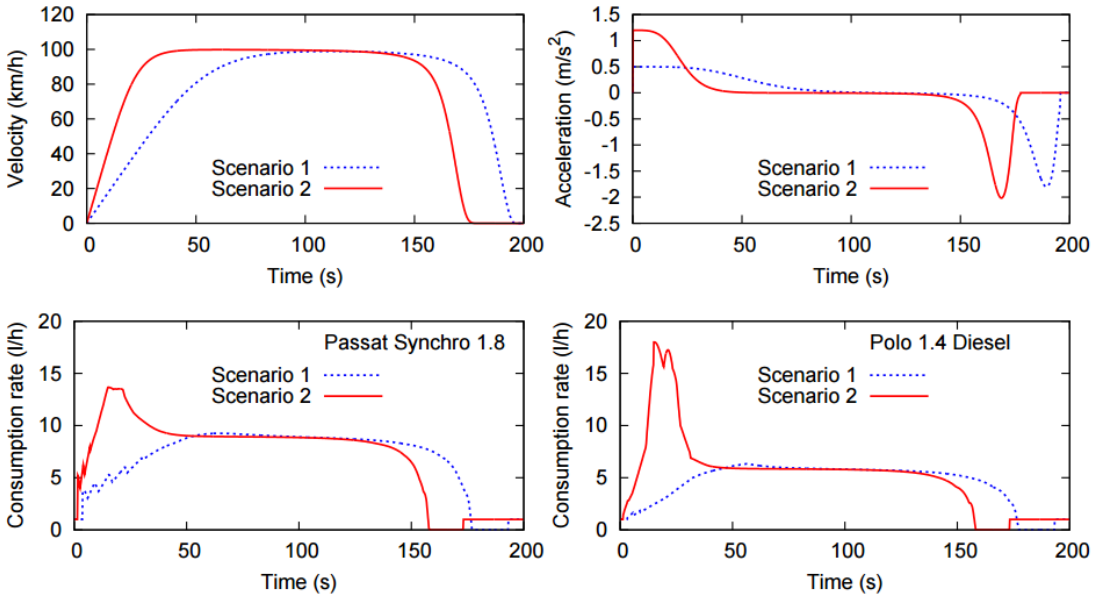

Figure 3.6. Sensitivity of fuel consumption due to application of different maximum acceleration constraint (Treiber, Kesting, & Thiemann, 2008)

The problem of unreasonable acceleration and deceleration is solved sometimes using pre-specified limits of acceleration for each defined speed range. That means the simulated trajectory of the vehicle is adjusted to follow a series of reasonable acceleration profiles to complete the acceleration and deceleration process. A simple sensitivity analysis varying the

maximum acceleration parameter from 0.5 m/s^2 (blue dotted line) to 1.2 m/s^2 (solid red line) using Intelligent Driver Model (IDM) is shown in Figure 3.6 (Treiber et al., 2008).

The enveloping of speed-acceleration removes outliers or unreasonable data points. This leads to the second limitation of simulated trajectories – lack of speed variation. In the constructed speed acceleration envelope the majority of the data points either lie on a horizontal line (constant speed with no acceleration) or at the envelope. However, there is significant variation inside the envelope in real world driving cycles that represents different levels of fuel consumption and emissions. Figure 3.7 shows instantaneous consumption (liters per 100 km) for different velocity acceleration ranges. This problem can be solved by adding random disturbances to the seemingly homogenous speed profiles or matching micro-trips for different episodes of vehicle activity (idling, cruising, acceleration, and deceleration). Although this approach was never implemented before in literature, micro-trip matching based trajectory reconstruction was suggested in a recent publication (Zhou et al., 2015). However, micro-trip matching would be an elaborate approach and will act as a hindrance to real time implementation of a traffic simulation model.

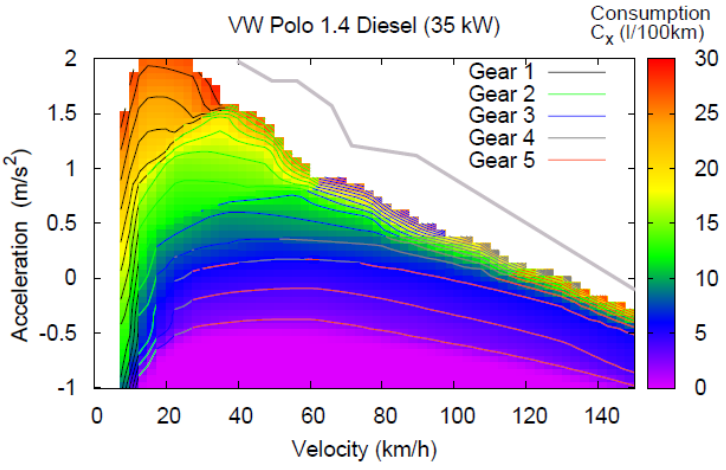

Figure 3.7. Instantaneous fuel consumption for VW Polo 1.4 Diesel at different speed-acceleration levels (Treiber et al., 2008)

3.1.5 Speed of trajectory generation process

The trajectory generation process is a post-processing step of mesoscopic traffic simulation. Accumulation of detailed vehicle activity information and consequent filtering or enhancement procedure for all the vehicles in the network is an elaborate process. In order to use simulation as a medium for observation of system inefficiency and efficiency gained through control measures, simulation should be performed at a near real time level. Therefore, adding all the various mitigation approaches mentioned in the earlier section should be applied in consideration of their speed of performance.

Several previous studies used clustering techniques to produce representative trajectories for a link: K-means clustering with Euclidian distance was used in one such study (Chamberlin, Swanson, Talbot, Dumont, & Pesci, 2011a) and hierarchical clustering based dynamic time warping based similarity distance was used in another (Aziz & Ukkusuri, 2015). Representative trajectories essentially arise from similar input levels in the trajectory generation procedure regarding link and vehicular parameters. Therefore, it is logical to assume that a set of unique input parameters can produce similar driving cycles.

3.1.6 Simulated trajectory post-processing methods

Post-processing of simulated trajectories from simplified trajectory generators is needed to generate more realistic trajectories. There are two post-processing options for the simulated trajectories in existing implementation of DTALite: unweighted moving average of space-time trajectories with fixed parameters, and control of excessive acceleration and deceleration using a speed acceleration envelope.

Unweighted moving average method

The current application of DTALite uses the simplest moving average (Hyndman & Athanasopoulos, 2014) of simulated trajectories in the space time domain with a fixed window or filter width. The moving average can be mathematically represented as a technique to smooth an array of raw (noisy) data [y_1, y_2, ……, y_n]. The "smoothed point" (y_k)s is the average of an odd number of consecutive 2n+1 (n = 1, 2, 3, …) points of the raw data y_{k-n}, y_{k-n+1},…., y_{k-1}, y_k, ….., y_{k+n-1}, y_{k+n} , i.e.

$$(y_k)_s = \sum_{i=-n}^{n} y_{k+1}/(2n+1)$$

The odd number 2n+1 is usually named the filter width or the window width. The greater the filter width the more intense is the smoothing effect.

Speed-acceleration envelope

This method is only available for application on a sample of vehicles in DTALite due to the high computational burden. The problem of undesirable high acceleration and deceleration can be tackled by adding boundary conditions at different speed levels. Boundary conditions can be found from extracting certain percentile values from empirical observations. In a previous study (Frey, Yazdani-Boroujeni, Hu, Liu, & Jiao, 2013) real-world vehicle activity data for 100 light duty vehicles were used to obtain the joint distribution of speed and acceleration. DTALite implemented a 95th percentile envelope for bounding acceleration and 5th percentile envelope for bounding deceleration at discretized levels of speeds (Liu & Frey, 2015).

Table 3.1. Speed-acceleration envelope from empirical observation (Liu & Frey, 2015)

Speed Range (mph)	**Acceleration (95th Percentile) (mph/s)**	**Deceleration (5th Percentile) (mph/s)**
0-1	0.6	-2
1-5	2.4	-3.7
5-10	5.6	-5.1
10-20	5	-4.5
20-30	3.6	-3.7
30-40	2.7	-2.9
40-50	1.7	-1.6
50-60	1	-1
60-70	1	-1
70 +	1	-1

The relationship in Table 3.1 can be utilized to remove outlier accelerations and decelerations using the following algorithm.

IF $a_t > \hat{a}_t(v_{t-1})$

INITIALIZE n = 1

WHILE $v_{t-n} > \hat{v}_{t-n}$ AND $v_{t-n} > 0$

DO $v_{t-n} = v_{t-n+1} - \hat{a}_t(v_{t-n})$

$n = n + 1$

To illustrate the algorithm for n = 1,

v_{t-1} = speed at time *t-1*

v_t = speed at time *t*

a_t = $v_t - v_{t-1}$ =acceleration at time *t*

$\hat{a}_t(v_{t-1})$ = maximum acceleration at time *t-1* with speed v_{t-1}

$\hat{v}_{t-1}$ = $v_t - \hat{a}_t(v_{t-1})$= Minimum possible speed at time (t-1)

3.1.7 Problems arising from post-processing trajectories

Although post-processing may improve some features of the synthetic trajectory, some other features and information may be lost if it is not done carefully. Some of the problems of post-processing are described in the following paragraphs.

Amplitude and frequency of peaks modified

Perhaps this is the most impactful among all the problems discussed before. Selection of an inappropriate post-processing method may significantly reduce the useful information contained inside the raw simulated trajectories.

First in first out (FIFO) violation

As post-processing methods are not included in the trajectory generation procedure, filters are almost always applied on individual trajectories without respecting the context of physical leader-follower relationship. Therefore, in some cases a follower may cross its leader and thus violates the inputs provided from the mesoscopic link performance generator module.

Unequal total distance traveled

Some post processing protocols skew the spatial stretch of vehicle activity time series to maintain their temporal stretch. This causes unequal distance traveled by a group of vehicles traveling over the same link. This inconsistency may lead to erroneous estimation of fuel use and emissions especially if instantaneous vehicle activity information is used.

3.1.8 Fuel use-emissions estimation models for simulated trajectories

Simulated driving activity is supplied to the fuel use-emissions estimation models. These estimation models are based on the relationship between externally observed driving activity and simultaneously measured fuel use-emissions. It is resource intensive to collect high resolution externally observed variables (EOV) such as speed and acceleration. Additionally,

filtering out measurement errors and noises is a theoretically and computationally challenging process. Therefore, widely used emission factor models such as MOBILE6 (National Research Council, 2000) and COPERT (Cloke et al., 1998) utilized low spatial and temporal resolution aggregated driving activity and fuel use-emissions data. Another accepted method is to stratify empirical data in defined modes based on estimated vehicle specific power or operating modes (Frey, Unal, Chen, Li, & Xuan, 2002). Modal based approaches provide averaged estimations of fuel use-emissions, therefore, do not utilize the full potential of a high-resolution simulated trajectory. In contrast, physically and statistically based fuel use-emissions estimators developed with high-resolution observed data suffers from autocorrelation among the temporally neighboring observations (Frey, Zhang, & Rouphail, 2010). To reduce the bias of autocorrelation and previously mentioned measurement noises, moving average post-processing is conducted on both time series of driving activity and fuel use-emissions. If a model is developed using post-processed (averaged) data, then the inputs for the model in the implementation phase is required to be post-processed similarly. The reason for post-processing of simulated trajectories as described earlier in this chapter is different from the reason for post-processing empirical data. Therefore, it is important to understand which fuel use-emissions estimation model is more applicable for the simulated trajectories post-processed in a certain manner.

One particular inconsistency in post-processed simulated trajectories is the reduction in amplitude and frequency of peaks in raw simulated trajectories. Alternative post-processing methods can be employed to preserve the peaks. However, these methods may overlook some undesired features of the simulated trajectory. Therefore, it is critical to

understand how important it is to preserve the peaks in simulated driving activity compared to the other irregularities.

3.2 Research Questions

The research described in this chapter addressed three key research questions as identified in the previous section:

a. Which post-processing method is most suitable for simulated trajectories derived from simplified trajectory generators in a mesoscopic simulation environment?
b. How to select parameters for different post-processing methods to realistically represent driving activity?
c. Are the existing externally observable variables (EOV) based fuel use estimation models suitable for high resolution synthetic trajectories?

3.3 Methodology

The issue of deriving vehicle position trajectories from DTA output is not trivial and prone to significant discretization errors. In the light of discussions regarding the limitations of the simplified trajectory generation procedure, it is important to know whether the amplitude and frequency of simulated acceleration/ deceleration is supported by empirical evidence. In this research, attempts will be made to compare the simulated activity information with the empirically observed one. Also, we will verify the extent of post processing that can be done on the simulated trajectories without significantly altering the parameters responsible (operating mode distribution) for emissions generation. The methodological flow for this work is depicted in Figure 3.8.

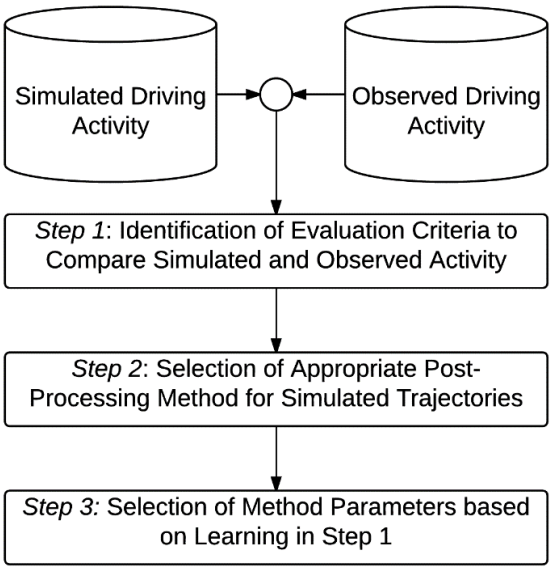

Figure 3.8. Methodology to select post-processing methods and parameters for synthetic trajectories generated from mesoscopic traffic simulation

The methods in this research included a selection of study locations to extract similar empirical trajectories as the simulated trajectories, setting up an integrated simulation, optimization, an evaluation platform for different post-processing methods, and the development of evaluation criteria for the post-processed trajectories with different fuel use estimation models.

The existing simplified trajectory generation method in DTALite is described in chapter 2. The method assumes that simplified trajectory generation procedure by Newell (Newell, 2002) is adequate in representing 'true' vehicle activity dynamics and kinematics. Therefore, the objectives of post-processing are to reduce inconsistencies in simplified trajectory generation procedure and enhance the realistic explanatory power of simulated vehicle activity in explaining fuel use and emissions. One way to verify that post-processed trajectories are realistic is by examining their operating mode distributions as defined in the

EPA MOVES model (Chamberlin, Swanson, Talbot, Dumont, & Pesci, 2011b). The definition of operating modes as adopted in EPA MOVES model is given in Table 3.2.

The fraction of time a vehicle spends in each operating modes of its driving cycle determines the characteristics of that cycle. However, the characteristics vary by the road facility being traveled such as freeways, arterials, local roads; operating conditions of the road such as free-flowing or congested. Therefore, calibrating parameters for post-processing methods can be conceived as an optimization problem where the objective function would be to minimize gap between the fraction of time in each operating mode bins in simulated trajectories and the ones in empirically observed trajectories. Empirically observed operating mode distributions can be classified into several road facility and operating conditions classes as shown in Table 3.3.

Table 3.2. Definition of Operating Modes in EPA MOVES (EPA, 2009)

0 mph< v_i ≤25 mph		**25 mph < v_i ≤50 mph**		**v_i >50 mph**	
OpMode ID	Description	OpMode ID	Description	OpMode ID	Description
11	VSP< 0	21	VSP< 0		
12	0≤VSP< 3	22	0≤VSP< 3		
13	3≤VSP< 6	23	3≤VSP< 6	33	VSP< 6
14	6≤VSP< 9	24	6≤VSP< 9	35	6≤VSP<12
15	9≤VSP<12	25	9≤VSP<12		
16	12≤VSP	27	12≤VSP<18	37	12≤VSP<18
Other:		28	18≤VSP<24	38	18≤VSP<24
0	Braking	29	24≤VSP<30	39	24≤VSP<30
1	Idling	30	30≤VSP	40	30≤VSP

Here v_i refers to instantaneous speed at time i

Table 3.3. Conceptual classes of distinct operating mode distributions[1]

Classes	Freeways	Local Roads
Uncongested	FFS[2] ↑ Average Speed / FFS ↑	FFS ↓ Average Speed / FFS ↑
Congested	FFS ↑ Average Speed / FFS ↓	FFS ↓ Average Speed / FFS ↓

3.3.1 Selection of study locations for empirical trajectories

The technology for collection, storage, and transmission of the empirical vehicle trajectories is discussed in Chapter 4. Six segments on local arterial streets and five segments on freeways were selected for collection of observed vehicle trajectories. All the arterial street segments were in the midblock between two intersections and all the selected freeway segment were outside of the ramp influence area. Segments were selected in a way that maximizes the ability to observe more trajectories in various operating conditions. Also, the arterial segments had posted speed of 45 mph and freeway segments had posted speed of 65 mph. A detailed description of the segments is provided in Table 3.4.

[1] ↑ means high, ↓ means low
[2] FFS is an abbreviated form of Free Flow Speed

Table 3.4. Description of Study Locations for Collection of Observed Driving Activity

Section Type (Posted Speed)	Location	Start Coordinate	End Coordinate	Length (meter)	Number of Lanes	Estimated Capacity[3] (vph/lane)
Arterial (45 mph)	Avent Ferry Rd. (EB)	35.769824, -78.689841	35.771996, -78.685552	460	2	1600
	Avent Ferry Rd. (WB)	35.771996, -78.685552	35.769824, -78.689841	460	2	1600
	Glenwood Ave. (WB)	35.813591, -78.651551	35.815463, -78.653425	270	2	1600
	Glenwood Ave. (EB)	35.815463, -78.653425	35.813591, -78.651551	270	2	1600
	Tryon Rd. (EB)	35.749737, -78.710901	35.749830, -78.708451	220	2	1600
	Tryon Rd. (WB)	35.749830, -78.708451	35.749737, -78.710901	220	2	1600
Freeway (65 mph)	I-540 (E)	35.894770, -78.802211	35.895281, -78.792327	890	4	2100
	I-440 (E)	35.773342, -78.716958	35.776467, -78.710204	700	2	2100
	I-440 (W)	35.776467, -78.710204	35.773342, -78.716958	700	2	2100
	I-40 (E)	35.752668, -78.629939	35.753609, -78.622152	710	3	2100
	I-40 (W)	35.753609, -78.622152	35.752668, -78.629939	710	3	2100

3.3.2 Extraction and processing empirical trajectories

The observed trajectories were extracted from a database using a process called ‘Geo-fencing’ where the microscale trip database is superimposed on a street network shapefile in ArcGIS and a buffer zone is created using the segment start and end coordinates. Trips which have a previous instance within the starting buffer and a later instance within the ending buffer are considered traveling on the segment. The last step of the extraction process involves querying the trip database for all the seconds between the two instances.

[3] Based on HCM

Extracted trajectories are categorized in three bins according to the 'speed ratio'. Speed ratio is used as an indicator for operating condition of the segment. The definition of speed ratio and operating condition bins was as follows.

Speed-ratio, $\rho = \frac{\bar{v}}{v_f}$

If $0.7 \geq \rho > 0.5$, Operating condition bin = 1 (Congested)

If $0.9 \geq \rho > 0.7$, Operating condition bin = 2 (Average)

If $1.1 \geq \rho > 0.9$, Operating condition bin = 3 (Uncongested)

Here,

$\bar{v} = \frac{Segment\ Length}{Segment\ Travel\ Time}$ = average travel speed on the segment

v_f = Posted speed limit or free-flow speed of the segment

3.3.3 Simulation configuration

It was inefficient to test different post-processing methods and parameters in the existing visual C++ based DTALite framework. The existing framework lacked readily available statistical packages and an interactive graphical user interface. A separate implementation in statistical programming software R was developed to overcome these problems. Although R does not have dynamic memory allocation and parallel processing capabilities, the added usability and functionality makes it a better platform to perform a wide range of post-processing experiments. As shown in Figure 3.9, the finalized version of post-processing method can be implemented back into DTALite.

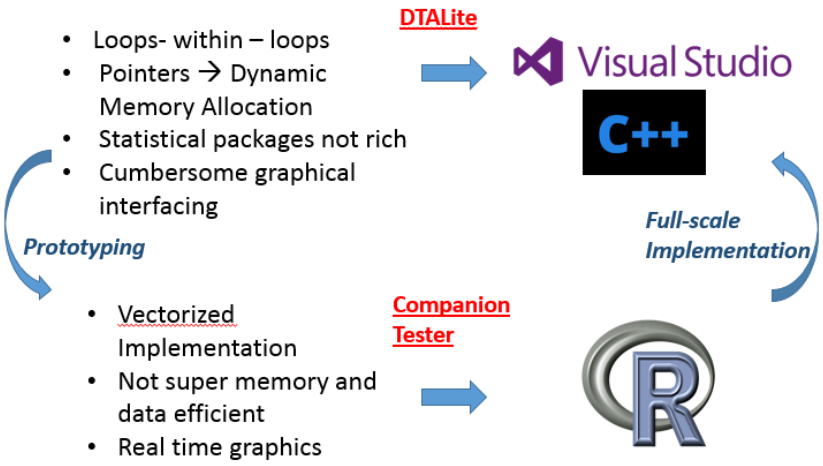

Figure 3.9. Prototyping of DTALite trajectory post-processing codes in R

The prototype includes three different modules which are integrated in a single framework for efficient evaluation of different facility types and operating conditions. The modules are-

a. Mesoscopic simulation module
b. Synthetic trajectory generation module
c. Post-processing module
d. Fuel use-emissions estimation module

The mesoscopic simulation module generates link arrival and departure times for each vehicle agents based on the entry flow rate. The entry flow rate is estimated from the Highway Capacity Manual (TRB, 2016) for the segment being modeled for a specific speed ratio, ρ. To effectively simulate the operating conditions of the segment, a corridor with multiple segments and varying downstream capacity was simulated.

The trajectory generation module uses the generated link arrival and departure times to calculate high resolution (10 Hz) space-time locations of each vehicle agents within the simulated segment. The post-processing module applies different post-processing methods on

the simulated trajectories. Finally, the fuel use-emissions estimation module calculates the vehicle specific power (VSP) for the trajectories and generates the operating mode bin distributions.

3.3.4 Synthetic trajectory post-processing methods

Post-processing methods can be classified in two broad categories – a) conventional signal smoothing algorithms, b) outlier removal and reconstruction based on some heuristics.

Signal smoothing

Unweighted moving average implemented as the default to post-process simulated trajectories is a form of signal smoothing. The results of this technique is deceptively impressive because it yields excessive filtering. The pre-existing information is lost or distorted because too much statistical weight is assigned to data points that are away from the central point.

The moving average method produces more erratic results when the peaks are narrower compared to the filter width. However, if the spike removal is of interest then a median filter is more desirable than a mean or average filter. The median method can result in the attenuation of peaks to a great extent. Therefore, if the spike / peak is of interest then a modification of analysis may be necessary.

Savitzky- Golay Algorithm (Savitzky & Golay, 1964)

This is the more generalized form of the simple moving average algorithm. A set of integers (A_{-n}, $A_{-(n-1)}$, ….., A_{n-1}, A_n) can be derived and used as the weighing coefficients to perform smoothing. These integers are known as “Convolution Integers”; makes the smoothing of points fitted as polynomials. The method can be given by the following equation:

$$(y_k)_s = \frac{\sum_{i=-n}^{n} A_i y_{k+i}}{\sum_{i=-n}^{n} A_i}$$

The advantage of this smoothing is that it is faster than other complex smoothing methods and is more effective in preserving features of a signal.

Lowess Smoothing (Cleveland, 1981)

This method applies weighted linear regression to fit data in the form of a second order quadratic polynomial. The regression weights are computed using the tricube function.

$$w_i = \left(1 - \left|\frac{y - y_i}{d(y)}\right|^3\right)^3$$

Where, w_i is regression weight, y is the value of interest, y_i is the value of nearest neighbors, d(y) is the distance of y from the furthest value in filter width.

The advantage of Loess smoothing is that it is very flexible. But calculating weights for each data point and applying smoothing overall is a computationally intensive process.

Micro-trip based trajectory reconstruction

The single speed-acceleration envelope may cause positioning of data points along the envelope border and the absence of data points in the central portion of joint distribution. This phenomenon occurs because speed-acceleration enveloping constrains high levels of acceleration or deceleration events to a fixed maximum or minimum, respectively.

Micro-trip based trajectory reconstruction approach involves adding noise to the simulated trajectories based on speed-levels and vehicle activity episode categories. Speed-levels can be discretized similar to the bins described in earlier section. The vehicle activity episodes can be characterized in four driving modes based upon time-averaged speed and acceleration as indicated in Table 3.5.

Table 3.5. Vehicle activity episodes determined from time-averaged simulated trajectories

Driving Mode	**Definition**
Idle	Speed =0 & Acceleration = 0
Acceleration	Speed > 0 & Acceleration ≥ 2 mph/s
Deceleration	Speed > 0 & Acceleration ≤ -2 mph/s
Cruise	Other situations than the above defined

Different amplitude and frequencies of noise (either white or Gaussian) can be added to different levels of speed- vehicle activity episodes to obtain realistic properties of simulated speeds. There may be other signal modulating or modification algorithms suitable for this purpose which will be explored in the later part of this research.

3.3.5 Selection of post-processing method and parameters

The root mean square error (RMSE) is used as an indicator of difference between simulated and observed trajectories. Different post-processing method and parameter combination were tried in the optimization module added in the previously described simulation platform. The RMSE is calculated using the following equation.

$$RMSE_{S,O} = \sqrt{\frac{\sum_{i=1}^{40}\left(f_{S,i} - f_{O,i}\right)^2}{n}} \times 100\%$$

Here,

S = Simulated trajectory

O = Observed trajectory

$RMSE_{S,O}$ = RSME of the operating mode bin distributions between S and O

$f_{S,i}$ = fraction of time in i^{th} operating mode bin in simulated trajectory

$f_{O,i}$ = fraction of time in i^{th} operating mode bin in observed trajectory

n = number of operating mode bins = 23

The optimization problem to specify the parameters of the post-processing method can be stated as follows.

SELECT parameter, $K\{k_1, k_2, \ldots, k_z\}$ for each condition, j for method, m

Objective function: min $\sum_{i=1}^{40}(f_{ijs} - f_{ijo})^2$

where,

i = 1, …….., 40 = Operating mode bin number

j = 1, 2, ……, n = Classes of road type (freeways and arterials) and operating conditions (congested, average, and uncongested)

f_{ijs}= fraction of time in operating mode bin i for representative ***simulated*** cycle / set of cycles in condition j.

f_{ijo}= fraction of time in operating mode bin i for representative ***real-world*** cycle / set of cycles in condition j.

Representative cycle from either simulation or real world at different conditions can be selected by random drawing because an averaging will destroy features in either of these trajectories. Then the optimization problem becomes stochastic in nature.

3.4 Results

Results are presented for (a) operating mode distribution for observed trajectories; (b) outputs from the mesoscopic simulation module of the prototype; (c) synthetic trajectories generated from different post-processing methods; (d) optimized parameters for post-processing methods; (e) fuel use estimations for the synthetic trajectories.

3.4.1 Operating mode distributions of empirical trajectories

The operating mode distributions of observed trajectories for freeways in different operating conditions is shown in Figure 3.10. Similar operating mode distributions are shown in Figure 3.11. The bars heights are the mean fraction of time in each of the operating mode bins and error bars represent 95% confidence interval.

The sample size was smaller under congested operating conditions ($0.7 \geq \rho > 0.5$) for both freeways and arterials compared to the sample sizes in average and uncongested conditions. In addition, more variability in the driving activity was observed under congested conditions.

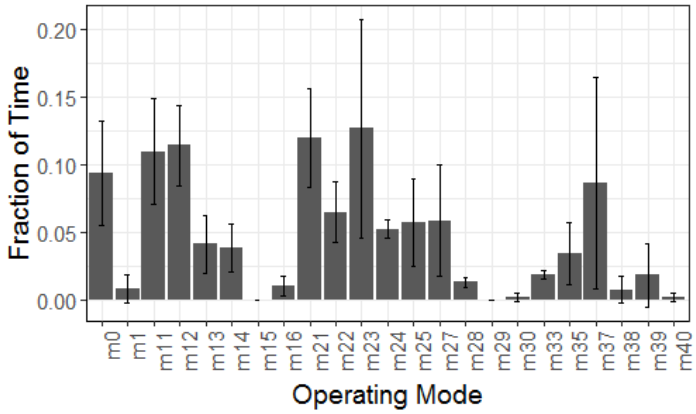

(a) Freeways (v_f = 65 mph); $0.7 \geq \rho > 0.5$; n= 17

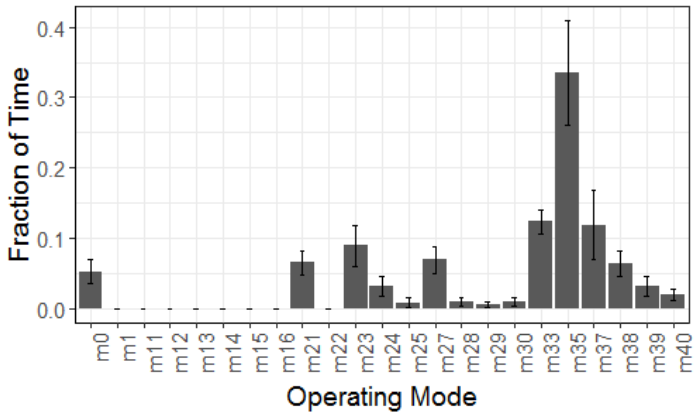

(b) Freeways (v_f = 65 mph); $0.9 \geq \rho > 0.7$; n= 97

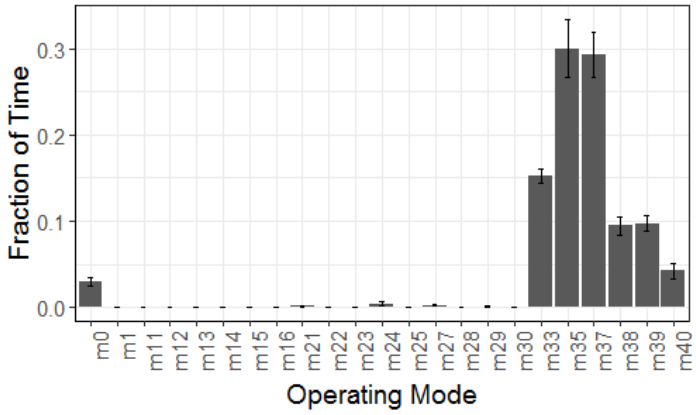

(c) Freeways (FFS = v_f mph); $1.1 \geq \rho > 0.9$; n = 133

Figure 3.10. Operating mode distribution of empirical trajectories for freeways under different operating conditions. The error bars represent 95% confidence interval. ρ = speed-ratio. n = number of extracted trajectories to draw the distribution. v_f = posted speed.

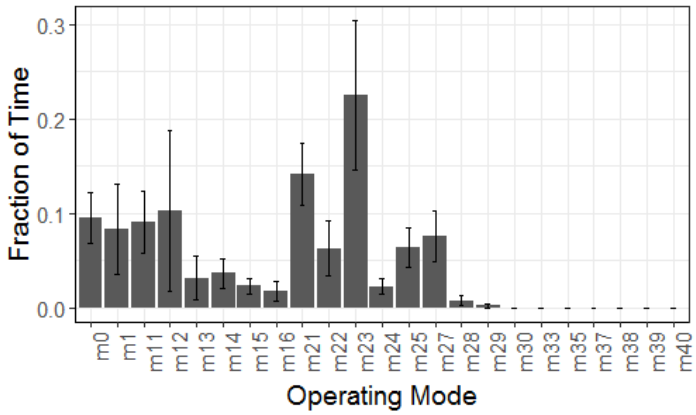

(a) Arterials (v_f = 45 mph); $0.7 \geq \rho > 0.5$; n= 96

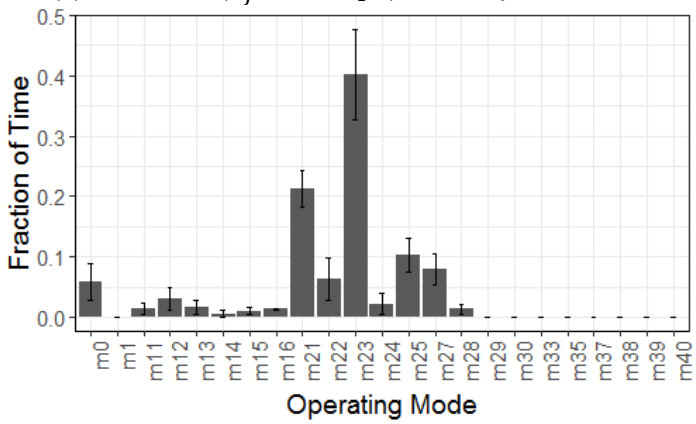

(b) Arterials (v_f = 45 mph); $0.9 \geq \rho > 0.7$; n= 212

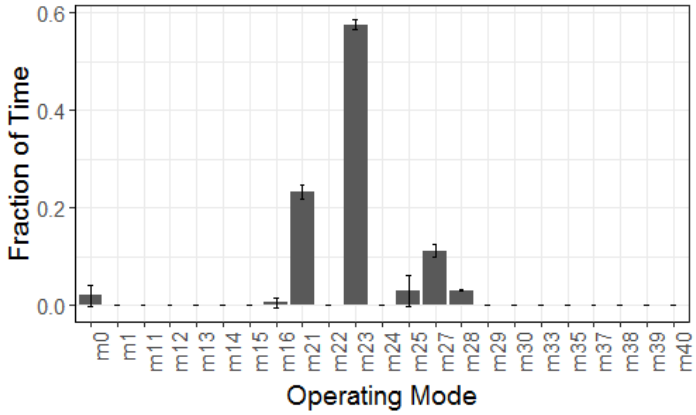

(c) Arterials (v_f = 45 mph); $1.1 \geq \rho > 0.9$; n = 167

Figure 3.11. Operating mode distribution of empirical trajectories for arterials under different operating conditions. The error bars represent 95% confidence interval. ρ = speed-ratio. n = number of extracted trajectories to draw the distribution. v_f = posted speed.

3.4.2 Outputs from the mesoscopic simulation module

A single origin-destination pair was formulated in the testing framework with only one corridor consisting of 10 links. Inflow was only possible in the first or entry link of the corridor. Operating conditions similar to the selected segments of the study locations was generated by limiting the capacity of a downstream link. In Figure 3.12, an example of the mesoscopic simulation output is presented. This example used inflow of 1200 vehicles per hour (vph). All links except for link 9 (capacity = 1,000 vph) were modeled with capacity 1600 vph. Inflow at the entry link sustained for a period of 2 minutes. During this time entry time for each individual vehicle agent was randomly generated from a uniform distribution, U(number of vehicles, min= 0, max = 2s*number of vehicles). Figure 3.12 (b) shows how the outflow capacity varied at different links with time. The outflow capacity at link 8 dropped from 1600 vph to 420 vph due to bottleneck initiated at link 9. As a result density increased in link 9 from 25 vehicles per mile (vpm) to about 125 vpm. All the upstream links had constant density of 25 vpm (= 1600 vph/ 65 mph). The only downstream link had a metered flow due to the bottleneck and therefore the density in link #10 was 15.38 vpm (= 1000 vph/65 mph).

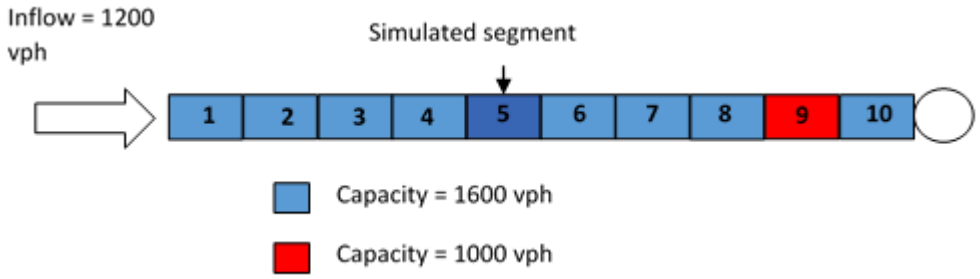

(a) Network configuration

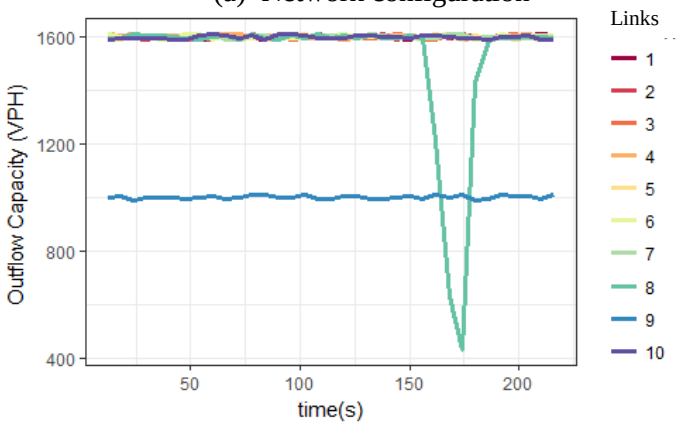

(b) Outflow capacity profiles at different links

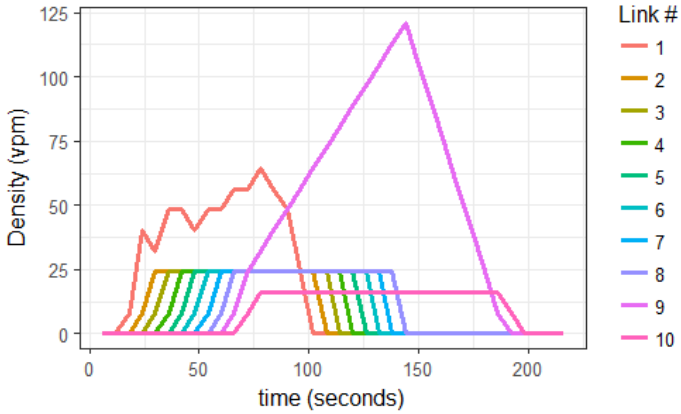

(c) Simulated densities at different links

Figure 3.12. Outputs from the mesoscopic simulation module for a 10 link single corridor with free-flow speed of 65 mph and backward wave speed of 12 mph.

3.4.3 Application of different post-processing methods and parameters

The current post-processing implementation of DTALite uses a simple unweighted moving average as its default post-processing method. The filter width is fixed at 7 intervals of simulation. The second method is a speed-acceleration enveloping (not set as a default post-processor; highly computationally intensive). Speed-acceleration enveloping can only be performed on a sample of vehicles because applying this method on the overall vehicle fleet is computationally infeasible.

In the simplest version of prototype, a single link is considered where all the inputs required to perform Newell's simplified trajectory generation procedure is generated based on mesoscopic simulation outputs and link attributes. Figure 3.13 shows raw space-time trajectories generated in the prototyped R code for a hypothetical 500m long freeway link with a free flow speed of 60 miles per hour and backward wave speed of 11.8 miles per hour. In the simplified case the minimum time and space gap between two consecutive vehicles are kept constant for all the vehicles in fleet. The speed and acceleration profile for the 7th vehicle (randomly chosen) in the fleet is shown in Figure 3.14. The speed-acceleration envelope for all the vehicles generated is shown in Figure 3.15.

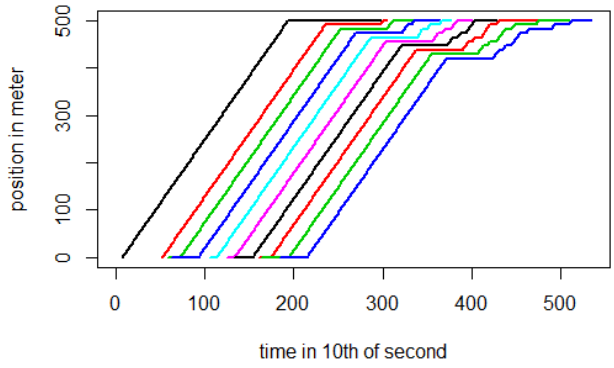

Figure 3.13. Unsmoothed space-time trajectories for 10 simulated vehicles on a link

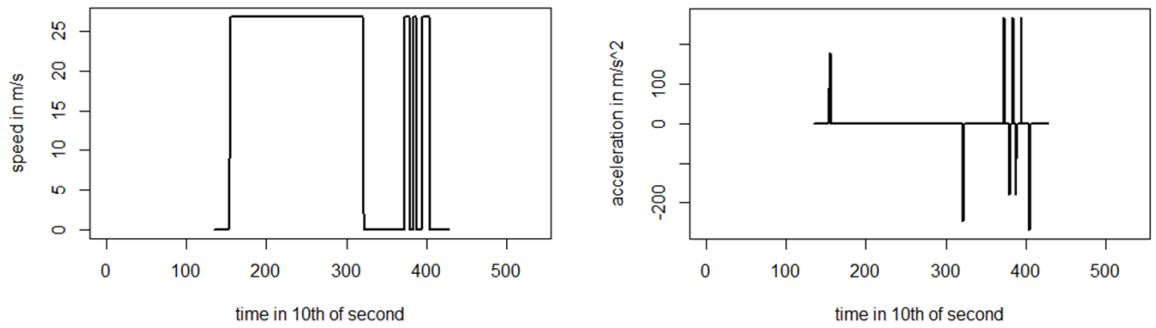

(a) (b)

Figure 3.14. (a) Speed profile and (b) acceleration profile for the 7th vehicle (shown black in Figure 3.13)

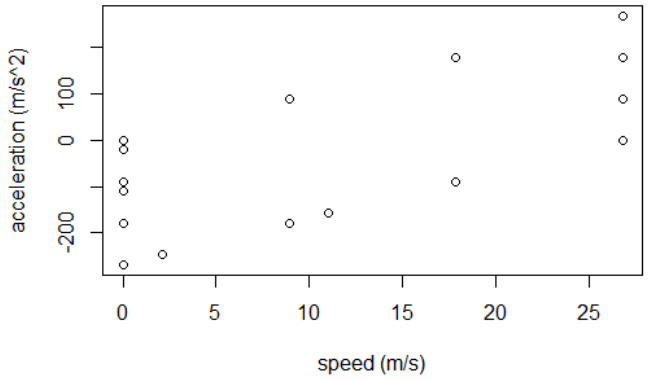

Figure 3.15. Speed-acceleration envelope for 10 simulated raw trajectories

Moving average method

The unweighted moving average method has one parameter – filter width. The prototyping framework has the capability to test different widths of filters and to examine the characteristics of post-processed trajectories. Figure 3.16 shows comparison of filter width 20 (2 seconds) and 160 (16 seconds).

Figure 3.16. (a) Space-time trajectories (b) speed profiles and (c) acceleration profiles for 2nd and 8th vehicles (d) speed-acceleration envelopes (e) VSP density plot (outliers removed) for filter width 20 and 160 simulation intervals using unweighted moving average method

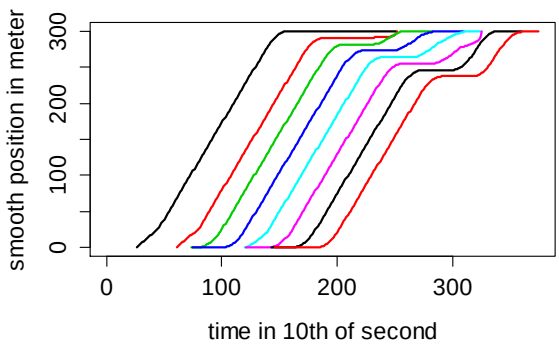

(a) Filter Width =20

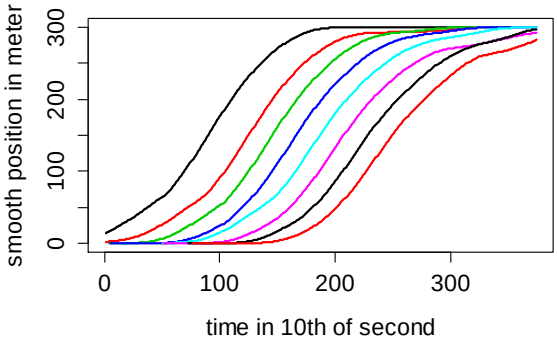

(a) Filter Width =160

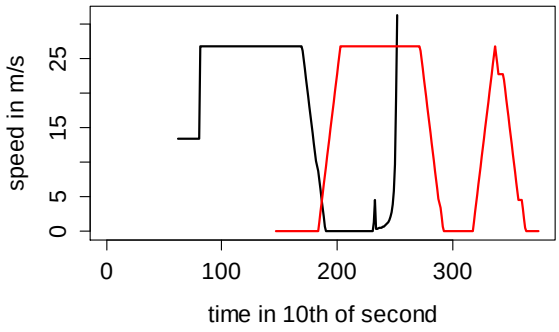

(b) Filter Width =20

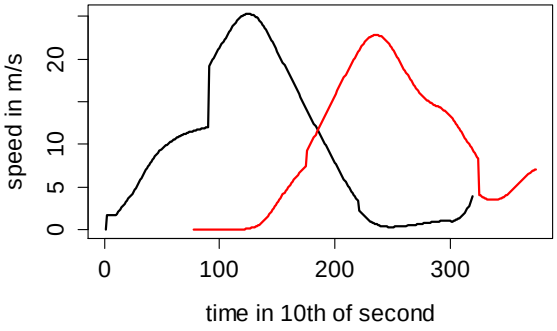

(b) Filter Width =160

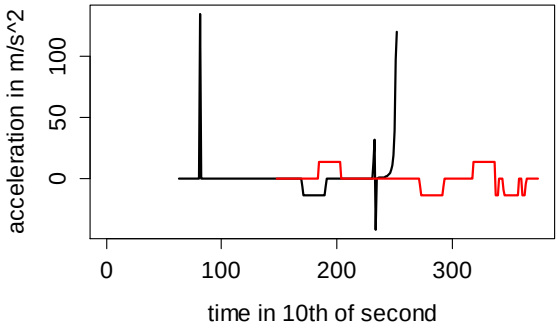

(c) Filter Width = 20

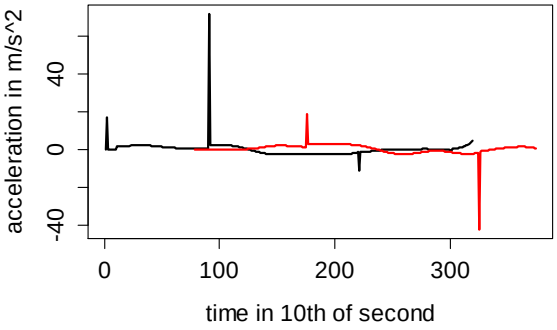

(c) Filter Width = 160

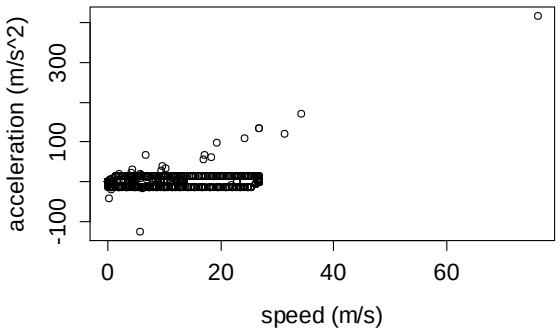

(d) Filter Width =20

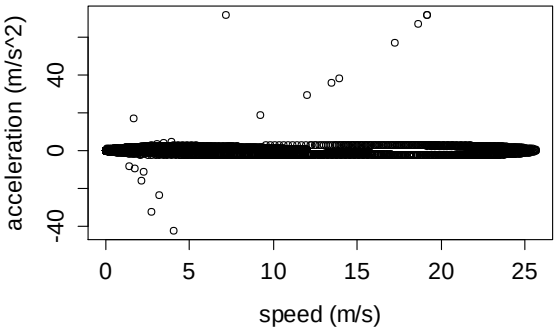

(d) Filter Width = 160

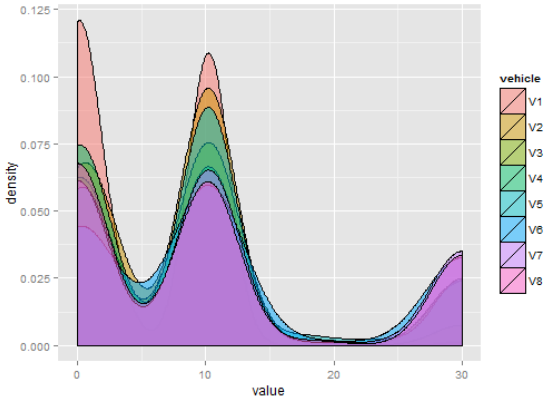

(e) Filter Width =20

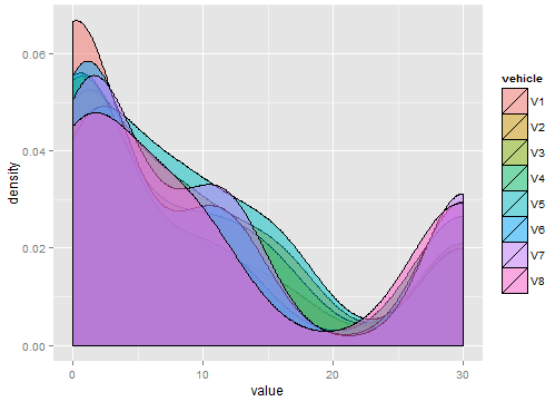

(e) Filter Width = 160

In this case a freeway link 300 meters long with 60 mph free-flow speed is simulated with 8 vehicles. It is to be noticed that the more smoothing is done the more features are lost in driving activity and the more inconsistencies arise in the physical representation of traffic stream behavior.

Overall, unweighted moving-average method causes loss in information in the original time series. However, The unweighted moving average is computationally less burdensome; therefore, can be used with other post-processing method as a complementary method.

Speed-acceleration enveloping

In a preliminary validation effort, randomly selected trajectory information of 344 vehicles in the Fort Worth network (Transportation Networks for Research Core Team,)was used to generate the speed-acceleration distribution (using a sample vehicle post-processing approach of speed-acceleration enveloping in existing DTALite). Only a subset of vehicles were used because the amount of second-by-second data points for all vehicles in that simulation is very large. The simulated speed-acceleration distribution is shown in Figure 3.17, and the 5th percentile and 95th percentile envelopes of acceleration from simulated trajectories and from real-world vehicle driving cycles are highlighted. The real-world vehicle activity information consist of data from 100 vehicles used in the study (Frey et al., 2013). A recent method (Liu & Frey, 2015) was used here to develop empirical speed-acceleration profile. For each vehicle, there are typically over 12,000 seconds of valid 1 Hz data.

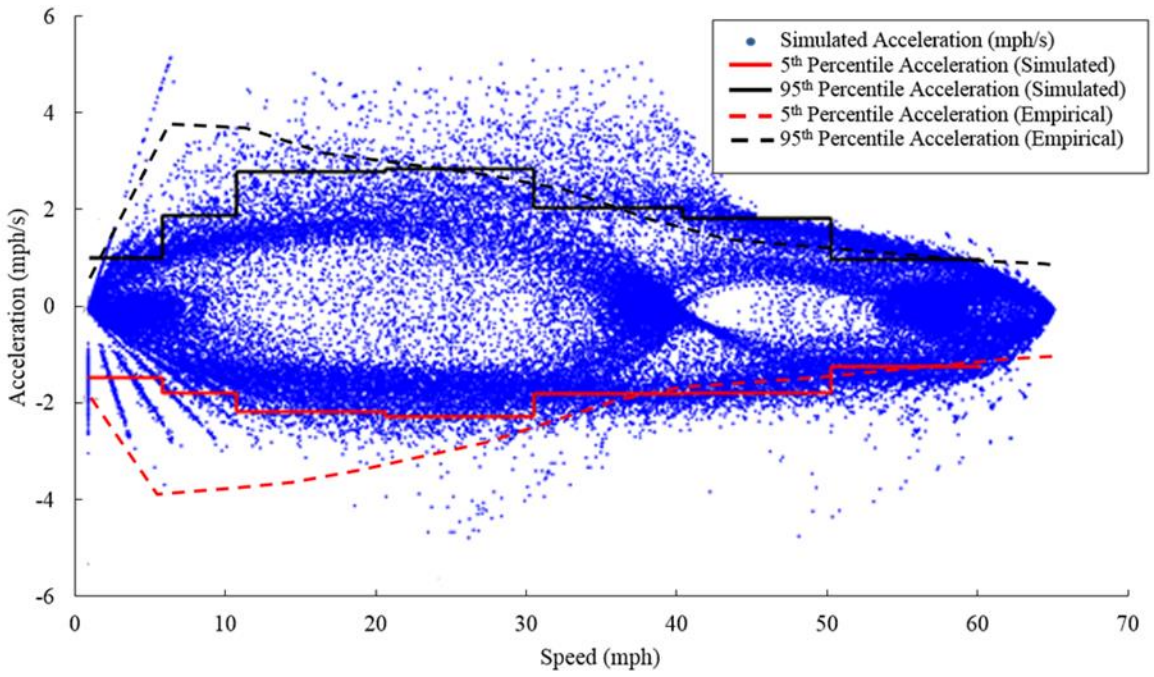

Figure 3.17. Joint speed-acceleration distribution: simulated vs. field-observed

It can be observed from Figure 3.17 that the empirical 90 percent frequency range of acceleration is wider than the simulated acceleration at lower speed bins. This indicates much more variability in acceleration or deceleration of field-measured vehicles at lower speed compared to the simulated trajectories. However, the widening of frequency ranges is evident at speeds from 10 mph to 30 mph. The simulated speed-acceleration distribution adheres more to the empirical distribution at speed ranges higher than 30 mph. A small number of data points in the joint speed-acceleration distribution of simulated trajectories correspond to very high acceleration and deceleration at lower speed ranges (0 mph to 10 mph). Also, there are many outliers in acceleration at mid speed range (20 mph to 45 mph).

Signal smoothing algorithms

Different signal smoothing algorithms in addition to the standard moving average method were tested in the prototype. Table 3.6 includes the list of different signal smoothing methods

and the range of test parameters. The Savitzky-Golay filter needed more parameters to determine the convolution co-efficient. To minimize the scope of parameter optimization a fixed filter order of 1 was used. The filter length for the Savitzky-Golay filter should be an odd number.

Table 3.6. Range of tested signal smoothing methods and parameters

Smoothing Algorithm	**Parameter 1**	**Range of Parameter 1**	**Parameter 2**	**Range of Parameter 2**
Unweighted Moving Average	Window Width	1/10 s ~ 10 s	Smoothing Iterations	1 ~ 50
Lowess (Locally Weigted) Smoothing	Window Width	1/10 s ~ 10 s	Smoothing Iterations	1 ~ 50
Savitzky–Golay filter	Filter Length	3/10 s ~ 13/10 s	Smoothing Iterations	1 ~ 70

In addition, smoothing algorithms were applied on the space-time trajectories and speed trajectories separately for all the combinations of road types (freeway and arterials) and operating conditions (uncongested, average, congested). Sample results from different smoothing algorithms are shown in Figure 3.18 to Figure 3.20.

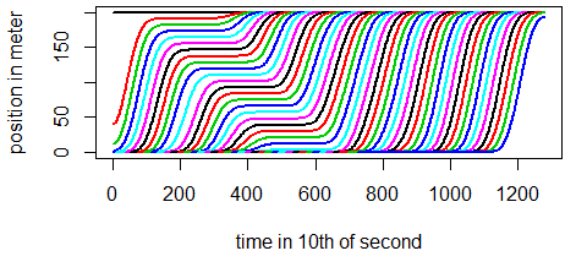

(a) Smoothed space-time trajectory (all the vehicles in simulated link)

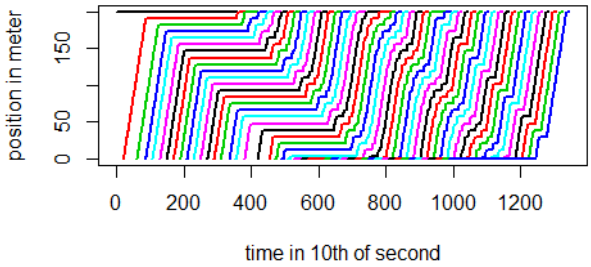

(d) Unsmoothed space-time trajectory (all the vehicles in simulated link)

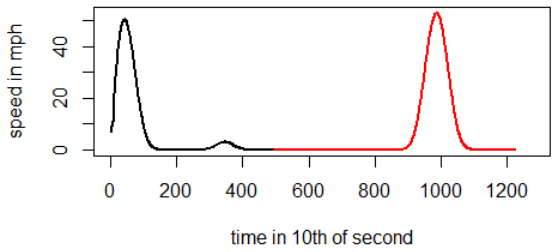

(b) Resulting speed trajectory (for the 3rd and 45th vehicle)

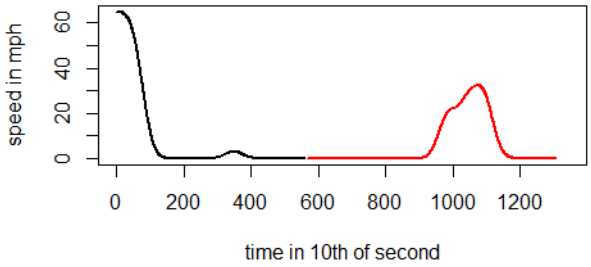

(e) Smoothed speed trajectory (for the 3rd and 45th vehicle)

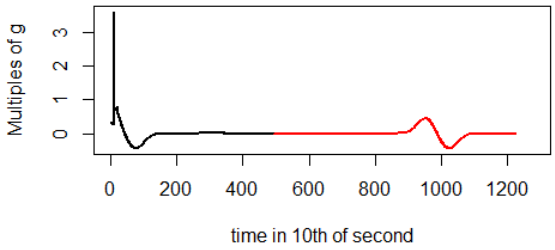

(c) Resulting acceleration trajectory from (b)

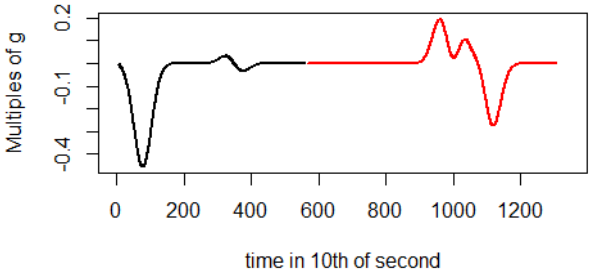

(f) Resulting acceleration trajectory from (e)

Figure 3.18 Modified trajectories from (a to c) smoothing space-time trajectories using unweighted moving average with window width of 3 sec and 10 smoothing iterations (d to f) smoothing speed trajectories using unweighted moving average with window width 3 sec and 20 smoothing iterations.

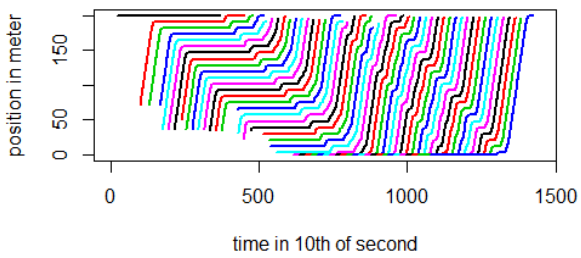

(a) Smoothed space-time trajectory (all the vehicles in simulated link)

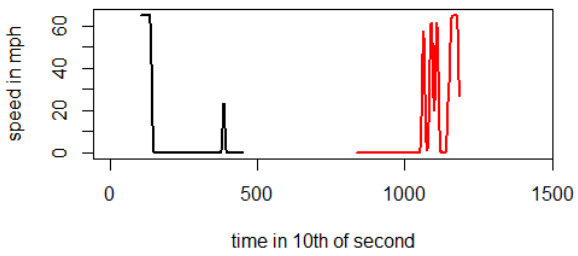

(b) Resulting speed trajectory (for the 3rd and 45th vehicle)

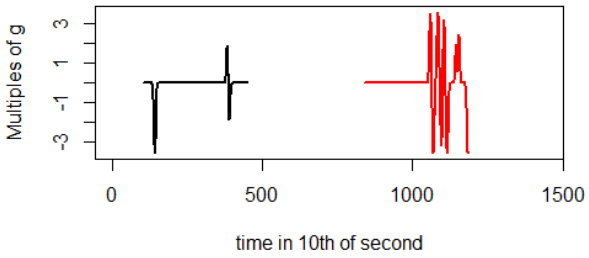

(c) Resulting acceleration trajectory from (b)

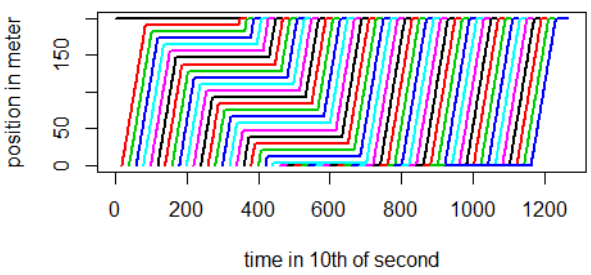

(d) Unsmoothed space-time trajectory (all the vehicles in simulated link)

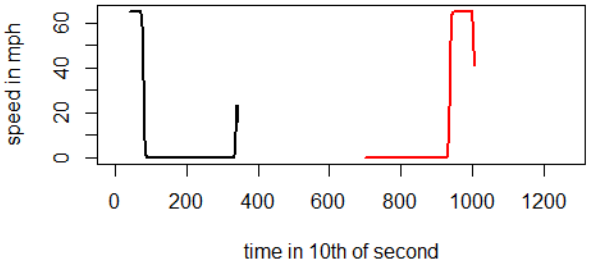

(e) Smoothed speed trajectory (for the 3rd and 45th vehicle)

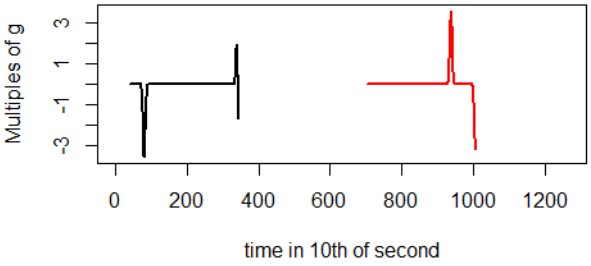

(f) Resulting acceleration trajectory from (e)

Figure 3.19. Modified trajectories from (a to c) smoothing space-time trajectories using Svitzky-Golay filter with filter length of 1/2 sec and 10 smoothing iterations. (d to f) smoothing speed trajectories using Svitzky-Golay filter with filter length 1/2 sec and 10 smoothing iterations.

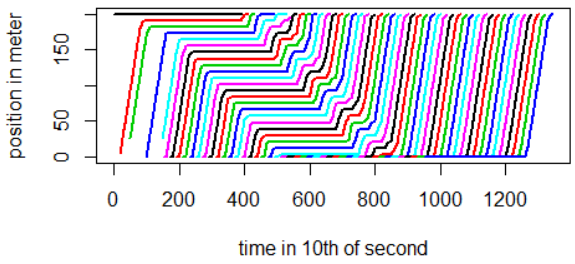

(a) Smoothed space-time trajectory (all the vehicles in simulated link)

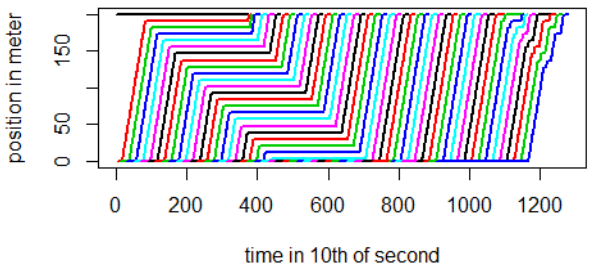

(d) Unsmoothed space-time trajectory (all the vehicles in simulated link)

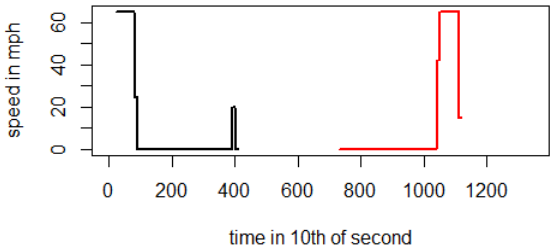

(b) Resulting speed trajectory (for the 3rd and 45th vehicle)

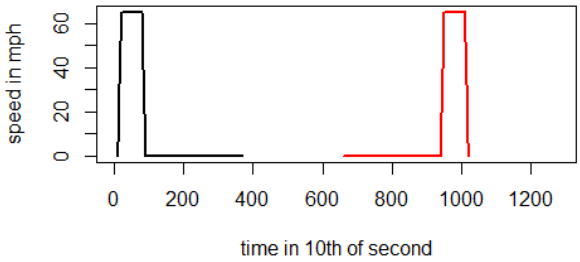

(e) Smoothed speed trajectory (for the 3rd and 45th vehicle)

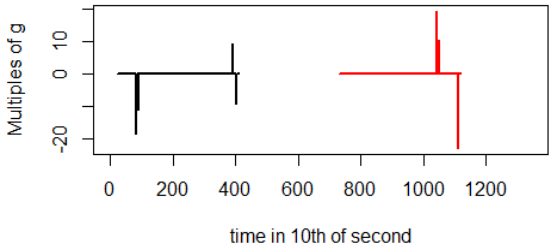

(c) Resulting acceleration trajectory from (b)

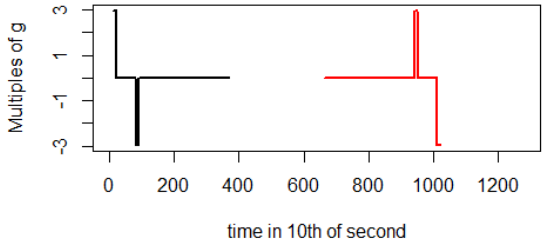

(f) Resulting acceleration trajectory from (e)

Figure 3.20. Modified trajectories from (a to c) smoothing space-time trajectories using Lowess smoothing with filter length of 1/2 sec and 10 smoothing iterations. (d to f) smoothing speed trajectories using Lowess smoothing with filter length 1/2 sec and 10 smoothing iterations.

Speed-acceleration enveloping

The existing implementation of speed-acceleration enveloping involves reducing the speeds of previous seconds for a high-acceleration event and later seconds for a high deceleration event until on each size zero speed is reached. This method have some unintended consequences of smoothing out small-accelerations or decelerations around a high-acceleration and deceleration event. In the developed optimization framework speed-

acceleration enveloping was executed using two parameters. The parameter values are listed as follows-

a) Enveloping zone: number of simulation interval before (for acceleration violations) or after (for deceleration violations) which speed-acceleration enveloping is not employed.
   Range: 1/10 s ~ 13/10 s
b) Enveloping iterations: number of passes of speed-acceleration enveloping. Each time the acceleration violation condition is checked.
   Range: 1 ~ 70

The result of speed-acceleration enveloping with enveloping zone 1/10 s and 50 iterations is shown in Figure 3.21.

Micro-trip based trajectory reconstruction

In this method random Gaussian noise was added to the segments of the trip corresponding to predefined events. There were four parameters for the trajectory reconstruction method with each parameter representing standard deviation for the Gaussian noise-generator. Since all the added noises were assumed to be white noises, the mean values for the noise-generators was set at 0.

The result for micro-trip based trajectory reconstruction for all the noise standard deviations set at 0.1 m/s is shown in Figure 3.21.

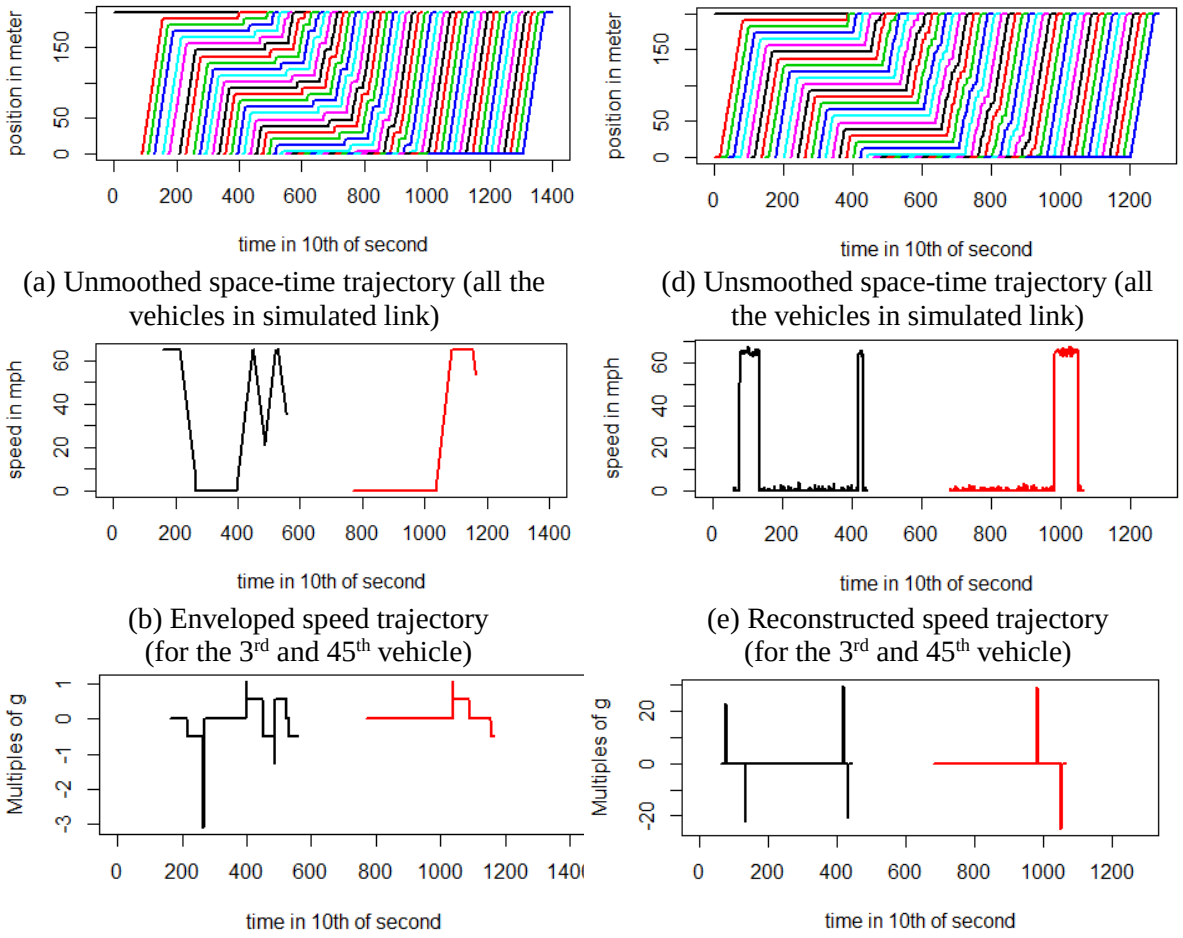

(a) Unmoothed space-time trajectory (all the vehicles in simulated link)

(d) Unsmoothed space-time trajectory (all the vehicles in simulated link)

(b) Enveloped speed trajectory (for the 3rd and 45th vehicle)

(e) Reconstructed speed trajectory (for the 3rd and 45th vehicle)

(c) Resulting acceleration trajectory from (b)

(f) Resulting acceleration trajectory from (e)

Figure 3.21 Modified trajectories from (a to c) speed-acceleration enveloping with enveloping zone 1/10 s and 50 iterations. (d to f) micro-trip based trajectory reconstruction for all the noise standard deviations set at 0.1 m/s.

3.4.4 Optimized parameters for post-processing methods

The optimized parameter values for freeways under three operating conditions with calculated average RMSE values are shown in Table 3.7. Similar numbers for arterials are shown in Table 3.8.

Table 3.7 Optimized parameters for freeways (v_f = 65 mph)

Operating Condition	Smoothing Type	Method	Optimized Window Width (1/10 s)	Optimized Iteration Number	Average RMSE
Uncongested ($1.1 \geq \rho > 0.9$)	Space-time Smoothing only	Unweighted Moving Average	41	1	14.83
		Savitzky-Golay Filter	5	31	11.62
		Lowess Smoothing	86	1	9.87*
	Speed Smoothing Only	Unweighted Moving Average	36	1	14.83
		Savitzky-Golay Filter	7	11	12.01
		Lowess Smoothing	76	21	12.88
	No Smoothing	Speed-Acc. Enveloping	13	21	15.27
Average ($0.9 \geq \rho > 0.7$)	Space-time Smoothing only	Unweighted Moving Average	6	11	13.9
		Savitzky-Golay Filter	7	11	11.49
		Lowess Smoothing	51	41	7.96*
	Speed Smoothing Only	Unweighted Moving Average	26	1	13.99
		Savitzky-Golay Filter	7	11	11.27
		Lowess Smoothing	81	11	11.59
	No Smoothing	Speed-Acc. Enveloping	7	51	13.02
Congested ($0.7 \geq \rho > 0.5$)	Space-time Smoothing only	Unweighted Moving Average	26	11	12.76
		Savitzky-Golay Filter	13	41	8.18
		Lowess Smoothing	96	26	11.04
	Speed Smoothing Only	Unweighted Moving Average	11	11	12.28
		Savitzky-Golay Filter	3	41	7.71*
		Lowess Smoothing	41	11	9.18
	No Smoothing	Speed-Acc. Enveloping	6	41	9.66

Table 3.8 Optimized parameters for arterials (v_f = 45 mph)

Operating Condition	Smoothing Type	Method	Optimized Window Width (1/10 s)	Optimized Iteration Number	Average RMSE
Uncongested ($1.1 \geq \rho > 0.9$)	Space-time Smoothing only	Unweighted Moving Average	51	1	15.12
		Savitzky-Golay Filter	7	11	12.12
		Lowess Smoothing	96	1	10.84
	Speed Smoothing Only	Unweighted Moving Average	16	1	14.13
		Savitzky-Golay Filter	5	31	12.53
		Lowess Smoothing	71	31	11.40
	No Smoothing	Speed-Acc. Enveloping	3	11	10.80
Average ($0.9 \geq \rho > 0.7$)	Space-time Smoothing only	Unweighted Moving Average	1	11	12.68
		Savitzky-Golay Filter	5	11	10.12
		Lowess Smoothing	56	21	8.87
	Speed Smoothing Only	Unweighted Moving Average	1	1	11.18
		Savitzky-Golay Filter	3	21	8.57
		Lowess Smoothing	66	41	8.39
	No Smoothing	Speed-Acc. Enveloping	1	41	7.45*
Congested ($0.7 \geq \rho > 0.5$)	Space-time Smoothing only	Unweighted Moving Average	61	1	8.70
		Savitzky-Golay Filter	9	21	7.36
		Lowess Smoothing	1	1	11.97
	Speed Smoothing Only	Unweighted Moving Average	6	11	9.99
		Savitzky-Golay Filter	11	11	6.35*
		Lowess Smoothing	76	31	6.86
	No Smoothing	Speed-Acc. Enveloping	1	31	7.66

Finding the optimized parameter values for micro-trip based trajectory reconstruction method are shown in Table 3.9.

Table 3.9 Parameters and average RMSE values for micro-trip based trajectory reconstruction method

Facility Type	**Operating Condition**	**Noise s.d.* Idle**	**Noise s.d.* Cruise**	**Noise s.d.* Acc.**	**Noise s.d.* Dec.**	**Average RMSE**
Freeways	Uncongested	2	2	0.5	0.5	9.87*
	Average	2	2	1	2	9.60
	Congested	1.5	1	0.5	0	9.73
Arterials	Uncongested	2	0.5	0.5	1.5	10.76*
	Average	2	0	0.5	1	8.42
	Congested	2	2	0	0	7.10

*s.d. = σ = standard deviation for a Gaussian distribution, $N(0,\sigma^2)$

In both freeway and arterial congested conditions, the Savitzky-Golay based speed-smoothing process performed better than other methods. This observation shows that the frequent stop and go motion created by the simplified trajectory generator in congested conditions is an important feature to preserve (since Savitzky-Golay algorithm is more capable of preserving important features in a time-series trace).

Wide width Lowess smoothers are shown to be providing less residuals. Lowess smoothing performed particularly well in uncongested and average operating conditions. However, Lowess smoothers needed more iterations with more congested conditions to provide satisfactory trajectories. Lowess smoother performed well when it is applied to speed trajectories only.

In addition to finding the optimized trajectories, the average RMSE or the residual of the relationship between simulated and observed operating mode distributions is calculated for the parameter space. Figure 3.22 shows the residual distribution for freeways in

congested condition. Similar analysis were done for other facility types and operating conditions are documented in appendix A.

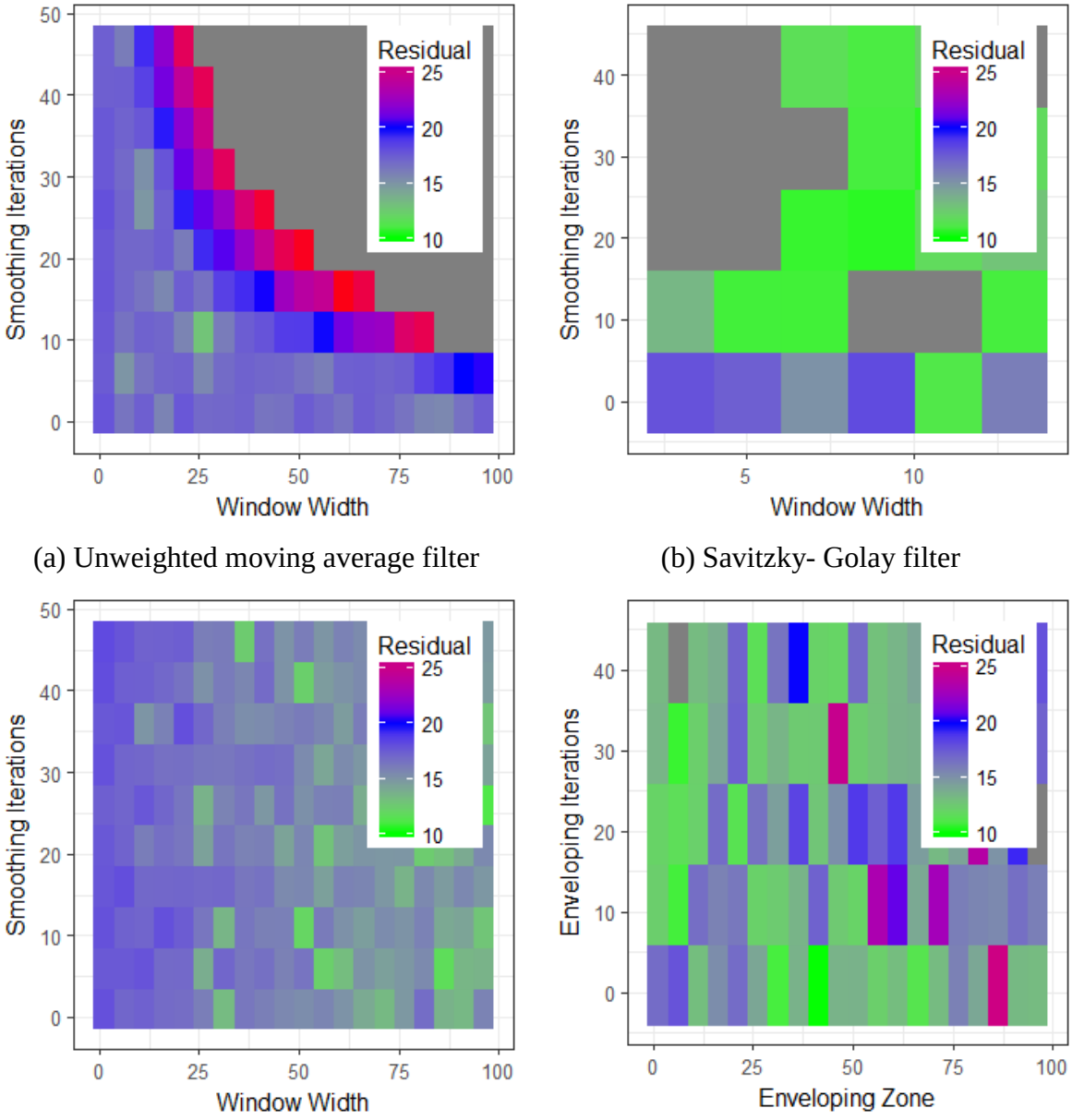

(a) Unweighted moving average filter

(b) Savitzky- Golay filter

(c) Lowess smoothing

(d) Speed-acceleration enveloping

Figure 3.22. Residual distribution for the post-processing parameter space with different post-processing methods. The grey cells represents values outside the plotting range.

In the moving average method, residual values decreased initially with increase in window width and smoothing iterations. However, at higher values of smoothing iterations the value for residual increased exponentially. In fact, moving average method shows

residual under 15 for all facility types and conditions when window width is kept in a range of 20 – 50 and smoothing iterations are kept under 10.The Savitzky – Golay filter performs better with higher number of smoothing iterations. In all the cases, specifically for congested condition, the residual decrease rapidly with smoothing iterations beyond 10 around window width of 5 – 20.

The Lowess smoothing and speed-acceleration enveloping did not follow a regular pattern. For Lowess smoothing, residual values generally decreased at high values of smoothing window width (> 50) and smoothing iterations (>20).

3.4.5 Fuel use estimations for the synthetic trajectories

Two different externally observed variables (EOV) based fuel use estimation models were applied to calculate fuel use for the unprocessed synthetic trajectory and the corresponding post-processed trajectories. The estimation models are as follows-

1) Vehicle specific power based model- a simple piecewise power function is used to express the relation between instantaneous VSP and fuel use in g/s. The relationship is then applied to the trajectory to determine total fuel use.
2) Operating mode based model- fixed fuel use rate (g/s) is assigned to each operating mode.

The total distance traveled (miles) in the trajectory was divided by the total fuel use (US gallons) to determine trajectory fuel mileage (mpg). Fuel mileage for observed trajectories under similar conditions were determined using internally observed variables (IOV) – moving average manifold absolute pressure and engine speed. The applied IOV based fuel use estimation model has a coefficient of determination (R^2) of 0.99 when it was fit (Frey et al., 2010).

Figure 3.23 shows a Savitzky-Golay filter with filter width of 7 and 10 filtering iterations brings the distribution of fuel mileage closer to the empirical distribution. In this figure, both empirical and simulated trajectories were collected for a freeway facility under congested operating condition. Similar findings were made in optimized simulated trajectories for all other conditions and facility types.

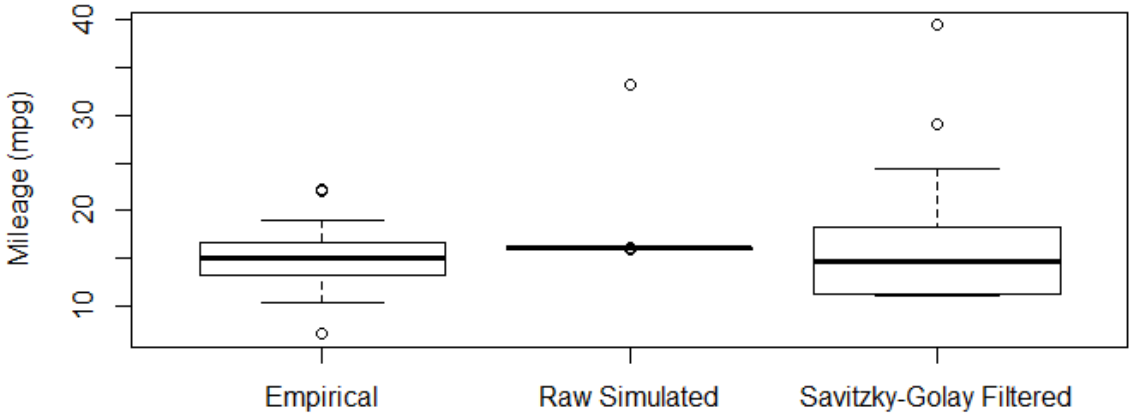

Figure 3.23. Comparison of estimated fuel mileage for empirical and simulated trajectories for freeways (v_f = 65 mph) in congested condition($0.7 \geq \rho > 0.5$).

For the operating mode bin based fuel use estimations, lesser variation was observed in estimated emissions of smoothed trajectories. The lack of variation in binning method may come from the functional relationship between VSP and fuel use rate. Both continuous function based and binning based fuel use estimators has similar mean estimates for all the conditions.

3.5 Conclusions

This chapter has presented an analysis of synthetic trajectories generated from mesoscopic traffic simulators. The effect of different post-processing methods in bringing the simulated

driving activity close to reality was examined. To compare simulated driving activity with real-world driving activity, observed trajectories were extracted from similar facility types and similar operating conditions as was simulated. In addition, a simulation-optimization-evaluation platform, as a prototype for the actual DTALite implementation of the mesoscopic simulator, was developed for better visualization and post-processing algorithm implementation. Conclusions were drawn on each of the research questions of this chapter as follows-

a. The selection of post-processing method most suitable for simulated trajectories derived from simplified trajectory generators in a mesoscopic simulation environment depends on the operating condition and the facility type. The Savitzky-Golay filter performed better than other methods in congested conditions. This finding suggests that the features in trajectories under congested conditions attributed by the simulated stop-and-go conditions are important to preserve in terms of representing reality. The Lowess smoothing performed better under average conditions. In average congested conditions, the Savitzky-Golay filter left some of the unnecessary irregularities in simulated trajectories, where the Lowess smoothing applied local smoothing to filter out those irregularities. Additionally, Lowess smoothing performed better than the moving average because moving average generally reduces the amplitude of the peaks in speed trajectories. Microtrip-based trajectory reconstruction performed best in uncongested condition. This findings suggest that the trajectory generator in general is working better in uncongested conditions than the other operating conditions. Indeed, the simplified trajectory generator propagates vehicles at free-flow speed as observed in reality; except in reality there is speed variation i.e. drift behavior due to oscillation in the car following

regime. Adding a noise component, specifically in the cruising part of the trajectory pushes the trajectory closer to reality. The simple unweighted moving average method, the *de-facto* smoother in DTALite, provide space-time trajectories which are visually appealing. However, unweighted moving average modifies the frequency and amplitude of the peaks in processed trajectories. Both unweighted moving average and speed-acceleration enveloping methods begin to perform poorly i.e. high residual values at high values of window width and smoothing iterations.

b. The recommendation on parameters to use for different post-processing methods is based upon the optimization platform designed. The fraction of time spent in each operating mode bin is used as the indicator for matching empirical and post-processed simulated trajectories. The objective function for optimization was set as the residual or the average root mean squared error (RMSE) between the empirical and simulated trajectories. In the optimization, no constraints on computational resources were imposed. The distribution of residuals in the sample space was explored to understand the recommended parameters. Based on the analysis, the Savitzky-Golay filter on the speed-trajectories with window width 7 and 10 windowing iteration is a balanced choice for congested condition. Lowess smoothing on the space-time trajectories with window width 40 and smoothing iterations 30 is recommended under average conditions. The micro-trip based trajectory reconstruction method is the preferred method for uncongested condition with addition of random Gaussian white noise of $N(0, 2^2)$ while idling, $N(0, 1^2)$ while cruising, $N(0, 0.5^2)$ in acceleration, and $N(0, 0.5^2)$ in deceleration instances. Combination of different post-processing methods will be explored as a future work.

c. Both continuous function based and operating mode bin based fuel use estimators provide similar estimation of average fuel mileage for both simulated and observed trajectories. However, the operating mode bin based estimation had lesser variability. Within the current scope of this research, it was not possible to evaluate whether the variability is due to the 'true' nature of the simulated trajectories or due to the noisy and oversensitive nature of the EOV model. This observation leads to the question, whether the existing continuous function based EOV models are developed to handle high-resolution VSP values appropriately (with peaks and features that may last for a small time ~ 1 s). On the other hand, for the binning approaches, if there is not significant variation in estimated fuel mileage to as an effect of within segment operational variabilities, then increasing the computational complexity to generate high-resolution trajectories becomes unnecessary. These questions are being investigated in details as a part of an ongoing research.

3.6 References

Ahn, S., Cassidy, M. J., & Laval, J. (2004). Verification of a simplified car-following theory. *Transportation Research Part B: Methodological, 38*(5), 431-440.

Aziz, H. M., & Ukkusuri, S. V. (2015). Finding the link driving schedules (LDS) for integrated traffic-emissions (EPA-MOVES) simulator by clustering with dynamic time warping measures. Paper presented at the *Transportation Research Board 94th Annual Meeting*, (15-5060)

Chamberlin, R., Swanson, B., Talbot, E., Dumont, J., & Pesci, S. (2011a). Analysis of MOVES and CMEM for evaluating the emissions impact of an intersection control change. Paper presented at the *Transportation Research Board 90th Annual Meeting*, (11-0673)

Chamberlin, R., Swanson, B., Talbot, E., Dumont, J., & Pesci, S. (2011b). Analysis of MOVES and CMEM for evaluating the emissions impact of an intersection control change. Paper presented at the *Transportation Research Board 90th Annual Meeting*, (11-0673)

Cleveland, W. S. (1981). LOWESS: A program for smoothing scatterplots by robust locally weighted regression. *The American Statistician, 35*(1), 54.

Cloke, J., Boulter, P., Davies, G. P., Hickman, A. J., Layfield, R. E., McCrae, I. S., & Nelson, P. M. (1998). Traffic management and air quality research programme. *Trl Report 327*,

da Rocha, T. V., Leclercq, L., Montanino, M., Parzani, C., Punzo, V., Ciuffo, B., & Villegas, D. (2015). Does traffic-related calibration of car-following models provide accurate estimations of vehicle emissions? *Transportation Research Part D: Transport and Environment, 34*, 267-280.

EPA. (2009). *MOVES software design and reference manual.* Ann Arbor, MI: EPA.

FHWA. (2015). Next generation simulation (NGSIM) http://Ops.fhwa.dot.gov/trafficanalysistools/ngsim.htm.

Frey, H. C., Unal, A., Chen, J., Li, S., & Xuan, C. (2002). Methodology for developing modal emission rates for EPA's multi-scale motor vehicle & equipment emission system. *Ann Arbor, Michigan: US Environmental Protection Agency,*

Frey, H. C., Zhang, K., & Rouphail, N. M. (2010). Vehicle-specific emissions modeling based upon on-road measurements. *Environmental Science & Technology, 44*(9), 3594-3600. doi:10.1021/es902835h; 10.1021/es902835h

Frey, H. C., Yazdani-Boroujeni, B., Hu, J., Liu, B., & Jiao, W. (2013). Field measurements of 1996 to 2013 model year light duty gasoline vehicles. Paper presented at the *Proceedings, 106th Annual Conference, Air & Waste Management Association, Chicago, IL,*

Hyndman, R. J., & Athanasopoulos, G. (2014). *Forecasting: Principles and practice* OTexts.

Jimenez-Palacios, J. L. (1998). *Understanding and quantifying motor vehicle emissions with vehicle specific power and TILDAS remote sensing*

Kesting, A., & Treiber, M. (2009). Calibration of car-following models using floating car data. *Traffic and granular Flow'07* (pp. 117-127) Springer.

Kleijnen, J. P., Cheng, R. C., & Bettonvil, B. (2000). VVA IV: Validation of trace-driven simulation models: More on bootstrap tests. Paper presented at the *Proceedings of the 32nd Conference on Winter Simulation,* 882-892.

Lighthill, M. J., & Whitham, G. B. (1955). On kinematic waves. II. A theory of traffic flow on long crowded roads. *Proceedings of the Royal Society of London.Series A.Mathematical and Physical Sciences, 229*(1178), 317-345.

Liu, B., & Frey, H. C. (2015). Measurement and evaluation of real-world speed and acceleration activity envelopes for light-duty vehicles. *Transportation Research Record: Journal of the Transportation Research Board,* (2503), 128-136.

Montanino, M., & Punzo, V. (2015). Trajectory data reconstruction and simulation-based validation against macroscopic traffic patterns. *Transportation Research Part B: Methodological, 80*, 82-106.

National Research Council. (2000). *Modeling mobile-source emissions* National Academies Press.

Newell, G. F. (2002). A simplified car-following theory: A lower order model. *Transportation Research Part B: Methodological, 36*(3), 195-205.

Savitzky, A., & Golay, M. J. (1964). Smoothing and differentiation of data by simplified least squares procedures. *Analytical Chemistry, 36*(8), 1627-1639.

Taylor, J., Zhou, X., Rouphail, N. M., & Porter, R. J. (2015). Method for investigating intradriver heterogeneity using vehicle trajectory data: A dynamic time warping approach. *Transportation Research Part B: Methodological, 73*, 59-80.

TRB. (2016). *Highway capacity manual, sixth edition: A guide for multimodal mobility analysis*. Washington DC: Transportation Research Board.

Treiber, M., Kesting, A., & Thiemann, C. (2008). How much does traffic congestion increase fuel consumption and emissions? applying a fuel consumption model to the NGSIM trajectory data. Paper presented at the *87th Annual Meeting of the Transportation Research Board,*

Zhou, X., Tanvir, S., Lei, H., Taylor, J., Liu, B., Rouphail, N. M., & Christopher Frey, H. (2015). Integrating a simplified emission estimation model and mesoscopic dynamic traffic simulator to efficiently evaluate emission impacts of traffic management strategies. *Transportation Research Part D: Transport and Environment, 37*, 123-136. doi://dx.doi.org/10.1016/j.trd.2015.04.013

Zhou, X., Taylor, J., & Pratico, F. (2014). DTALite: A queue-based mesoscopic traffic simulator for fast model evaluation and calibration. *Cogent Engineering, 1*(1), 961345.

CHAPTER 4

EFFECT OF LIGHT DUTY VEHICLE PERFORMANCE ON A DRIVING STYLE METRIC[*]

4.1 Introduction

The transportation sector in the United States consumed about 36 quadrillion Btu of energy in the form of petroleum in 2016 *(U.S. Energy Information Administration, 2017)*. In addition to producing greenhouse gases (GHG), petroleum dependence makes the economy vulnerable to price shocks *(Kilian & Park, 2009)*. Many fuel consumption reduction measures have been attempted such as improving vehicle technology, reducing travel demand, increasing vehicle occupancy and transit use, among others *(Bandivadekar et al., 2008)*. However, the effectiveness of these countermeasures have shown mixed results because of the expense and inconvenience involved in their adoption *(Graham-Rowe, Skippon, Gardner, & Abraham, 2011)*. In contrast, 'Eco-driving' which involves changing the behavior or the style of driving to achieve energy efficiency is less costly than other options; however, is more difficult to administer. The estimated benefit from eco-driving is reported from 5 percent to 40 percent *(Bin & Dowlatabadi, 2005; Onoda, 2009)*. High benefit values are generally estimated for a very idealistic condition where the drivers can choose the cruising speed and the level of acceleration and deceleration. However, in a naturalistic environment, drivers are constrained by congestion on their routes, road geometry, traffic control, weather, and vehicle performance. In this paper, we will explore the effect of vehicle performance on driving style.

[*] Paper accepted for publication as Tanvir, S., Frey, H. C., & Rouphail, N. M. (2018) Effect of Light Duty Vehicle Performance on a Driving Style Metric. Transportation Research Record: Journal of the Transportation Research Board.

Driving style is a generic term which is sometimes used interchangeably with the term ‘driver aggressiveness’. Generally, driving style refers to the accumulated microscale driving activity such as speed or acceleration over a single or a set of synthetic or real-world drive cycle/s gathered from the same driver-vehicle combination. Synthetic drive cycles such as the Federal Test Procedure (FTP) and Highway Fuel Economy Driving Schedule (HWFET) are mainly used for certification purposes in chassis dynamometer tests. In contrast, real-world or naturalistic drive cycles are manifested as the driving style reacts to both in-vehicle and out-of-vehicle environments.

Vehicle performance is the capability of a vehicle to accelerate or decelerate under particular speed conditions. Malliaris et al., 1976 *(Malliaris, Hsia, & Gould, 1976)* found an inverse power relation between vehicle time to accelerate from 0 to 60 mph and its power-to-weight ratio. Vehicle performance delineates the limiting conditions on the driving style. The effect of power-to-weight ratio, as a surrogate for vehicle performance, has been studied in previous research *(Brundell-Freij & Ericsson, 2005; Fontaras, Zacharof, & Ciuffo, 2017).*

Most studies examined vehicle performance and driving styles in a disjointed way – by not considering the effect of driver-vehicle interaction on the specified driving style metric. In other words, heterogeneity in driving styles across different drivers was not considered while measuring the effect of vehicle performance. Absence of consideration for driver-vehicle interaction may have led to wide variability in the measured effect of vehicle performance on driving style.

In the next section, we present a review of the literature on the measures of driving style and methods of testing the effect of vehicle performance on driving style. Methods and

data for the paper are discussed in the subsequent sections. Next, we discussed the results and followed by the conclusions from this analysis.

4.1.1 Review of driving style measures

Several approaches have been proposed to characterize driving style or the 'aggressiveness' of driving styles. The most common way to characterize driving style is by characterizing microscale driving activity. Descriptive statistics of instantaneous speed and acceleration over the drive cycle such as average speed, standard deviation of speed, average positive acceleration, standard deviation of positive acceleration, percentage trip time accelerating over a threshold, and jerk frequency, among others, have been used to characterize driving style *(Evans, 1978; J. Liu, Khattak, & Wang, 2017)*. However, aggregate cycle based characteristics are not very useful in comparing multiple driving styles in terms of fuel consumption. Another mode of characterizing driving style is to use a normalized energy consumption measure. In this approach, fuel efficiency (measured in miles per gallon) or the ratio of cycle average speed to energy consumption *(Ericsson, 2000)* is used to describe driving style. A major shortfall of this approach is that the direct measurement of fuel consumption is needed. In addition, aggregate measures do not consider the differences in drivers' reactions to different dynamics which exist at different speed levels.

To account for vehicle speed-acceleration dynamics, joint distribution of speed and acceleration has been suggested as a characteristics of driving style. EPA (*Federal test procedure review project: Preliminary technical report. technical report.*1993) used the fraction of speed-acceleration instances falling outside the range of standard drive cycles such as FTP or HWFET to characterize driver aggressiveness. Berry, 2010 *(Berry, 2010)* proposed the use of an 'Aggressiveness Factor' from microscale driving activity data by

calculating the amount of extra work relative to steady-state driving. She defined three separate ‘aggressiveness factors’ based on trip average speeds to distinguish neighborhood (below 20 mph), city (between 20 and 45 mph), and highway (above 45 mph) driving. Along the same philosophy, Stichter, 2012 *(Stichter, 2012)* developed a ‘proposed aggressivity metric’ using average positive and negative acceleration frequencies for trucks. These single number driving style metrics overlook the distribution of deviations of observed microscale activities from the standardized cycles or steady-state driving style. To explain the dynamics of deviation, Liu and Frey, 2015 *(B. Liu & Frey, 2015)* suggested using ‘activity envelopes’ for light duty vehicles. They defined activity envelope as the 95 percent frequency range of acceleration for each of 15 speed bins from 0 to 75 mph in intervals of 5 mph, and one bin for speeds greater than 75 mph. This discretized way of portraying driving style provided more information than a single number metric. However, the entire distribution of acceleration activities in relation to the standardized cycles was not explicitly considered in their metric.

4.1.2 Review of experimental designs

The method for experimenting with driving styles and vehicle performances has varied substantially across the literature. In most cases, the objective of the research was not to measure the effect of vehicle performance on driving style; rather the focus was on finding the joint impact of driving style and vehicle characteristics on energy consumption or emissions while controlling for other factors such as route and congestion. Common approaches to gather microscale driving activity are through engine dynamometers across predetermined drive cycles *(Sharer, Leydier, & Rousseau, 2007)* and microscopic vehicle simulation *(Berry, 2010)*. However, these simulated driving styles cannot always accurately

represent real-world characteristics of individual drivers *(Anya, Rouphail, Frey, & Schroeder, 2014; Song, Yu, & Zhang, 2012)*. Frey et al., 2003 *(Frey, Unal, Rouphail, & Colyar, 2003)* used portable emissions measurement systems along with vehicle on-board diagnostic (OBD) information to characterize real-world driving style and associated emissions. Experiments controlling for routes, time of day, road grade, and vehicles *(Frey, Zhang, & Rouphail, 2008; Van Mierlo, Maggetto, Van de Burgwal, & Gense, 2004)* have been conducted to examine the resulting fuel use and emissions. However, these studies did not examine the variation in individual driver driving style at different levels of vehicle performance. In contrast to the controlled experiments, naturalistic driving studies can provide long-term information on a driver's driving style. In naturalistic driving, personal vehicles are equipped with microscale driving activity recorders that collect data during regular driving. Due to the expense involved in equipping the vehicles, naturalistic driving studies are typically conducted in randomized assignments of drivers for a long period or, in case of factorial design trials, multiple driver-vehicle combinations are monitored in short phases. In the first case, even with a long term study, true impact of vehicle performance on driving style cannot be properly characterized due to heterogeneities in driving style in the driver population. In case of short-duration studies, observed driving style do not stabilize due to variabilities in the choice of routes and departure times.

On the basis of the review of literature presented above, three main limitations can be gleaned: (a) lack of an effective driving style metric, (b) lack of controlled experiments to investigate the impact of vehicle performance on individual driver driving style (c) even fewer long term factorial design driver-vehicle experiments have been conducted.

4.2 Research Questions

The key research questions addressed in this paper are – (a) How different is a single driver's driving style when operating vehicles with different performances? And (b) How different are the driving styles of different drivers operating vehicles of similar performance in the context of both controlled experiments and naturalistic studies?

4.3 Methods

Methods of this study include a proposed approach to characterize driving style, a procedure to compare among different driving styles, and a plan to classify vehicle performance.

4.3.1 Characterizing driving style

The speed-acceleration joint distribution provides a comprehensive signature of driving style for a driver. All the driving style measures discussed in the literature review section are abstractions of the speed-acceleration joint distribution. Liu and Frey, 2015 *(B. Liu & Frey, 2015)* developed vehicle activity envelopes for 100 light-duty vehicles including conventional passenger cars, passenger trucks, and hybrid electric vehicles. Vehicle activity envelope were defined as the 97.5^{th} percentile and 2.5^{th} percentile acceleration values at each of the 16 speed bins. The envelope values were examined across factors such as type of vehicle, type of transmission, road grade, engine horsepower, and power-to-weight ratio. Since the acceleration envelope values were found to be robust across all the factors considered, the combined activity envelope can be considered as the benchmark of real-world driving. Liu and Frey corrected the instantaneous accelerations with the measured road grades as shown in Equation 4.1 *(Bachman, 1998)*.

$$a_e = a + 35.66 \times \frac{RG}{100} \quad (4.1)$$

a_e =effective acceleration, km/h per second
a =acceleration, km/h per second
RG =percent increase in elevation per unit distance (%)

The adjustments made it possible to consistently compare microscale driving activities while accounting for grade. The activity envelope values for effective acceleration of a real world fleet is listed in Table 4.1. Envelopes for standard drive cycles such as FTP, HWFET, SCO3, and US06 have been compared against the envelope of real-world vehicle fleet. However, no numerical measure of comparison was defined in their work. In this paper we define a new metric termed 'envelope deviation' to quantitatively characterize the deviation of joint speed-acceleration distribution of drive cycles in relation to the real-world vehicle fleet envelope. Instantaneous envelope deviation is defined as the difference of absolute values of instantaneous acceleration, and the absolute values of envelope acceleration for the mode i.e. positive acceleration or negative acceleration/deceleration (Equation 4.2).

$$d_t = \left|a_{e,t}\right| - \left|E_{\bar{\bar{v}},m}\right| \quad (4.2)$$

d_t = instantaneous envelope deviation at time t (mph/s)
$E_{\bar{\bar{v}},m}$ = effective envelope acceleration for speed bin $\bar{\bar{v}}$ and mode m (mph/s)
$a_{e,t}$ = instantaneous effective acceleration at time t
$\bar{\bar{v}}$ = speed bins as left-open right-closed (mph; 16 from 0 -75+ mph) at time t
m = logical at time t; 1 if $a_{e,t} \geq 0$ (for acceleration), else 0 (for deceleration)

For example, if a driver has a positive acceleration (m=1) while driving at 33 mph ($\bar{\bar{v}}$ = 30-35 mph), then the effective envelope acceleration would be the 97.5th percentile acceleration for the speed bin ($E_{30-35,1}$= 3.84 mph/s). In contrast, if a driver has a negative

acceleration (m=0) while driving at 50 mph ($\bar{\bar{v}}$ = 50-55 mph), then the effective envelope acceleration would be the 2.5th percentile acceleration for the speed bin ($E_{50-55,0}$= -1.94 mph/s).

Table 4.1. Activity Envelope Values for Real-World Vehicle Fleet *(B. Liu & Frey, 2015)*

Speed Bin, $\bar{\bar{v}}$ (mph)	**Bounds of Acceleration Envelopes by Speed Bin**	
	Effective 97.5th Percentile Acceleration, $E_{\bar{\bar{v}},1}$ (mph/s)	Effective 2.5th Percentile Acceleration, $E_{\bar{\bar{v}},0}$ (mph/s)
0-5	1.69	-2.97
5-10	5.70	-6.04
10-15	5.48	-6.01
15-20	4.87	-5.77
20-25	4.75	-5.21
25-30	4.50	-4.75
30-35	3.84	-4.12
35-40	3.08	-3.39
40-45	2.37	-2.68
45-50	2.12	-2.20
50-55	1.89	-1.94
55-60	1.75	-1.85
60-65	1.66	-1.62
65-70	1.38	-1.44
70-75	1.35	-1.22
75+	1.44	-1.05

The empirical distribution of d_t provides aggressiveness characteristics of the drive cycles. Negative deviation values mean the acceleration or deceleration response for that instance was within the real-world vehicle fleet envelope. In contrast, positive deviation values suggests the instantaneous acceleration and deceleration values are more aggressive than the envelope. If the distribution of d_t were drawn for the accumulated real-world vehicle fleet, 95 percent of the distribution will fall in the negative side and 5 percent of the

distribution will fall in the positive side. Distributions of envelope deviation for standard driving cycles are shown in Figure 4.1.

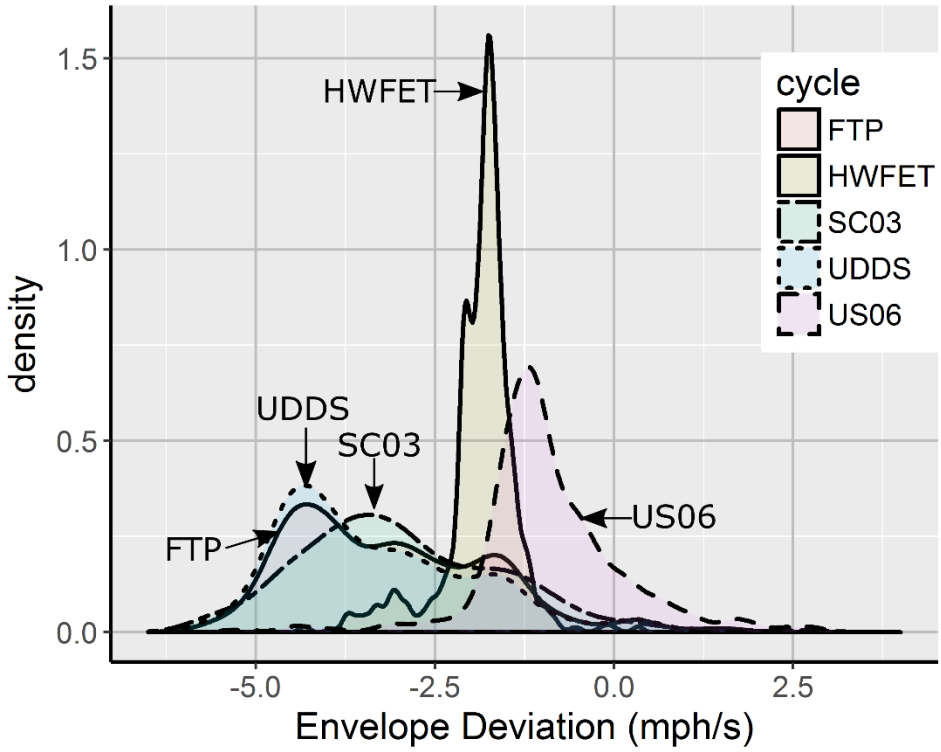

Figure 4.1. Distributions of envelope deviation for standard driving cycles

The FTP cycle has about 3.4% of the envelope deviation distribution in the positive side and the mass of the distribution is flatter compared to the other drive cycles. The HWFET cycle has only 0.52% in the positive envelope deviation zone with a sharp peak close to the zero deviation value. The UDDS and SC03 cycles follows the FTP distribution closely with 3.5% and 2.9% in the positive envelope deviation zones respectively. The US06 driving cycle has 15.3% in the positive zone with a peak concentrated near the zero deviation. US06 is a well-known aggressive cycle; where FTP and UDDS (UDDS is a part of the FTP cycle) are mild cycles i.e. acceleration is limited around 3.5 mph/s. Hence, envelope deviation analysis of standard drive cycles meets expectation.

4.3.2 Comparing driving styles

Driving styles are compared by comparing the empirical distributions of d_t based on 1 Hz data. No assumptions regarding the underlying distribution of envelope deviation was made. The two-sample Kolmogorov–Smirnov test (K–S test) was selected as the nonparametric method to compare two distributions, as it has sensitivity to differences in both the location and shape of the empirical distributions of the two samples. The test statistic for two-sample K-S test, D represents the maximum distance between the two empirical cumulative density functions under consideration. Although the test statistic, D is robust in presence of ties in values of underlying distributions and large sample sizes, the p- value is not. Therefore, even if the null hypothesis is rejected i.e. p-value < significance level (α) it does not always infer that the two-samples came from different populations. In this paper, comparison of driving styles will be conducted by calculating K-S test statistics, D of the two microscale activity samples, termed as 'Distance'. Only when the null hypothesis is accepted i.e. p-value > α, the condition is reported.

4.3.3 Classifying vehicle performance

Vehicle performance depends on multiple factors such as engine size, fuel type, transmission types, weight, engine horse power, and can depend on mileage, age, and other factors. In the context of understanding vehicle performance impact on driving style, only the factors which directly affect microscale activity are considered. The vehicle power-to-weight ratio has been found to be inversely correlated with vehicle acceleration potential i.e. time for 0 to 60 mph. However, very few studies verified the impact of vehicle power-to-weight ratio on real-world driving style. Andre, 2006 *(Andre, Joumard, Vidon, Tassel, & Perret, 2006)* found that vehicles with power-to-weight ratio greater than 0.037 hp/lb enabled higher aggressiveness

than vehicles with less power-to-weight ratio. Berry, 2010 *(Berry, 2010)* found that drivers of vehicles with power-to-weight ratio between 0.04 hp/lb and 0.05 hp/lb have significantly higher aggressiveness than those operating vehicles of power-to-weight ratio greater than 0.05 hp/lb or less than 0.04 hp/lb. Since a complete range of vehicle power-to-weight ratio cannot be tested in both the controlled experiments and naturalistic studies conducted in this study, each vehicle has been assigned to one of three classes of power-to-weight ratio. Low performance vehicles were chosen to be with power-to-weight ratio less than 0.037 hp/lb, medium performance vehicles were selected as having power-to-weight ratio between 0.037 hp/lb and 0.05 hp/lb, while vehicles with power-to-weight ratio greater than 0.05 hp/lb were considered as high performance vehicle. No super-high-performance vehicle such as sports cars (usually power-to-weight > 0.06 hp/lb) and supercars was used as a part of this study.

4.4 Study Data

Both controlled experiments and naturalistic driving studies were performed to understand the effect of vehicle performance on driving style. Microscale driving activity and vehicle dynamics information on predetermined routes were gathered from controlled experiments. In contrast, the naturalistic study focused on a smaller number of drivers over a longer time period.

4.4.1 Controlled experiment data

The details of the controlled experiment including selection of vehicles, drivers, route, time-of-day, and quality control process is described in Frey et al, 2008 *(Frey et al., 2008).* Field measurements of microscale vehicle activity and tailpipe emissions were conducted for 5 drivers tagged randomly to preserve anonymity. The measurements resulted in 17 driving trials with Driver 1, 2, 3, 4, and 5 operating 7, 4, 2, 2, and 2 different vehicles respectively.

Driver and vehicle attributes were recorded at the beginning of each experiment. The specifications of the selected vehicles are shown in Table 4.2.

Two origin destination (O-D) pairs – one from North Carolina State University campus to North Raleigh and another from North Raleigh to Research Triangle Park were selected as the real-world routes to conduct the controlled experiment. The routes are selected to include a wide range of variability in the regular traveling conditions. A combination of roads with different functional categories such as freeways, ramps, major arterials, minor arterials, and feeder/collector streets were part of the selected routes. Also, the operating condition of the selected routes captured a broad range of engine load which was suitable for studying the impact of vehicle performance on driving style.

Instantaneous vehicle speed was recorded from the CANbus system of the vehicles though the on-board diagnostic (OBD) port. An OBD link scan tool was used as a recorder of the engine data. Instantaneous acceleration (1 Hz) was calculated from the speed by subtracting the previous speed instance from the current instance. Location of the vehicles were measured using Global Positioning System (GPS) receivers. The height information from the GPS integrated with data from a barometric altimeter provided estimation of the road grade *(Yazdani Boroujeni & Frey, 2014)*.

Tagging for the Test ID field in Table 4.2 is done in such a way that the first part of the test ID contains driver ID, the second part consists of the vehicle performance class ID (1, 2, 3 represents low performance, medium performance, and high performance vehicles), the third part contains unique vehicle ID, and the fourth part represents the test year (YY format).

Table 4.2 Specifications of the Vehicles Analyzed in the Controlled Experiment

Driver ID	Test ID[1]	Body Type	Model Year	Make and Model	Engine Disp. (L)	Power (hp)	Curb Weight (lbs)	Power-to-Weight (hp/lb)
1	1-1-1-13	Minivan	2006	Dodge Caravan	3.3	180	4,350	0.033
1	1-1-2-13	SUV	2013	GMC Terrain	2.4	182	3,853	0.037
1	1-2-3-13	Sedan	2012	Ford Fusion	2.5	175	3,285	0.039
1	1-2-4-13	Sedan	2012	Dodge Avenger	2.4	173	3,400	0.038
1	1-2-5-13	Minivan	2012	Toyota Sienna	3.5	266	4,310	0.044
1	1-2-6-13	Sedan	2012	VW Passat	2.5	170	3,166	0.038
1	1-3-7-13	Sedan	2008	Chevy Impala	3.5	211	2,655	0.059
2	2-2-8-13	Sedan	2012	Ford Fusion	2.5	175	3,285	0.039
2	2-2-9-13	Sedan	2007	Honda Accord	2.4	166	3,321	0.040
2	2-2-10-16	Minivan	2017	Kia Sedona	3.3	276	4,443	0.045
2	2-3-11-16	Sedan	2013	Chevy Impala	3.6	301	3,555	0.067
3	3-1-12-13	Sedan	2003	VW Jetta	2.0	115	2,934	0.030
3	3-2-13-16	Sedan	2007	Volvo S60	2.5	208	3,501	0.046
4	4-3-14-16	Sedan	2016	Chev. Impala	3.6	305	3,841	0.064
4	4-3-15-16	SUV	2017	Kia Sorento	3.3	290	4,369	0.053
5	5-2-16-13	SUV	2008	Nissan Xterra	4.0	261	4,387	0.048
5	5-2-17-16	Sedan	1998	Nissan Maxima	3.0	190	3,025	0.044

[1]Test ID represent four parts as Driver ID-Vehicle Class ID-Vehicle ID-Test Year

4.5 Naturalistic driving dataset

Naturalistic driving data for this study were collected using an on-board logging system called ‘i2D’ *(Livedrive,)*. The system consists of an on board unit (OBU), a mobile communications network (via M2M protocols), and a secure cloud database. The OBU connects to the vehicle OBD-II interface, and includes a GPS sensor along with a 3D accelerometer and a barometric altimeter. Multiple engine and vehicle dynamics measures are acquired from the OBU at high resolution (1 Hz) and transmitted to the cloud database using mobile communications every 23 seconds. An illustration of the device is shown in **Figure 4.2**.

Figure 4.2 (Left) i2D device connected to the vehicle. (Right) I. the device II. antenna III. OBD-II connector cable

Participation in this study was voluntary and 35 drivers were recruited randomly in Raleigh, NC. The study participants were anonymized and were not provided with any specific instructions during the study. The observed vehicles used were personal vehicles of

the participants. Participants were not required to disclose their vehicle specific information to maintain anonymity. Participants were mostly university staff and students with age ranging from 20 years to 68 years. Out of the 35 participants, 25 were male and 10 were female. A total of 24 months of data were collected. Data collection started in April 2014 and ended in March 2016.

Participants were asked whether they would volunteer to disclose their vehicle type and usage information through a questionnaire. Out of the 35 participants, we received responses from only 5 drivers; of those only 2 used multiple vehicles during the study. To protect the privacy of the questionnaire respondents, only generic information regarding their vehicles such as fuel type, engine size, horse power, and gross vehicle weight were asked.

Table 4.3 includes information of the 7 driver-vehicle combinations studied from the naturalistic driving experiment based on the drivers who provided sufficient information. Tagging for the Test ID is done in a way which preserves both the vehicle and the driver information. The first letter part indicates the driver and the second numeric part represents the vehicle performance class.

Table 4.3 Specifications of the Selected Vehicles in the Naturalistic Driving Experiment

Driver ID	Test ID	Engine Disp. (L)	Power (hp)	Curb Weight (lbs)	Power-to-Weight (hp/lb)
A	A2	5.3	320	5,400	0.048
A	A1	1.8	126	2,700	0.035
B	B2-1	2.5	165	3,140	0.039
B	B2-2	2.0	148	2,696	0.041
C	C1	2.2	136	2,998	0.035
D	D1	2.0	146	2,809	0.037
E	E2	3.0	200	3,340	0.045

4.6 Results and Discussion

Aggregate driving activity statistics for different Test IDs were analyzed. The joint speed acceleration distributions across different groups were compared. The driving style measure 'envelope deviation' was calculated for each driving styles and the effect of different vehicle power-to-weight classes on the estimated measure is discussed.

4.6.1 Aggregate microscale driving statistics

The distributions of acceleration regardless of speed, for most driving styles appears to be surprisingly similar, with sharp peaks around 0 mph/s (Figure 4.3). Even after adjusting for idling time, acceleration distribution peaked sharply on the mean (mode and mean are similar because of symmetry in distribution), which is consistent with previous studies (*Federal test procedure review project: Preliminary technical report. technical report.*1993). Another feature to notice is the discrete nature of acceleration; as speed is recorded in the naturalistic study as discrete integers, there are a finite number of accelerations possible for the finite combinations of speeds.

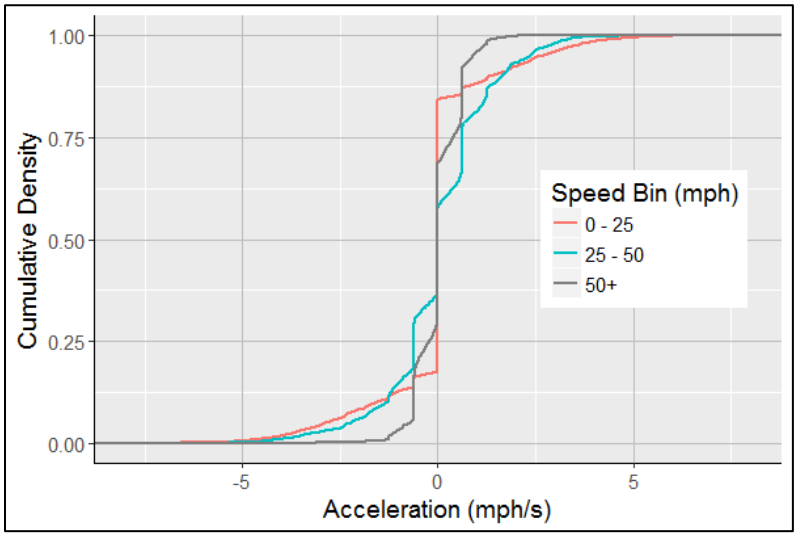

Figure 4.3 Cumulative Density Function of Acceleration for Dodge Caravan (1-1-1-13) at different speed bins [n=15,450]

4.6.2 Joint speed-acceleration distributions

The joint speed-acceleration distribution for the *same driver* of the controlled experiment operating two vehicles with varying performance classes is shown in Figure 4.4. The black lines represent real-world fleet activity envelope to provide context to the joint distribution. The visual representation of the distribution gives indication of the range of performance from these vehicles.

The overlapping nature of the points is shown in the heat-map style binned density plot. There are more extreme points in high performance vehicle class than low performance vehicles. For example, instances of acceleration greater than 5 mph/s in speeds over 40 mph were found in high performance vehicle class. However, those points are sporadic and random; suggesting that even though there is the capability to perform high acceleration and deceleration events in high performance vehicles, the driver is rarely taking advantage of them.

Similar comparisons were done for other drivers for both controlled and naturalistic studies using multiple vehicle performance classes. The speed-acceleration joint distributions were found to be similar with varying levels diffusion of the points near the edge of the distributions.

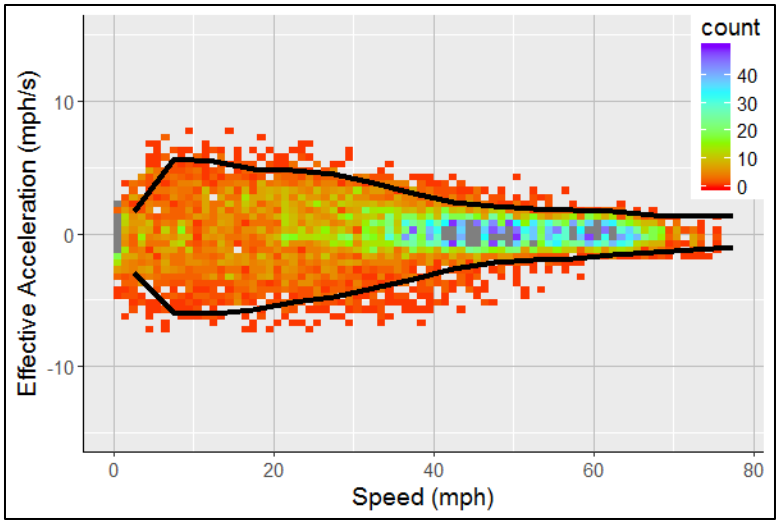

(a)

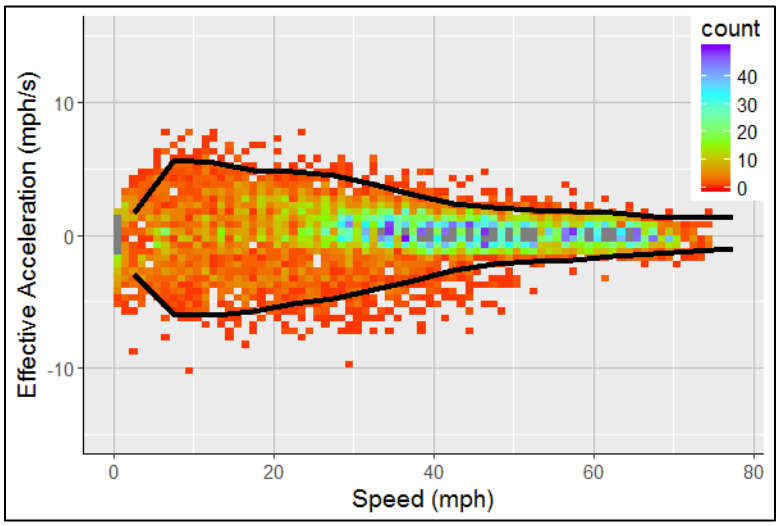

(b)

Figure 4.4 Joint speed-acceleration distribution binned density plot for (a) Dodge Caravan (1-1-1-13) (b) Chevrolet Impala (1-3-7-13). Black lines represents real-world vehicle activity envelope

4.6.3 Envelope deviation in controlled experiments

Descriptive statistics such as percent of area in positive, mean, and median of the developed measure envelope deviation were calculated. By plotting all these variables against vehicle power-to-weight ratio, a very weak relationship with considerable variability was observed (Figure 4.5). Also, the slopes of the fitted lines in Figure 4.5 do not imply significant relationships.

The common expectation is that the more powerful the vehicle, the more they will generate deviations that exceed the real-world activity envelope i.e. by greater than 5%. In this study, 12 out of 16 cycles surpassed the 5% threshold. There was no indication of high-performance vehicles exceeding the threshold more than the low performance vehicles; in fact medium performance vehicles generated both the highest and lowest aggressive cycles (p-value for the regression slope in Figure 4.5a was 0.74). The most aggressive cycle from a 2012 VW Passat and the least aggressive cycle from a 2012 Ford Fusion had power-to-weight ratios 0.038 hp/lb and 0.039 hp/lb respectively. In addition, the lack of samples from very low and very high performance vehicle categories may have contributed to the insignificance of the relationship.

Pairwise comparisons of the cycles using all data for each cycle under consideration were done using the two-sample K-S test statistic, D. Comparison of cycles from driver 1 with the cycles from driver 2 showed high D values ranging from 0.11 to 0.18. However, no pattern was detected which shows cycles from medium performance vehicles in driver 1 had greater similarity with the ones from driver 2. The cycles recorded with driver 1 showed high variability in observed D – 0.04 to 0.15. It shows that the true signal of a driving style may get unclear from the noise induced by the traffic conditions (even the controlled experiments cannot control for all the nuances of the testing routes).

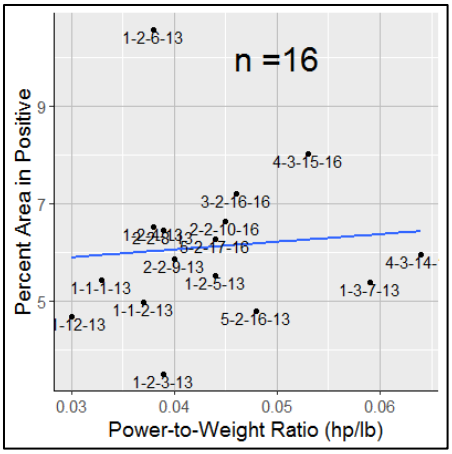

(a)

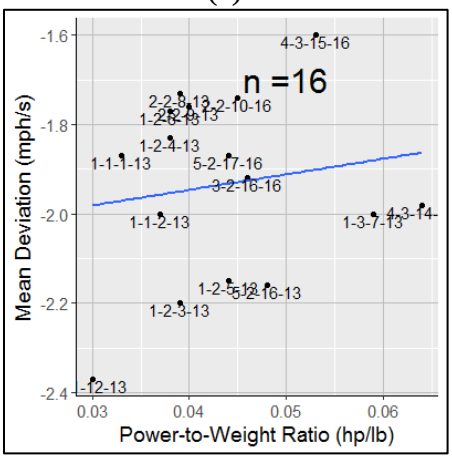

(b)

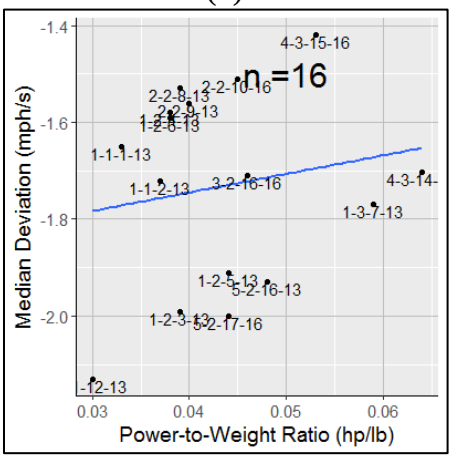

(c)

Figure 4.5. Measured variabilities in the summaries of envelope deviation distributions under varying power-to-weight (a) percent of area in positive (b) mean deviation (mph/s) (c) median deviation (mph/s)

Table 4.4 includes a sample of the comparison between selected cycles from driver 1 and driver 2. Comparison of cycles from driver 1 with the cycles from driver 2 showed high D values ranging from 0.11 to 0.18. However, no pattern was detected which shows cycles from medium performance vehicles in driver 1 had greater similarity with the ones from driver 2. The cycles recorded with driver 1 showed high variability in observed D – 0.04 to 0.15. It shows that the true signal of a driving style may get unclear from the noise induced by the traffic conditions (even the controlled experiments cannot control for all the nuances of the testing routes).

Table 4.4 Example Two-Sample K-S Test Statistics, D for Pairwise Comparison of Deviation Distributions from Baseline in Controlled Experiments

ID	**1-1-1-13**	**1-2-3-13**	**1-2-4-13**	**1-2-5-13**	**1-2-6-13**	**1-3-7-13**	**2-2-8-13**	**2-2-9-13**	**3-2-13-16**
1-1-1-13	0*	0.13	0.05*	0.12	0.09	0.06	0.17	0.16	0.10
1-2-3-13		0*	0.13	0.04	0.15	0.08	0.17	0.18	0.16
1-2-4-13			0*	0.11	0.05	0.09	0.14	0.15	0.21
1-2-5-13				0*	0.12	0.06	0.15	0.16	0.18
1-2-6-13					0*	0.12	0.18	0.19	0.12
1-3-7-13						0*	0.11	0.11	0.06
2-2-8-13							0*	0.002*	0.26
2-2-9-13								0*	0.25
3-2-13-16									0*

*represents failure to reject the null hypothesis. Dark grey shaded cells represent intra-driver-vehicle variability for Driver 1- Vehicle Performance Class 2. Dark grey and light orange shaded cells in combination represent inter-vehicle heterogeneity for Driver 1.

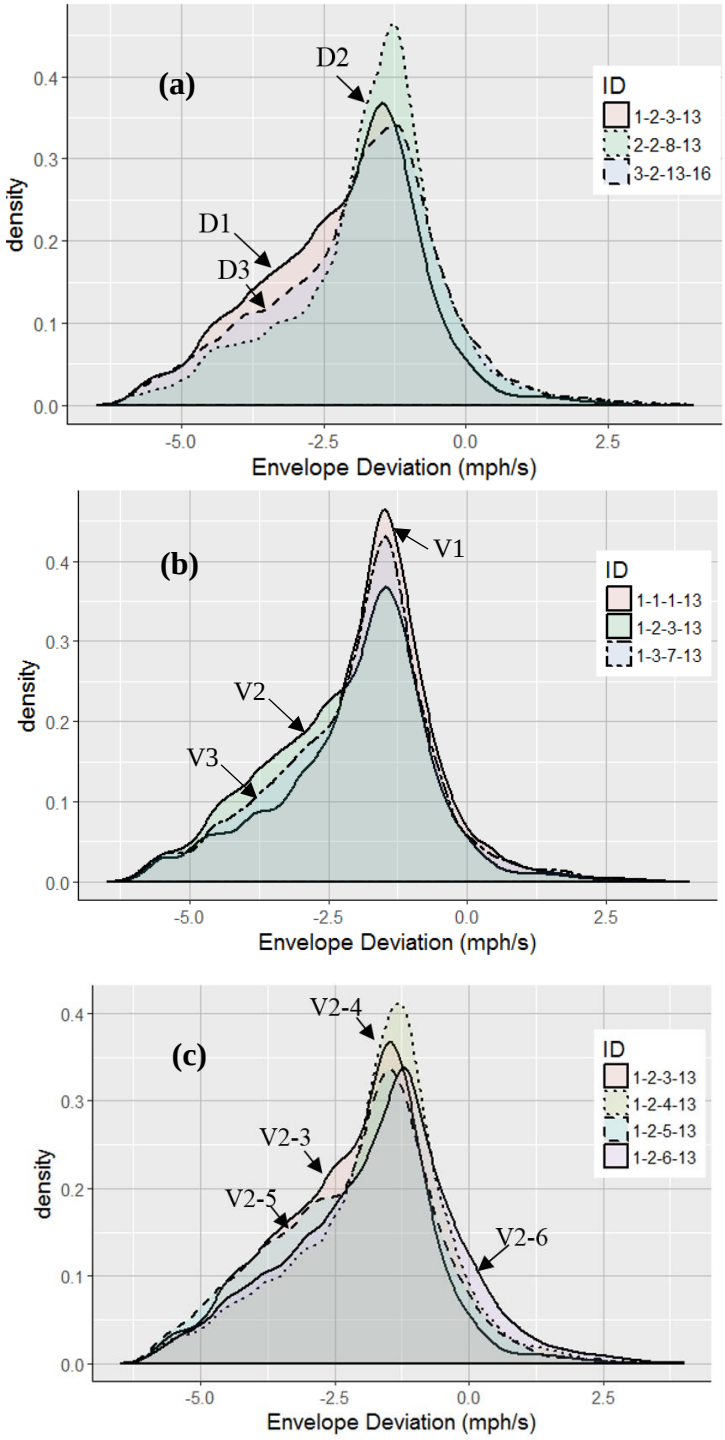

Figure 4.6. Comparison of envelope deviation distributions for the controlled experiment (a) driver 1,2, and 3 tested in medium performance vehicles (0.037 hp/lb < power-to-weight < 0.05 hp/lb) (b) for driver 1 for three vehicle performance classes (c) driver 1 tested at multiple medium performance vehicles

Distances among the envelope deviation distributions for the same driver were found to be in the range of 0.002 – 0.13. This is the inter-vehicle heterogeneity component of driving style controlling for the driver. The mean distances among the vehicles used by driver 1 was 0.09 (found from averaging all the shaded items in Table 4.4), by driver 2 was 0.002, driver 3 was 0.03, driver 4 was 0.05, and driver 5 was 0.03. The average of the mean driver distance was 0.044.

To compare drivers assuming vehicle performance is the same, distances among the empirical envelope deviation distributions for the same vehicle performance class were calculated. This distance is a measure of inter-driver heterogeneity of driving style when controlling for vehicle performance classes (Figure 4.6a). Inter-driver heterogeneity was found in the range of 0.002 – 0.19. The mean distance among the drivers driving low performance vehicles is 0.08, among drivers driving medium performance vehicles is 0.11, and among drivers driving high performance vehicles is 0.12. The average K-S test statistics representing the inter-vehicle component of driving style was 0.1, which is about 2.5 times higher than the case when controlling for the driver but varying vehicle performance.

Both of the previous measures were calculated while controlling for either vehicles or for the driver. However, there were conditions in this experiment where the same driver-vehicle combination were replicated multiple times. If hypothetical 'true' styles for each driver-vehicle combinations were present, multiple observations would help us identify those. In this case, multiple observations were used to quantify the variability of the measured statistic, D. This variability is termed as the intra-driver-vehicle variability.

For example, the intra-driver-vehicle variability for Driver 1 in medium vehicle performance group was 0.10. Intra-driver-vehicle variability for Driver 2 in medium vehicle

performance group was small, at 0.002. The high variability in the first case may be due to unobserved variation by congestion along the test route on a particular day. Only observable congestion indicators on the test routes were average speed on the routes which were 27.8 mph (1-2-3-13), 30.1 mph (1-2-4-13), 29.3 mph (1-2-5-13), and 31.3 mph (1-2-6-13). Intra-driver-vehicle variabilities did not show any correlation to the observed cycle average speed.

4.6.4 Envelope deviation in naturalistic studies

The envelope deviation distributions for the naturalistic study are plotted together in Figure 4.7. The amount of variability in distances among the 7 driver-vehicle combinations were found similar to that of the controlled experiment driving cycles. However, the percent of the area in positive in the naturalistic observations was in the range of 5% to 7% which is narrower than the range for controlled experiments (4% to 10%).

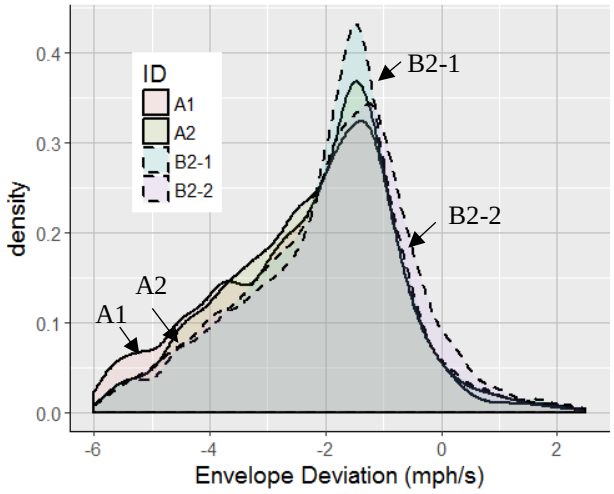

Figure 4.7. Comparison of envelope deviation distributions for 7 naturalistic driver-vehicle combinations

Both driver A and driver B had each generated long-term microscale activity data from two different vehicles. One of the vehicles used by driver A (ID = A2) had very

different engine characteristics than the other. However, the K-S test statistic between A1 and A2 were found to be 0.05, which is comparable to the inter-vehicle heterogeneities estimated for controlled experiments. The two vehicles used by driver B were from medium vehicle performance class. Distance between B2-1 and B2-2 was found 0.04.

Driver E was found to be the most aggressive driver in the naturalistic vehicle fleet. This may either be attributed to the higher performance of the vehicle relative to the vehicles of the fleet or to the inherently 'aggressive' nature of the driver. Such conclusions cannot be drawn without collecting more data.

4.7 Conclusions and Future Work

The proposed envelope deviation distribution is found to be an effective way of describing driving style. It is essentially a transformation of the joint speed-acceleration distribution of a cycle with respect to the typical real-world driving cycle. Typical real-world drive cycle was defined by the vehicle activity envelope developed from a collection of 100 light-duty vehicles. Hence, envelope deviation distribution is a metric of driver aggressiveness which quantifies the amount of deviation of driving style from the typical vehicle activity.

The standard drive cycles such as FTP, HWFET, SC03, US06, UDDS were compared using envelope deviation distribution. The findings suggest consistency of the envelope deviation with other established measures. However, the advantage of envelope deviation distribution is that it preserves overall dynamics of cycle aggressiveness and enables comprehensive comparison of driving style. This paper has proposed to use *distance* (term given to the two sample K-S test statistic, D) among driving cycles to compare and understand variabilities in driving styles.

To understand variabilities in driving styles with vehicle performance, each controlled and naturalistic study driving cycle was assigned to one of the three vehicle performance classes i.e. low, medium, and high. It was found that difference in driving styles measured as distance can be decomposed into three components – inter-driver heterogeneity, inter-vehicle heterogeneity, and intra-driver-vehicle variability. Inter-driver heterogeneity is variabilities in estimated distances among drive cycles assuming the vehicle performance class was kept the same. Whereas, inter-vehicle heterogeneity is variabilities in measured distances while controlling for the driver. Intra-driver-vehicle variability is the measure of repeatability in estimated driving style metrics for the same vehicle performance class and driver combination.

The decomposition of driving style helped us to answer both the research questions asked previously. Significant differences in a driver driving style at different vehicle performance classes can be implied if the inter-vehicle heterogeneity is significantly higher than the repeatability of the driving cycle measurements i.e. intra-driver-vehicle variability. In contrast, significance in differences among driving styles of different drivers operating vehicles of similar performance can be confirmed when the inter-driver heterogeneity is significantly higher than the intra-driver-vehicle variability component.

In both the controlled experiments and the limited scope of the naturalistic study (not all vehicle classes were available in naturalistic data), it was found that the inter-vehicle heterogeneity is not significantly higher than the intra-driver-vehicle variability. However, inter-driver heterogeneity was significantly higher than the intra-driver-vehicle variability. These findings imply that operating vehicles of different performance classes do not result in significantly different driving styles. Such implication is a useful information for designing

eco-driving schemes where microscale driving data is passively collected from devices such as GPS enabled smartphones, navigation units, among others. While the passive mode of retrieving driving style information helps to substantially increase participation in eco-driving schemes, vehicle related information from the participants is seldom available due to privacy concerns. With the assumption that driving style can be characterized without vehicle related information, information and incentives pertaining to driving style improvements can be provided to the driver directly.

Generalization of the observations from this research is not possible until significant amount of replications are available for a multitude of driver-vehicle combination group. In the future the experimental dataset will be expanded to include more samples of low and high performance vehicle classes. Additional vehicle performance indicators will be explored to examine the high variability of driving styles in the medium vehicle performance class.

4.8 Acknowledgements

This research is funded partially by the US Department of Energy (DOE) Advanced Research Project Agency - Energy (ARPA-E). The authors acknowledge the students of Frey Research Group for collecting and processing real world microscale vehicle activity data. Thomas Chase and Behzad Agdashi from the Institute for Transportation Research and Education have helped with the collection of naturalistic driving data.

4.9 References

Andre, M., R. Joumard, R. Vidon, P. Tassel, and P. Perret. Real-World European Driving Cycles, for Measuring Pollutant Emissions from High-and Low-Powered Cars. *Atmospheric Environment*, Vol. 40, No. 31, 2006, pp. 5944-5953.

Anya, A., N. Rouphail, H. Frey, and B. Schroeder. Application of AIMSUN Microsimulation Model to Estimate Emissions on Signalized Arterial Corridors. Transportation Research Record: Journal of the Transportation Research Board, No. 2428, 2014, pp. 75-86.

Bachman, W. H. *A GIS-Based Modal Model of Automobile Exhaust Emissions*. United States Environmental Protection Agency, Research and Development, National Risk Management Research Laboratory, 1998.

Bandivadekar, A., L. Cheah, C. Evans, T. Groode, J. Heywood, E. Kasseris, M. Kromer, and M. Weiss. Reducing the Fuel use and Greenhouse Gas Emissions of the US Vehicle Fleet. *Energy Policy*, Vol. 36, No. 7, 2008, pp. 2754-2760.

Berry, I. M. *The Effects of Driving Style and Vehicle Performance on the Real-World Fuel Consumption of US Light-Duty Vehicles*. Doctoral dissertation, Massachusetts Institute of Technology, 2010.

Bin, S., and H. Dowlatabadi. Consumer Lifestyle Approach to US Energy use and the Related CO2 Emissions. *Energy Policy*, Vol. 33, No. 2, 2005, pp. 197-208.

Brundell-Freij, K., and E. Ericsson. Influence of Street Characteristics, Driver Category and Car Performance on Urban Driving Patterns. *Transportation Research Part D: Transport and Environment*, Vol. 10, No. 3, 2005, pp. 213-229.

Ericsson, E. Variability in Urban Driving Patterns. *Transportation Research Part D: Transport and Environment*, Vol. 5, No. 5, 2000, pp. 337-354.

Evans, L. *Driver Behavior Effects on Fuel Consumption in Urban Driving*. In Proceedings of the Human Factors Society Annual Meeting, Sage Publications Sage CA: Los Angeles, CA, 1978, pp. 437-442.

Fontaras, G., N. Zacharof, and B. Ciuffo. Fuel Consumption and CO2 Emissions from Passenger Cars in Europe – Laboratory Versus Real-World Emissions. *Progress in Energy and Combustion Science*, Vol. 60, 2017, pp. 97-131.

Frey, H. C., A. Unal, N. M. Rouphail, and J. D. Colyar. On-Road Measurement of Vehicle Tailpipe Emissions using a Portable Instrument. *Journal of the Air & Waste Management Association*, Vol. 53, No. 8, 2003, pp. 992-1002.

Frey, H. C., K. Zhang, and N. M. Rouphail. Fuel use and Emissions Comparisons for Alternative Routes, Time of Day, Road Grade, and Vehicles Based on in-use Measurements. *Environmental Science & Technology*, Vol. 42, No. 7, 2008, pp. 2483-2489.

Graham-Rowe, E., S. Skippon, B. Gardner, and C. Abraham. Can we Reduce Car use and, if so, how? A Review of Available Evidence. *Transportation Research Part A: Policy and Practice*, Vol. 45, No. 5, 2011, pp. 401-418.

Johansson, H., P. Gustafsson, M. Henke, and M. Rosengren. *Impact of EcoDriving on Emissions*. In International Scientific Symposium on Transport and Air Pollution, Avignon, France, Citeseer, 2003.

Kilian, L., and C. Park. The Impact of Oil Price Shocks on the US Stock Market. *International Economic Review*, Vol. 50, No. 4, 2009, pp. 1267-1287.

Liu, B., and H. C. Frey. Measurement and Evaluation of Real-World Speed and Acceleration Activity Envelopes for Light-Duty Vehicles. *Transportation Research Record: Journal of the Transportation Research Board*, Vol. 2503, 2015, pp. 128-136.

Liu, J., A. Khattak, and X. Wang. A Comparative Study of Driving Performance in Metropolitan Regions using Large-Scale Vehicle Trajectory Data: Implications for Sustainable Cities. *International Journal of Sustainable Transportation*, Vol. 11, No. 3, 2017, pp. 170-185.

Livedrive. *i2D Telematics: How does it Work*. www.i2d.co/i2dpubportal/portal/tec.xvw, Accessed August 1, 2017.

Malliaris, A. C., H. Hsia, and H. Gould. *Concise Description of Auto Fuel Economy and Performance in Recent Model Years*. No. 760045. SAE Technical Paper, 1976.

Onoda, T. IEA policies—G8 Recommendations and an Afterwards. *Energy Policy*, Vol. 37, No. 10, 2009, pp. 3823-3831.

Sharer, P., R. Leydier, and A. Rousseau. Impact of Drive Cycle Aggressiveness and Speed on HEVs Fuel Consumption Sensitivity. *SAE Technical Paper*, Vol. 01, No. 0281, 2007.

Song, G., L. Yu, and Y. Zhang. Applicability of Traffic Micro-Simulation Models in Vehicle Emission Estimations: A Case Study of VISSIM. In 91st Annual Meeting of the Transportation Research Board, Washington, DC, 2012.

Stichter, J. S. *Investigation of Vehicle and Driver Aggressivity and Relation to Fuel Economy Testing*. Masters thesis, The University of Iowa, 2012.

Tanvir, S., N. Karmakar, N. M. Rouphail, and B. J. Schroeder. Modeling Freeway Work Zones with Mesoscopic Dynamic Traffic Simulator: Validation, Gaps, and Guidance. *Transportation Research Record: Journal of the Transportation Research Board*. No. 2567, 2016, pp. 122-130.

U.S. Energy Information Administration. *Monthly Energy Review*, 2017.

USEPA. *Federal Test Procedure Review Project: Preliminary Technical Report*. EPA 420-R-93-007. United States Environmental Protection Agency, 1993.

Van Mierlo, J., G. Maggetto, E. Van de Burgwal, and R. Gense. Driving Style and Traffic Measures-Influence on Vehicle Emissions and Fuel Consumption. *Proceedings of the Institution of Mechanical Engineers, Part D: Journal of Automobile Engineering*, Vol. 218, No. 1, 2004, pp. 43-50.

Yazdani Boroujeni, B., and H. C. Frey. Road Grade Quantification Based on Global Positioning System Data obtained from Real-World Vehicle Fuel use and Emissions Measurements. *Atmospheric Environment*, Vol. 85, 2014, pp. 179-186.

Zhou, X., S. Tanvir, H. Lei, J. Taylor, B. Liu, N. M. Rouphail, and H. C. Frey. Integrating a simplified emission estimation model and mesoscopic dynamic traffic simulator to efficiently evaluate emission impacts of traffic management strategies. *Transportation Research Part D: Transport and Environment*, Vol.37, 2015, pp.123-136.

CHAPTER 5

HETEROGENEITY AND CONSISTENCY OF ECO-DRIVING METRICS USING NATURALISTIC DRIVING DATA*

5.1 Introduction

The transportation sector accounts for more than 25% of the total energy supply of the United States. In 2015, petroleum fuels provided about 92% of the total energy used by the transportation sector totaling about 25,000 trillion BTU (US Energy Information Administration, 2016). Personal transportation contributed to 26% of total carbon dioxide (CO_2) emissions (USEPA, 2016). Any policy and operational improvement in reduction of personal transportation petroleum fuel consumption can significantly reduce emissions of greenhouse gases and save millions of dollars in energy import cost. Improvements of vehicle and fuel technologies have significantly increased fuel efficiencies of modern vehicles. Diversified energy sources such as bio-fuels and electric cars have provided means to reduce overall transportation fuel consumption. However, the penetration of improved technologies in the market is gradual due to prohibitive cost of new vehicles; only about 7% of vehicles replaced in a single year (Oak Ridge National Laboratory, 2015). An alternative option is to reduce the vehicle miles traveled that involves either making fewer trips or reducing trip lengths. Unfortunately, any travel demand reduction policy suffers from low acceptance and attainment rates except in densely populated urban areas where commuters have more opportunities for transit and carpooling. Another promising approach is to alter the drivers' current driving style to improve fuel efficiency. This relatively newer approach,

* Part of this chapter is submitted as a paper and in review with Journal of Intelligent Transportation Systems: Technology, Planning, and Operations.

termed eco-driving, is more feasible now than ever before. High resolution driving style can be observed at real-time with the advancements in sensor and communication technologies and information can be provided to the driver through real time wireless communication or internet with advanced analytics at the back-end. As opposed to static eco-driving where instructions to improve driving style is given beforehand and instructions do not change depending on a driver's current driving style, dynamic eco-driving is changing instructions to better suit a particular driver at specific conditions. This paper will focus on dynamic eco-driving capabilities in naturalistic driving.

Effectiveness of an eco-driving scheme depends on how often a driver is following the instruction and to what extent the benefits from saving fuel consumption is important to the driver (Barkenbus, 2010). Drivers may be too accustomed to their usual driving styles. Short-term fuel efficiency can be improved by 25% (Ford Motor Company,), however, without feedback can go down to 5% or no improvements at all. A solution to improve long-term fuel efficiency is to provide feedback and incentives (either monetary or non-monetary) to the drivers. Non-punitive financial controls such as coupons, tax relief, etc. can provide personal incentive to reduce fuel consumption. However, such personal incentive delivery requires a universal tracking method of driving style which is not impacted by the vehicle type and route chosen by the driver. Incentives can be provided when a driver's driving style has improved from a previous time period or when a driver is maintaining an optimal driving style. Therefore, there is a need to develop an unbiased metric of driving style which can be tracked over time and applied similarly to all the drivers participating in an eco-driving scheme.

The purpose of this paper is to develop eco-driving metrics for naturalistic driving where there is no control over the drivers' choice of vehicle and route. An eco-driving metric needs to serve as a benchmark of driving styles. In addition to scoring, the metric needs to enable ranking and grading drivers. Previously, empirical fuel consumption was monitored to serve as an indicator of fuel efficiency and comparison of drivers' fuel efficiency was only possible if vehicle type and route characteristics were controlled. Such controlled experiments are suitable for understanding the effect of vehicle, route, or drivers separately. However, fuel consumption alone without any adjustments for other choices cannot serve as a metric for naturalistic eco-driving schemes.

In the next section, the related literature is reviewed to understand factors influencing actual fuel consumption. Later, data and methodology are described. Results and discussions followed by conclusions are described in the last two sections.

5.2 Literature Review

Actual fuel consumption of a vehicle is affected by multiple factors – vehicle type, roadway factors, meteorological conditions, traffic factors, and driving styles. Vehicle type has the highest impact among all others; EPA reported fuel economy can be as high as 107 miles per gallon for small electric vehicles and as low as 12 miles per gallon (USDOE,). Roadway factors such as road grade and pavement condition has significant effect on fuel economy. Fuel economy of a flat route was found 15% to 20% higher than that of a hilly route (Boriboonsomsin & Barth, 2009). Meteorological conditions such as wind, barometric pressure, and ambient temperature has small impact on the fuel economy. Traffic related factors such as speed and variability of speed due to facility conditions or traffic control devices have significantly greater effect on fuel economy than driving styles

(Boriboonsomsin, Vu, & Barth, 2010). At urban conditions, average speed can explain more than 70% variability in fuel consumption (Evans, Herman, & Lam, 1976). Many later researches argued for the inclusion of acceleration and different functional forms of speed and acceleration to better estimate fuel consumption (Ahn, Rakha, Trani, & Van Aerde, 2002; Jimenez-Palacios, 1998). However, there are small differences between the factors to be considered as traffic stream related and driving style factors. Average speed can be considered as a traffic stream factor for a congested road as drivers need to follow preceding vehicle. In contrast, amount and frequency of acceleration and deceleration is a part of the driving style.

Most previous eco-driving experiments in the literature have, for the most part, included controls on vehicle type and route selection. In controlled experiments a small group of participants are instructed to drive along fixed routes using a pre-defined and similar vehicle (Ishiguro, 1997; Lenner, 1995); comparison among driving styles is made using actual fuel consumption. Barth and Boriboonsomsin used real-time information as speed advisories at different level of services (Barth & Boriboonsomsin, 2009). However, the study was limited to freeways and comparison was done for the same vehicle type and same route. Beusen *et al.* used on-board logging devices to track the long term impact of a static eco-driving scheme using actual fuel savings (Beusen et al., 2009). Rolim *et al.* used similar devices to track the effectiveness of an eco-driving program; however, they used frequency and level of excessive acceleration and declaration to quantify the improvement (Rolim, Baptista, Duarte, & Farias, 2014). Song and Yu normalized average fuel consumption rates with the idling rate to eliminate the effects of engine size, fuel type, and vehicle mass (Song & Yu, 2009). The normalized fuel consumption rate was suitable for estimation of vehicle

type independent fuel economy, however, lacked the quality to serve as a benchmark in comparing trips of different route choice by the same driver.

Dynamic eco-driving metrics needs to allow not only delivery of information but also delivery of incentives. Information delivery as done by Barth and Boriboonsomsin (Barth & Boriboonsomsin, 2009) is a two stage process where driving style is observed and information is delivered. In contrast, incentive delivery requires an additional feedback stage where the driver s performance is observed after information delivery and based on the performance incentive is provided. An eco-driving metric needs to serve as a performance indicator in that case. Performance indicators such as speed and braking are used by an insurance company, Progressive Casualty Insurance Co. (McQueen, 2008), to provide incentives for safety in naturalistic driving. However, there is no reported performance indicator for eco-driving applications that can be used for delivery of incentives.

Observation of long-term eco-driving behavior can provide better insight into driver consistency. Wahlberg (af Wåhlberg, 2007) monitored fuel consumption of buses during 12 months after an eco-driving training and found drivers returned to their previous habits within a small time period. Beusen et al. observed 10 drivers over the course of 10 months (Beusen et al., 2009) including before and after eco-driving training. They found scatter of average weekly fuel consumptions in both stages; making it difficult to measure any significant effect of driving styles. Therefore, it is important to understand usual randomness in driving styles of individual drivers through long-term studies.

On the basis of the review of literature presented above, three main limitations can be gleaned:

a. There is no agreed upon metric which can distinguish the effect of driving styles on fuel consumption from other confounding factors.

b. There is no comparative benchmark of driver behavior that can support the application of eco-driving incentives.
c. Few long-term longitudinal studies of individual driver's driving style were found that can assess the consistency of driving styles over an extended period of time.

5.3 Research Questions

This study attempts at addressing the following research questions:

a. How to develop eco-driving metrics that consider heterogeneity among driving styles only?
b. Are the developed metrics consistent and reasonable as benchmarks?
c. Can the developed metrics be used to rank or grade drivers for incentive development purposes?

5.4 Methodology

Methods of this study includes (a) a description of study data (b) method for benchmarking driving styles (c) method for development of eco-driving metrics (d) methods for characterization of heterogeneity and consistency in driving styles.

5.4.1 Data source

Naturalistic driving data for this study are collected using an on-board logging system called 'i2D'. The system consists of an on board unit (OBU), a mobile communications network (via M2M protocols), and a secure cloud database. The OBU connects to the vehicle's OBD-II interface, and includes a GPS sensor along with a 3D accelerometer and a barometric altimeter (song et al. 2015). Multiple engine and vehicle dynamics measures are acquired from the OBU at high resolution (1 Hz) and transmitted to the cloud database using mobile communications every 23 seconds. An illustration of the device is shown in Figure 5.1.

Participation in this study was completely voluntary and 35 drivers were recruited randomly in Raleigh NC. The study participants were anonymized and were not provided with any specific instructions during the study. All the vehicles used in this study were personal vehicles of the participants and participants were not required to disclose their vehicle specific information to maintain anonymity. Participants were mostly university staff and students with age ranging from 20 years to 68 years. Out of the 35 participants 25 were male and 10 were female. A total of 24 months of data were collected. Data collection started in April 2014 and ended in March 2016.

Figure 5.1. (Left) i2D device connected to the vehicle. (Right) I. the device II. antenna III. OBD-II connector cable

The system assigned a unique trip ID every time drivers started their vehicles. All second-by-second data for a particular trip was tagged with that trip ID. The second-by-second data included engine information such as revolution per minute (RPM), intake air temperature (IAT), manifold pressure (MAP) and vehicle dynamics information such as

vehicle speed. The drivers required to provide their vehicle information such as vehicle model, gross vehicle mass, fuel type at the time of recruitment. Integration of vehicle and engine information enabled the real world instantaneous fuel consumption during a trip. Previous studies have reported that estimation of fuel consumption using internally observed variables can explain 99% of the variability in empirical measurements (Frey, Zhang, & Rouphail, 2008).

In contrast to estimating fuel consumption using internally observed variables, instantaneous fuel consumption can be estimated using vehicle speed, acceleration, and road grade with previous knowledge of the vehicle specification. The latter approach is more suitable for observing driver behavior since the actual fuel consumption is governed by the type of vehicle driven. In the next section, the methodology for benchmarking driving style is discussed based on estimated fuel consumption using instantaneous vehicle speed.

5.4.2 Benchmarking driving styles through standardized fuel use

Driving style of a driver can be observed through the driver's actions. Actions which can possibly affect fuel consumption are speed, acceleration, and braking of the vehicle. Therefore, a benchmark of driving style and consequent fuel consumption needs to be standardized by the actions. Comparing two driver's empirical fuel consumption without standardization is only possible when they are driving the same vehicle type and driving in similar operating conditions.

Benchmarking of a driver's driving style requires standardization for choice of vehicle type and choice of route. This paper deals with standardization for vehicle type choice by assuming all drivers are operating a standard car as their vehicle. The standard car in this study is a 2007 Honda Accord with 2.4L 4-cylinder, 160 hp gasoline engine and a

3100 lb curb weight. Specifications of the standard car along with instantaneous speed, acceleration, and road grade can be combined to get estimate of vehicle specific power (VSP). VSP is a function of vehicle speed, acceleration, and road grade and expresses a vehicle's engine power demand. VSP has been found as an excellent predictor of vehicle fuel use (Jimenez-Palacios, 1998). VSP can be expressed by Equation 5.1. The coefficients in Equation 1 depend on the type of vehicle and for this paper specifications of the standard vehicle (A=0.1565 kW-sec/m, B=2.002×10^{-3} kW-sec^2/m^2, C=4.926×10^{-4} kW-sec^3/m^3, and m=1.479 tonne) were used to estimate all second-by-second VSP values for all drivers. Instantaneous VSP values were mapped into 23 operating mode bins which is a combination of VSP and speed. There is one operating mode bin for braking, one for idling, 6 bins for speeds from 1 mph to 25 mph, 9 bins for speeds 25 mph to 50 mph, and 6 bins for speeds above 50 mph. Corresponding instantaneous fuel consumption values (f_t) were estimated from a previously established relationship between operating modes and fuel consumption for the standard car (Frey & Liu, 2013).

$$\mathrm{VSP} = (\mathrm{A} \times \mathrm{V_t} + \mathrm{B} \times \mathrm{V_t^2} + \mathrm{C} \times \mathrm{V_t^3} + \mathrm{m} \times \mathrm{V_t} \times \mathrm{a_t})/\mathrm{m} \qquad (5.1)$$

Where,

VSP = vehicle specific power, kW/tonne
V_t = speed at time t, m/s
a_t = acceleration at time t, m/s^2
A = rolling resistance coefficient, kW-sec/m
B = rotational resistance coefficient, kW-sec^2/m^2
C = aerodynamic drag coefficient, kW-sec^3/m^3
m = vehicle mass, tonne.

This paper used instantaneous or trip average vehicle speed as a surrogate to express route characteristics. The main route characteristics which change by driver's choice are sequence of facility type (freeway vs. arterial), departure time (pre-peak, peak, or off-peak), and operating conditions of the route (congested vs. uncongested or signalized vs. roundabout). In most cases, average speed for a given trip is controlled by the route characteristics, not by driver's driving style. Standardization of fuel consumption for route choice is possible through fitting multiple expected fuel consumption models at different speed levels. In the next section, two different eco-driving metrics are introduced which incorporates successive standardization of fuel consumption; first for vehicle type choice and then for route choice.

5.4.3 Eco-driving metrics development

The purpose of an eco-driving metric is to compare driving styles across multiple drivers in a naturalistic driving study. The metric is required to reflect changes in driving styles only, not changes in vehicle type choice and route choice. The metric needs to be consistent over time for a given driver if no changes were made in the driver's driving style. Also, the metric needs to be sensitive to the heterogeneity in driving styles among drivers. Variation in the metric is required to be small enough for a given driver to identify significant changes in driving styles across reporting periods.

Another consideration for an eco-driving metric is to demonstrate improvement in driving style when a specific behavior is targeted. In the case of overall driving style improvement, a trip perspective of fuel usage is appropriate to track overall driver behavior change. However, studies exploring trip-level fuel consumption differences when only targeting behavior during parts of the trip (such as braking events), may lack the power to

identify change when all driving events are aggregated into trips. A metric based on trajectory level analysis provides for the ability to segment trips into unique events in order to perform paired comparisons solely on the events of interest.

Standardized fuel consumption cannot be used as eco-driving metrics for several reasons – a) it has no practical meaning to the driver; therefore, it is prone to misinterpretation, b) it does not consider factors such as congestion and route type which is out of driver's control, and c) it has a very low variability within the corresponding trip average speed bin (Figure 5.2 (b)). Therefore, there is a need to make adjustments to the standardized fuel consumption.

Aggregation of instantaneous standard fuel consumption at different resolutions leads to multiple approaches for adjustments by speeds. In each reporting interval (week or month) for an individual driver, adjustments can either be applied to each trip according to trip average speed or at trajectory level according to driver's behavior for each instantaneous speed level across all the trips made by that driver. In this paper two different eco-driving metrics for naturalistic driving are introduced: one based on summary trip characteristics and another based on overall trajectory characteristics.

5.4.4 Fuel efficiency score (FES)

For this study, information from about 42,000 trips were collected. Only trips over 1 mile in length and 1 minute in duration are selected for computing the metric. Trip average speed ($\overline{v_{ik}}$) can be calculated as average of OBD based instantaneous speeds for all the seconds of a trip. Miles per gallon of standard fuel consumption (F_{ik}) was chosen as the indicator of fuel efficiency for the trip.

$$\overline{\mathrm{v_{ik}}} = \frac{\sum_t^T \mathrm{v_{tik}}}{N} \tag{5.2}$$

$$F_{ik} = \frac{2800 * T}{3600} \frac{\sum_t^T \mathrm{v_{tik}}}{\sum_t^T \mathrm{f_{tik}}} \tag{5.3}$$

Where,

$\overline{v_{ik}}$ = average speed for trip *i* for driver *k*, miles/hour

v_{tik} = instantaneous speed for trip *i* at time *t* by driver *k*, miles/hour

F_{ik} = standard vehicle fuel economy for trip *i* by driver *k*, miles per gallon (MPG)

f_{tik} = instantaneous standard vehicle fuel consumption for trip *i* at time *t*, grams/sec.

T = duration of trip *i* in seconds

The relationship between trip average speed ($\overline{v_i}$) and standard MPG (F_i) is shown in Figure 5.2(a). The blue line is a quadratic function (LM) fit to the plot which shows a dip down in MPG at higher trip average speed. However, when a generalized additive model (GAM) was fit with a smooth on average speed as a predictor (considering dimension of basis function as 3), the fit stayed close to an optimal value of standard MPG. The shape of the fit suggests that there are separate distributions for standard MPG values at different speed levels. Cumulative distributions for standard MPG at 10 mph speed bins are shown in Figure 5.2(b). The shape of all the distributions followed similar pattern with long tails on both sides. The median MPG values increased with increase in trip average speed. However, for the last (highest) two speed bins the distributions overlap.

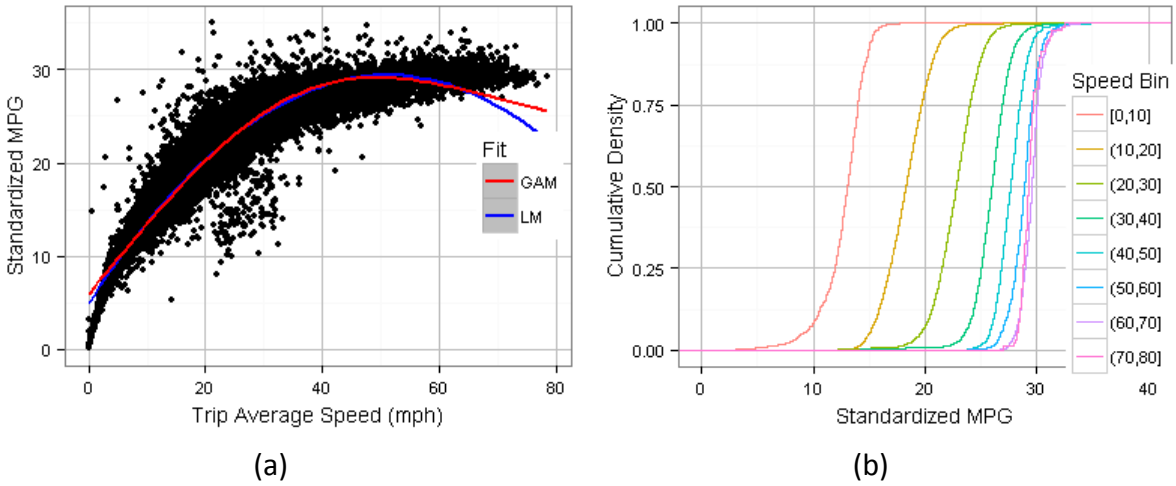

(a) (b)

Figure 5.2. (a) Standardized MPG vs trip average speed (b) Cumulative distribution for standardized MPG at 10 mph trip average speed bins.

The trip based eco-driving metric fuel efficiency score (FES) is developed from the insight gained from Figure 2(b). Since the distributions shown in Figure 2(b) are Gaussian and non-skewed it is safe to assume FES changing linearly between two extreme values. The relative fuel efficiency of the trip with respect to all other trips can be assessed if the trip average speed and trip standardized MPG are known. FES for an individual trip (FES_i) is scaled to vary from 20 to 100, with the minimum value occurring when trip standardized MPG (F_{ik}) is lower than the 10 percentile MPG value (l_j) for the speed bin and maximum value occurring when fi is greater than 90 percentile MPG value (u_j) for the corresponding speed bin. Minimum FES of 20 is chosen because displayed score under 20 may discourage drivers from following the e. Combined FES for all the trips (1, 2, 3,……., I) made during a reporting period (τ) is the trip length weighted summation of FES_{ik} .

$$\text{FES}_{\text{ik}} = 100; if\ F_{ik} > u_j$$

$$\text{FES}_{\text{ik}} = 20; if\ F_{ik} < l_j \tag{5.4}$$

$$\text{FES}_{\text{ik}} = 20 + \frac{(F_{ik} - l_j)}{(u_j - l_j)} * (100 - 20); if\ \ u_j \geq F_{ik} \geq l_j$$

$$FES_k = \frac{\sum_i^I FES_{ik} * \ L_{ik}}{\sum L_{ik}} \tag{5.5}$$

Where,

FES_{ik} = fuel efficiency score for trip *i* for driver *k*

F_{ik} = standard vehicle fuel economy for trip *i* for driver *k*, miles per gallon (MPG)

l_j = 10th percentile standardized MPG at speed bin *j*, interval 10 mph

u_j = 90th percentile standardized MPG at speed bin *j*, interval 10 mph

L_{ik} = trip length for trip *i* for driver *k*, miles

FES_k = fuel efficiency score for *I* trips made during reporting period τ by driver *k*

5.4.5 Fuel use difference (FUD)

The same trips used in calculating FES were also analyzed at the trajectory level. Observations of speed, acceleration, and instantaneous fuel consumption along with other information on vehicle performance are collected in one second intervals. A total of 20,947,617 observations were used in the following analysis after removing all trips shorter than one mile in distance or one minute in travel time. The trajectory level analysis aims to identify trends in standardized fuel consumption among drivers that can be aggregated at the trip or event level in order to track improvements in driver behavior.

The proposed metric for trajectory level analysis is the Fuel Use Difference (FUD), which is calculated as the percentage of instantaneous standard vehicle fuel consumption above or below the estimated fuel consumption at a given instantaneous speed. Fuel

consumption was modeled using a segmented quadratic regression on driver average fuel consumption for a given speed range (fit in 2mph speed bins). Figure 5.3(a) shows the observations of driver average fuel usage (in grams/sec.) for each 2 mph speed bin, meaning that the maximum number of observations in each speed bin is equal to the number of drivers in the sample. Model fitting was performed using a weighted least squares regression on a segmented quadratic model that provides for equal value and slope at the breakpoint. Each driver average fuel usage observation was weighted by the number of seconds of data included in the averaging. The best fit model is described in Equation 5.6, resulting in a standard error of 0.035 g/s.

$$\begin{aligned} &if\ v < 30mph \quad && y = -0.000802v^2 + 0.0498v + 0.266 \\ &else && y = 0.000432v^2 + 0.0243v + 1.377 \end{aligned} \tag{5.6}$$

Where

y = Estimated standardized instantaneous fuel consumption in grams per second

v = Speed bin median (mph)

Using the model fit to driver average fuel usage, FUD is then calculated for each observation of speed according to Equation 5. This value can be averaged for a driver's individual trips or across any subset of a trip depending on the comparison of interest.

$$\begin{aligned} &if\ v_{tk} < 30mph \quad && y_t = -0.000802v_{tk}^2 + 0.0498v_{tk} + 0.266 \\ &else && y_t = 0.000432v_{tk}^2 + 0.0243v_{tk} + 1.377 \\ & && FUD_{tk} = \frac{f_{tk} - y_t}{y_t} * 100 \end{aligned} \tag{5.7}$$

Where,

FUD_{tk} = Fuel use difference at time *t* for driver *k*

y_t = Estimated standardized instantaneous fuel consumption in grams per second at time *t*

f_{tk} = Actual standardized instantaneous fuel consumption in grams per second at time, *t* for driver *k*

v_{tk} = Instantaneous speed in mph at time *t* for driver *k*

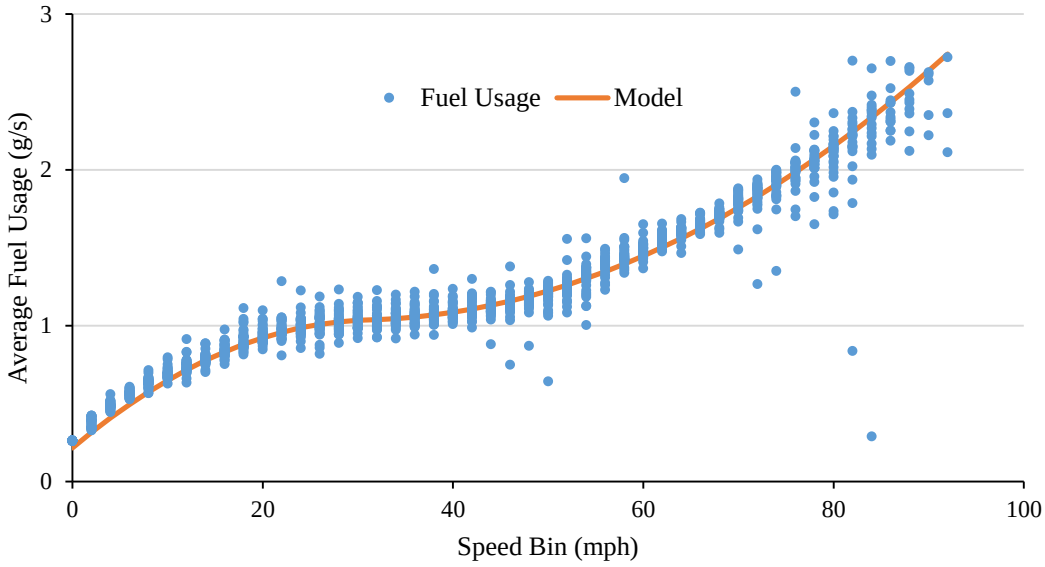

(a)

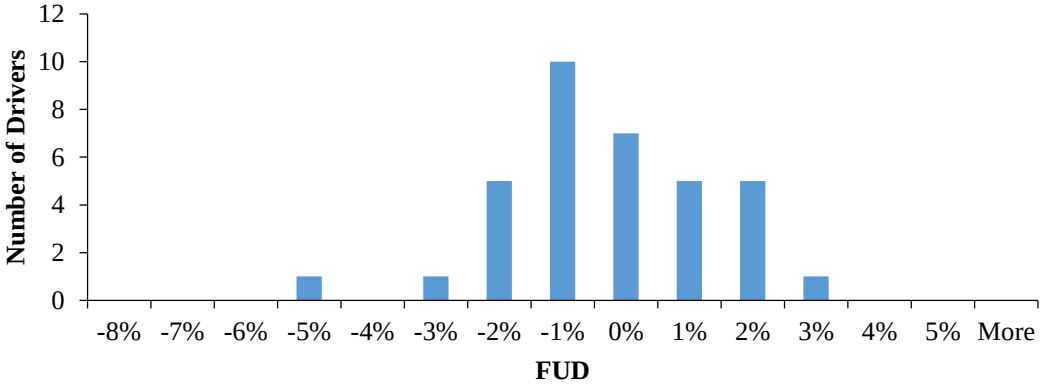

(b)

Figure 5.3. (a) Speed binned average fuel usage by driver vs. segmented model (b) Histogram of overall FUD by driver.

Figure 5.3 (b) shows the distribution of overall driver average FUD across the entire study period. It is important to note that as FUD is aggregated across larger time spans, the

values will tend towards the mean according to the law of large numbers, so these values do not necessarily explain the full range of fuel use differences between drivers.

5.4.6 Characterizing heterogeneity and consistency in driving style

The essence of eco-driving lies in the ability for improving a driver's driving style to reduce fuel use. This infers that at least some drivers in the population are following an optimal style and some drivers are significantly lacking in fuel economy due to their inefficient style. Therefore, an eco-driving metric needs to identify this significant heterogeneity among drivers' styles. This paper uses the Tukey's honest significant difference (HSD) to test whether the monthly scores of a pair of drivers are significantly different. The choice of month as reporting interval as opposed to week may cause a metric to be more centered on the driver mean.

Consistency of a metric requires it remain unchanged for an individual driver if no significant changes have been observed to his/her style. It also infers robustness of a measure. In this study, it is assumed that no changes have been made in drivers' driving styles as no instructions or incentives were given to them. Therefore, consistency of a metric means that its value across the reporting period should not be significantly different across reporting periods for all drivers. Thus, the presence of any time trend such as continuously increasing or decreasing value of the metric would violate the consistency requirement.

5.5 Results and Discussion

FUD is plotted against FES scores at monthly reporting period levels in Figure 5.4(a). Each point is colored by the number of trips used to generate the metrics. The linear fit suggests an inverse relation (slope of -1.37) between the two metrics; meaning the higher the FES, the lower is the FUD (negative FUD implies improved driving style). This is expected as more

fuel efficient drivers are, fewer fuel will be consumed relative to the average fuel consumption.

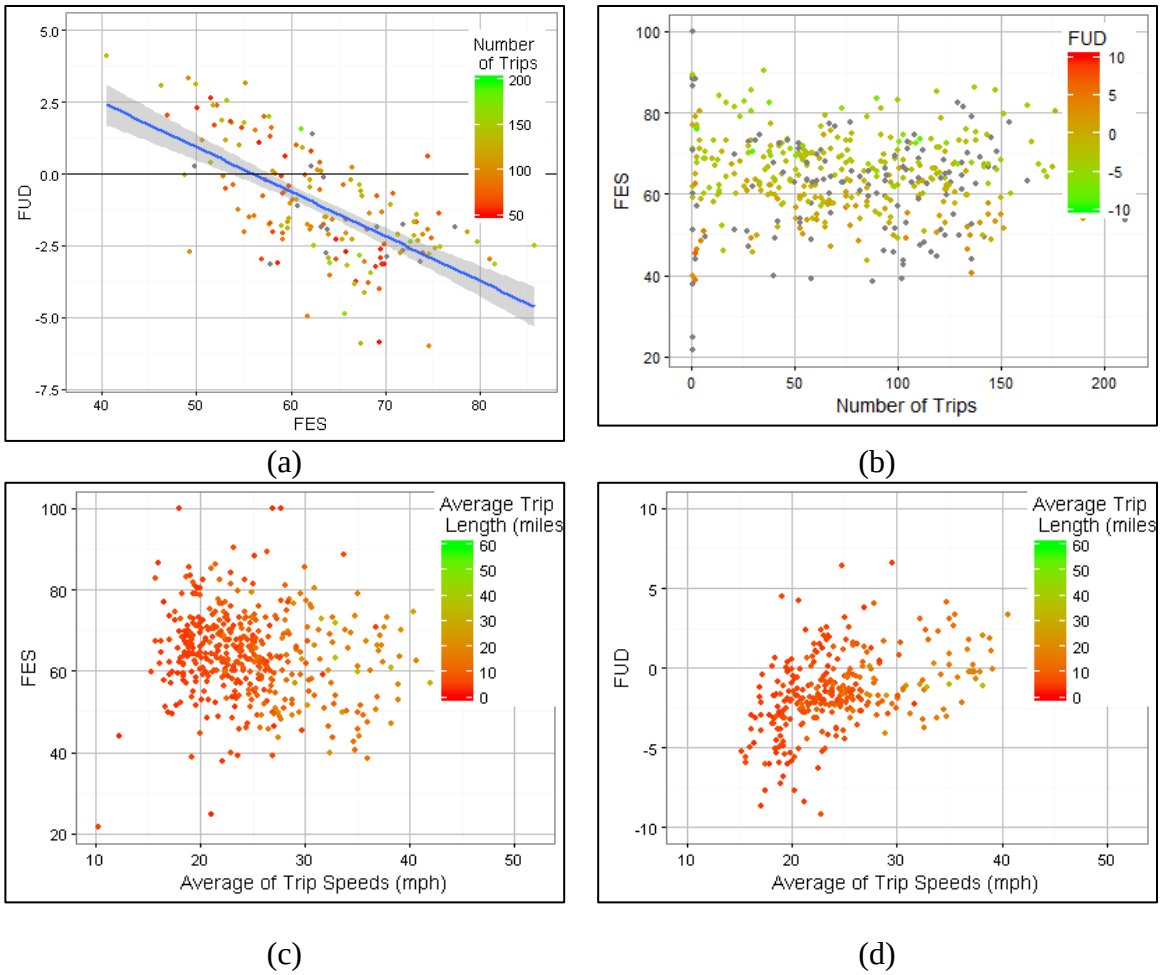

Figure 5.4. (a) Relation between driver FES and FUD at monthly aggregation level (b) Relation of FES and FUD with number of trips. Monthly aggregated eco-driving metrics VS. average of trip average speeds (c) FES (d) FUD.

Even though the overall trend in the relation between FES and FUD matches expectations, the scatter is very high (multiple R^2 value is 0.28); suggesting that calculating one metric and converting them to the other may not provide reliable estimate of the other.

Scatterplots of the two developed metrics against averages of trip average speed and average trip length at monthly reporting period level is shown in Figure 5.4 (c) and (d). Since FES was developed using adjustments for trip average speed, there is no systematic pattern in monthly aggregated FES with average trip speed observed in Figure 5.4(a). However, there appears to be a positive correlation of FUD with average of trip average speeds (Figure 5.4 (b)). This suggests a collection of higher average speed trips during a month will cause FUD to increase; where in reality the same driver could be using different facilities or the operating conditions have changed. There is no significant effect of average trip length on both metrics.

Monthly FES boxplots for each driver across the study period is shown in Figure 5.5. In addition to the 1 minute trip duration and 1 mile trip length filter, only driver-month combinations containing more than 30 trips were selected to remove bias in sample. Simple one-way analysis of variance (ANOVA) test was done with driver as a factor to test if FES varied significantly across drivers. Driver was found to be a significant factor from ANOVA.

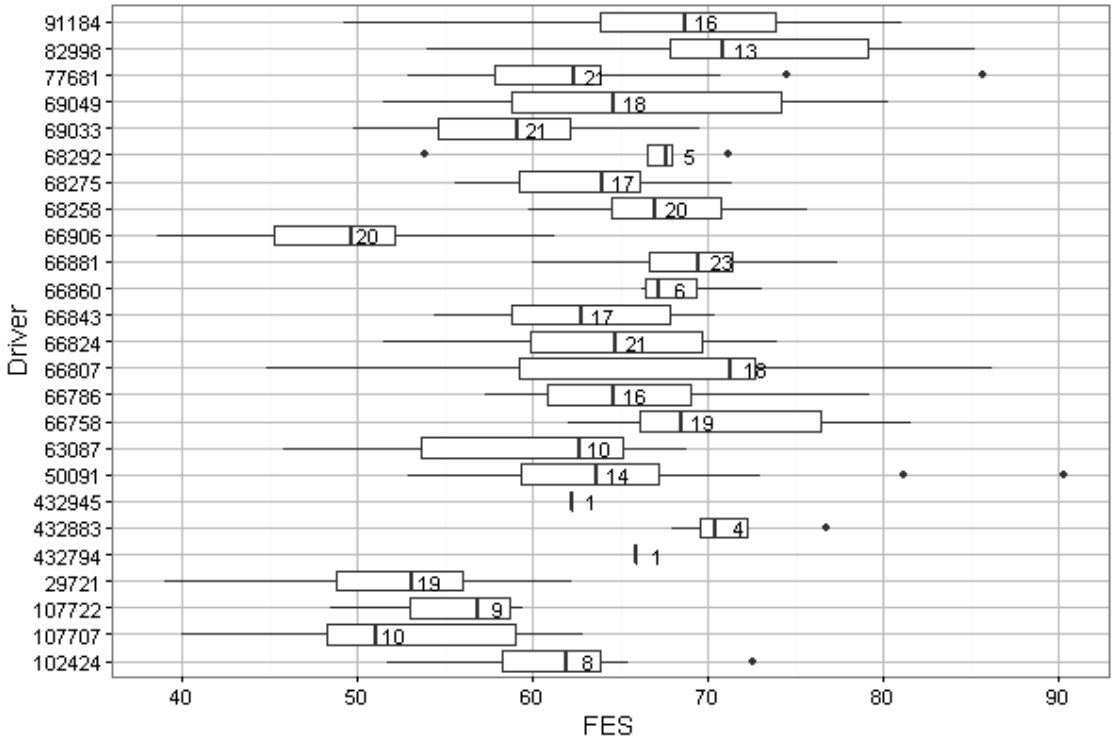

Figure 5.5. Boxplots of monthly FES for each driver across the study period. Number inside the box indicate total number of months of data used to generate that boxplot.

The result from ANOVA was used to compute Tukey's HSD for pairwise comparison. Tukey's HSD of 8.6 was computed for the monthly FES. Based on this, Table 5.1 was generated to group drivers into similar clusters. Only drivers having at least 10 months of FES score were included in this grouping. Drivers with the same letter group are not significantly different. The mean FES value for the drivers ranged from 73 to 49. Four categories of drivers can be found in the data – 2 drivers with FES above 70, 8 drivers having FES in 65-70 range, 5 drivers in FES 55-65 range, and 3 drivers with FES below 55. In summary, this analysis has confirmed the hypothesis of the presence of heterogeneity across drivers based on their driving style.

Table 5.1. Grouping of Drivers according to Monthly FES

Tukey's HSD Groups							Treatments (Driver ID)	Means (FES)
A							82998	73
A	B						66758	71
A	B	C					66881	69
A	B	C	D				91184	68
A	B	C	D				66807	68
A	B	C	D				68258	68
A	B	C	D	E			66786	66
A	B	C	D	E			69049	66
A	B	C	D	E			50091	66
A	B	C	D	E			66824	65
	B	C	D	E			68275	63
		C	D	E			77681	63
		C	D	E			66843	63
			D	E	F		63087	59
				E	F		69033	59
					F	G	107707	52
					F	G	29721	52
						G	66906	49

Consistency of the developed metrics were tested in three steps – first the temporal progression of the metric was modeled with month as a predictor using one-way ANOVA. Second, individual driver time series were tested for stationarity. Finally, the coefficient of variation or standard deviation of a metric for an individual driver was calculated as a measure of dispersion.

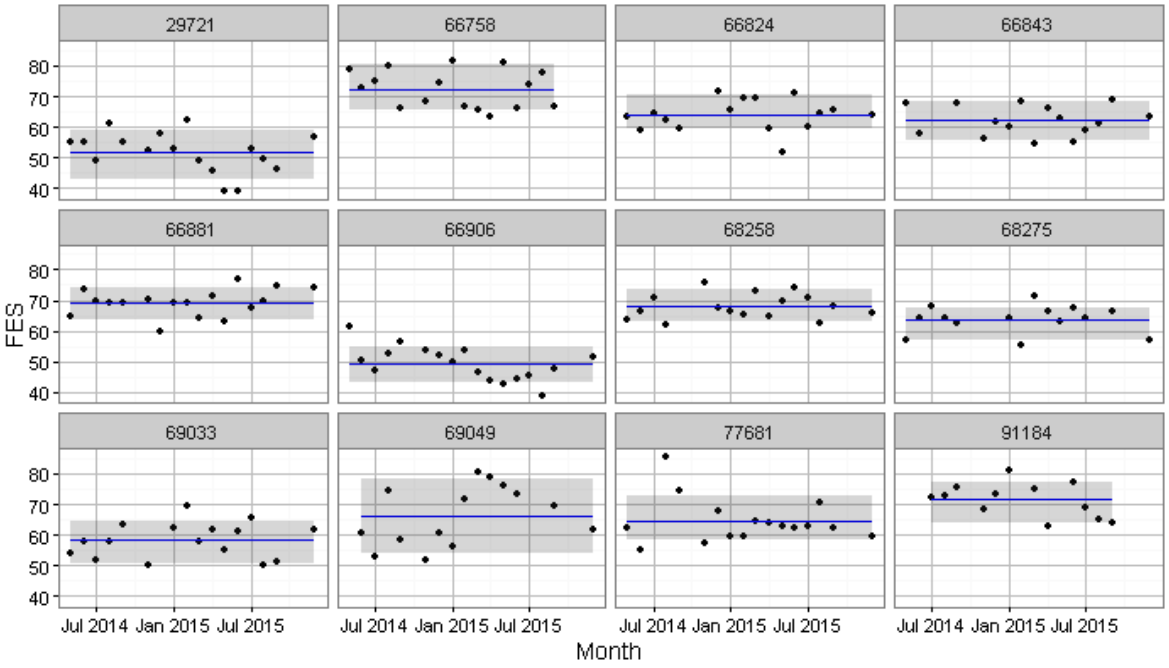

Figure 5.6. Progression of FES for individual drivers. Blue line indicates the mean FES and the grey ribbon shows 80 percent confidence interval.

FES progression for the selected group of drivers is shown in Figure 5.6. In most cases driver FES scores are scattered around the mean with a few outlier months where their driving style deviated significantly. FES modeled with one-way ANOVA resulted in month as an insignificant predictor. The probability that all monthly mean FESs are equal is 0.985.

A stationary time series is one whose statistical properties such as mean, variance, autocorrelation are all constant over time. Individual driver time series are tested for stationarity using autocorrelation plots and Dickey Fuller test (Dickey & Fuller, 1981) for a unit root with drift and deterministic time trend. Both test results indicated that the times series for FES and FUD are stationary across the months.

The coefficient of variation (standard deviation/ mean *100) for monthly FES values for the selected drivers were calculated across the two year study. Coefficient of variation for

FES varied from 6.2 to 13.9 with the mean value around 9.6. Since the mean value of FUD lies around 0 (due to presence of both positive and negative values), using the coefficient of variation for FUD is misleading to judge dispersion. Instead the standard deviation of FUD was calculated. Standard deviation of FUD varied from 0.50 to 1.84 with the median value at 0.98. In sum, considering all three consistency tests for both eco-driving metrics, it is reasonable to assume that they both are consistent individually. However, internal consistency of the two metrics are required to be tested. All drivers at a particular reporting period were ranked according to the values of their monthly metrics. Ranking of two drivers is shown in Figure 5.7. Driver ID 66758 had the second highest overall mean FES value and driver 66906 has the lowest overall mean FES. Even though both were consistently making the same number of trips across the months, their scores fluctuated and so did their ranking. However, their ranking fluctuated within a certain range. Ranking of the intermediate drivers fluctuated more frequently and their relative position changed. This infers that slight fluctuations in FES for intermediate drivers could result in large shifts in their ranking. This finding is consistent with the results in Table 5.1; intermediate drivers have overall FES that are not significantly different from each other.

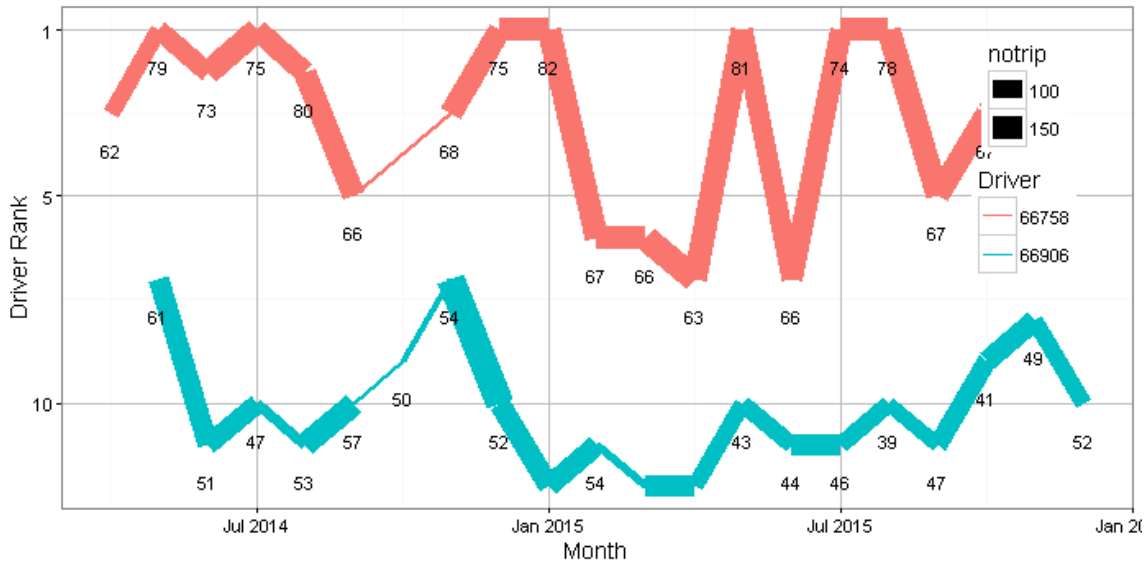

Figure 5.7. Ranking of two drivers across months according to monthly FES for two drivers. Numbers adjacent to the lines show actual FES.

5.6 Conclusions and Future Work

The purpose of an eco-driving metric that benchmarks driving style is to remove the impacts of vehicle and route choice from fuel use while still identifying heterogeneity among drivers. Effects of vehicle type choice is standardized using instantaneous driving activity for a standard car. Average speed is used to standardize the differences in fuel consumption from route choice.

Studies of eco-driving may alternatively focus on complete trips or discrete events, and an eco-driving metric must be tailored to the study need. Based on the two perspectives of eco-driving analysis this study developed two metrics: a trip based metric (FES) designed to analyze overall trip fuel efficiency while accounting for trip average speed; the second based on trajectory level fuel usage difference (FUD) from estimated usage accounting for instantaneous speed.

Both FES and FUD were found to be capable of distinguishing heterogeneous driving styles. Individual drivers' scores on both metrics are consistent over time – there is no trend or level shifts in their behavior without any intervention. However, dispersion of metrics around the mean may cause confusions in judging effectiveness on an intervention. In that case, Tukey's HSD for pairwise comparison between before and after eco-driving interventions can be used to detect significance of differences. Incentive tracking and delivery can be done by grading the drivers according to eco-driving metrics.

FES can be implemented by eco-driving schemes where aggregate trip based measures are available. In contrast, fuel use difference (FUD) can be implemented at sub-trip level where improvements during certain behaviors such as braking, accelerating-from-rest, cruising, etc. can be tracked separately. FES is more geared to post hoc delivery of eco-driving advisory and performance tracking; whereas FUD is suitable at microscopic level even when the trip is not yet completed. Calculation of FES is less data intensive compared to FUD.

FES and FUD have a significant inverse relationship with a lot of scatter. Conversion between two metrics is possible at an aggregate level, however, will not be reliable at a trip level. Since FES is already standardized by average trip speed, it does not show a trend against trip average speed. However, FUD was standardized by instantaneous speed and has slight positive slope with trip speed. FES and FUD are very different from one trip to another and aggregation at weekly or monthly level causes it to center. According to law of large numbers variability in either metric is reduced at higher aggregation levels. Reduced variability at higher aggregation level causes heterogeneity among drivers less distinguishable. However, the statistical analysis shows presence of groups of drivers with

different fuel efficiency levels. Therefore, grading the drivers at discrete groups can be significant in order to communicate improvements immediately to the driver.

This research has provided a footing to benchmark the driving styles for a vehicle fleet. The researchers are currently acquiring additional naturalistic driving data in the DC-Baltimore region to verify robustness of the model parameters. Future research will be directed towards finding out the specific associations between trip level driving behaviors such as braking, accelerating, speeding and the developed eco-driving metrics. Personalized recommendations thus developed along with personalized incentives will serve as a basis for 'nudging' drivers to choose optimized driving styles.

5.7 Acknowledgements

This research is funded partially by the US Department of Energy (DOE) Advanced Research Project Agency - Energy (ARPA-E) through its TRANSNET Program and a project led by the National Transportation Center at the University of Maryland. Findings presented in this paper do not necessarily represent the official views of DOE or ARPA-E. The authors are solely responsible for all statements in the paper.

5.8 References

af Wåhlberg, A. E. (2007). Long-term effects of training in economical driving: Fuel consumption, accidents, driver acceleration behavior and technical feedback. *International Journal of Industrial Ergonomics, 37*(4), 333-343.

Ahn, K., Rakha, H., Trani, A., & Van Aerde, M. (2002). Estimating vehicle fuel consumption and emissions based on instantaneous speed and acceleration levels. *Journal of Transportation Engineering, 128*(2), 182-190.

Barkenbus, J. N. (2010). Eco-driving: An overlooked climate change initiative. *Energy Policy, 38*(2), 762-769.

Barth, M., & Boriboonsomsin, K. (2009). Energy and emissions impacts of a freeway-based dynamic eco-driving system. *Transportation Research Part D: Transport and Environment, 14*(6), 400-410.

Beusen, B., Broekx, S., Denys, T., Beckx, C., Degraeuwe, B., Gijsbers, M., . . . Panis, L. I. (2009). Using on-board logging devices to study the longer-term impact of an eco-driving course. *Transportation Research Part D: Transport and Environment, 14*(7), 514-520.

Boriboonsomsin, K., & Barth, M. (2009). Impacts of road grade on fuel consumption and carbon dioxide emissions evidenced by use of advanced navigation systems. *Transportation Research Record: Journal of the Transportation Research Board,* (2139), 21-30.

Boriboonsomsin, K., Vu, A., & Barth, M. (2010). Eco-driving: Pilot evaluation of driving behavior changes among us drivers. *University of California Transportation Center,*

Dickey, D. A., & Fuller, W. A. (1981). Likelihood ratio statistics for autoregressive time series with a unit root. *Econometrica: Journal of the Econometric Society,* , 1057-1072.

Evans, L., Herman, R., & Lam, T. (1976). Multivariate analysis of traffic factors related to fuel consumption in urban driving. *Transportation Science, 10*(2), 205-215.

Ford Motor Company.Sustainability report 2014/15 spotlight: Ford driving skills for life/ eco-driving. Retrieved from https://corporate.ford.com/microsites/sustainability-report-2014-15/environment-spotlight-ecodriving.html

Frey, H. C., Zhang, K., & Rouphail, N. M. (2008). Fuel use and emissions comparisons for alternative routes, time of day, road grade, and vehicles based on in-use measurements. *Environmental Science & Technology, 42*(7), 2483-2489.

Frey, H. C., & Liu, B. (2014) Development and evaluation of a simplified version of MOVES for coupling with a traffic simulation model. *Proceedings, 91st Annual Meeting of the Transportation Research Board,*

Ishiguro, S. (1997). No title. *Heavy-Duty Truck Fuel Economy Test in Actual Road Traffic,*

Jimenez-Palacios, J. L. (1998). *Understanding and quantifying motor vehicle emissions with vehicle specific power and TILDAS remote sensing*

Lenner, M. (1995). Measurements by on board apparatus, of passenger cars'real-world exhaust emissions and fuel consumption. *Vti Meddelande,* (771A)

McQueen, M. P. (2008, How technology can help trip auto insurance. *The Wall Street Journal, June 26*

Oak Ridge National Laboratory. (2015). *Transportation energy data book edition 34*. Oak Ridge TN: Center for Transportation Analysis ORNL.

Rolim, C. C., Baptista, P. C., Duarte, G. O., & Farias, T. L. (2014). Impacts of on-board devices and training on light duty vehicle driving behavior. *Procedia-Social and Behavioral Sciences, 111*, 711-720.

Song, G., & Yu, L. (2009). Estimation of fuel efficiency of road traffic by characterization of vehicle-specific power and speed based on floating car data. *Transportation Research Record: Journal of the Transportation Research Board,* (2139), 11-20.

US Energy Information Administration. (2016). *Monthly energy review*. (). Washington DC: Office of Energy Statistics. US Department of Energy.

USDOE.2016 best and worst fuel economy vehicles. Retrieved from https://www.fueleconomy.gov/feg/best-worst.shtml

USEPA. (2016). *Inventory of U.S. greenhouse gas emissions and sinks: 1990 - 2014*. (No. EPA 430-R-16-002). Washington DC: US Environmental Protection Agency.

CHAPTER 6

CONCLUSIONS AND FUTURE WORKS

6.1 Summary and Key Findings

The research presented in this dissertation improves the understanding of simulation and control of driving activity. A framework was developed within the existing implementation of a mesoscopic simulator, DTALite. Different policy and operational interventions were tested in the framework to understand the effect of dynamic demand-supply interactions on simulated driving activity and consequent estimated emissions. In addition, a prototype simulation-optimization-evaluation framework was developed. Observed driving activities at different facility types and operating conditions were used to select appropriate post-processing methods for simulated driving activity. Understanding of relative importance of different features in simulated driving activity can be implemented to improve accuracy of energy use-emissions estimation. To understand the effect of vehicle performance and driver on observed driving activity two questions were posed in observed driving activity – (1) how different is an individual driver driving style when operating vehicles with differences in performance?; and (2) how dissimilar are the driving styles of different drivers when operating vehicles that have similar performance? The findings suggested that the choice of vehicle does not significantly alter the natural driving style of a driver. Moreover, a database of observed microscale (1 Hz) driving activity was used to develop two metrics: a trip based measure called the Fuel Efficiency Score (FES), and a difference in fuel use metric that uses the second by second observations called the Fuel Use Difference (FUD). Both measures passed the test of consistency so that, at the driver level, both revealed no temporal trend in

the scores from month to month across a period of two years. Moreover, the FES metric passed the heterogeneity test. It was able to identify four distinct clusters of driving styles.

Key scientific findings and conclusions from this research are summarized below.

6.1.1 Findings on simulation of driving activity

- A framework was developed to quantify network level mobility and emissions impacts of Transportation Management Strategies (TMS) when applied to a regional network at a mesoscopic modeling scale. The core of the multi-resolution modeling framework is the generation of synthetic driving activity from link-based traffic characteristics.
- A Mode Shift (MS) strategy from single occupancy vehicle (SOV) to high occupancy vehicle (HOV) travel reduces total emissions. But emissions per VMT may increase for some pollutants because at an existing uncongested network reduction of demand may provide stimulation for speeding and consequently higher emissions.
- In a bounding case involving total (100%) fleet replacements (FR) to 'Tier 2' regulatory classes on a regional network in North Carolina, reductions of 81%, 78%, and 91% in NO_X, CO and HC levels respectively were estimated. CO_2 reduction is insignificant (1%) as there is not much difference between the EPA 'Tier 1' and 'Tier 2' standards for this pollutant. FR does not affect traffic flow characteristics such as speed or travel time.
- In bounding case of peak spreading (PS) with uniform demand across the peak period, not only emissions per VMT were reduced, but also the peak emission level dropped. By lowering the ambient concentration and adjusting the temporal distribution of emissions, one can reduce the exposure level and generation of secondary pollutants such as Ozone.

- In case of incidents with variable message signs (VMS), travelers on the path of incident experienced an increase in NO_X emission of 155% (average VMT basis) even though there was a 30% diversion from the incident link.
- The selection of post-processing method most suitable for simulated trajectories derived from simplified trajectory generators in a mesoscopic simulation environment depends on the operating condition and the facility type.
- Savitzky-Golay filters, Lowess filters, and micro-trip based trajectory reconstruction methods performed best in post-processing trajectories from simplified trajectory generators in congested, average, and uncongested conditions respectively.
- The operating mode bin based fuel use estimation models showed lower variability in estimated emissions than continuous function based models for the optimally post-processed trajectories. Both model types have similar average estimated fuel use in miles per gallon.

6.1.2 Findings on control of driving activity

- The proposed envelope deviation distribution is found to be an effective way of describing driving style. It is essentially a transformation of the joint speed-acceleration distribution of a cycle with respect to the typical real-world driving cycle.
- The measured difference in driving styles were decomposed into three components – inter-driver heterogeneity, inter-vehicle heterogeneity, and intra-driver-vehicle variability.
- Inter-vehicle heterogeneity was found not significantly higher than the intra-driver-vehicle variability. Inter-driver heterogeneity was significantly higher than the intra-driver-vehicle variability.

- Operating vehicles of different performance classes do not result in significantly different driving styles.
- Two eco-driving metrics were developed: Fuel Efficiency Score (FES) to analyze overall trip fuel efficiency while accounting for trip average speed; Fuel Use Difference (FUD) from estimated fuel usage accounting for instantaneous speed.
- Both FES and FUD were found to be capable of distinguishing heterogeneous driving styles.
- Individual drivers' scores on both metrics are consistent over time – there is no trend or level shifts in their behavior without any intervention.
- Eco-driving Incentive tracking and delivery can be done by grading the drivers according to eco-driving metrics. Grading the drivers at discrete groups can be significant in order to communicate improvements immediately to the driver.

6.2 Future Works

The findings in the research of simulation and control of driving activity have given rise to multiple research questions and opportunities for further extension. Following are some research ideas based on the works described in this dissertation-

Improved fuel use-emissions estimation models

Current fuel use estimation models do not explicitly consider the non-linear lag phenomenon between the observed fuel use and driving activity. Additionally, the peaks in a time-series of driving activity are not treated differently in existing fuel use-emissions estimation models. Since simulated trajectories from mesoscopic simulators have realistic shockwave propagation and queueing behavior, estimation models which treats sudden changes in driving activity explicitly will improve the usability of simplified trajectory generator.

Method for faster fuel use and emissions calculation

All the post-processing methods described in chapter 3 results in added computational complexity and expense on the simplified trajectory generation procedure. The link based trajectory generation and post-processing in existing DTALite framework works in a third layer of loops where additional computations increase computational complexity as a cubic function of network number of links, number of vehicles, and number of simulation time steps. This phenomenon restricts the use of existing DTALite framework for real-time implementation. A reduced-form implementation of the trajectory generator in DTALite may reduce the computational complexity. The reduced-form implementation can be achieved through high dimensional mapping between input parameters and cycle attributes such as cycle correction factor (CCF) used in MOVESLite.

Generation of recommended activity for eco-driving participants

Certain driving activities are responsible for energy inefficiencies. The core of this research under development is to identify thresholds in driving activity variables which causes standardized fuel efficiencies (as defined in chapter 5) to decrease.

Smartphone based driving activity monitoring and eco-driving

Trip based eco-driving metric FES (chapter 5) is extensible at a smartphone environment. To test the capability of smartphone sensors to capture similar driving activity data as the onboard data logger, simultaneous data collection was conducted. The smartphone lacked usable road grade information. Research is underway to modify the vehicle specific power generated without road grade information with location specific information about road grades.

Generating optimized trajectory for autonomous vehicles at mixed flow condition

At low penetration levels, autonomous vehicles will still be subjected to the macroscopic level nuances of the traffic stream. In those mixed flow conditions, autonomous vehicle have significant potential to reduce fuel use-emissions of the follower human driven vehicles by setting optimal driving activities to follow. The synthetic trajectory generator is capable of simulating agents with special microscopic characteristics such as safe following distance and reaction time. The prototyping framework discussed in chapter 3 is currently being extended to optimize microscopic trajectories of selected agents set as autonomous vehicles.

Simulating system models with heterogeneous driving styles under incentives

Existing agent based system models are not capable of addressing heterogeneity in driving styles in terms of estimated fuel use-emissions. Distribution of eco-driving metrics across the population provides quantification of the heterogeneity. In addition, similar distributions in the treatment groups involving different monetary and non-monetary incentives indicate the efficacy of the treatments. These observed and experimentally derived distributions can be applied at the system model agent generation stage to characterize the impacts of incentives in an eco-driving scheme.

APPENDICES

Appendix A

Supplementary materials for the task of optimizing post-processing methods

Optimization Contours for Post-Processing

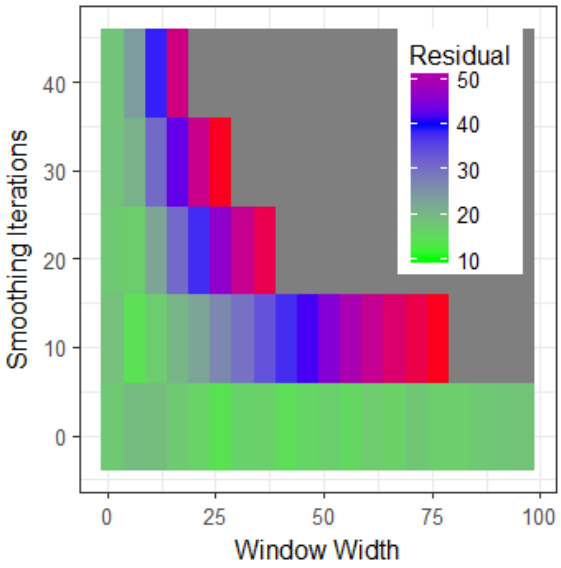

1200, 65 MA (6, 11, 13.9)

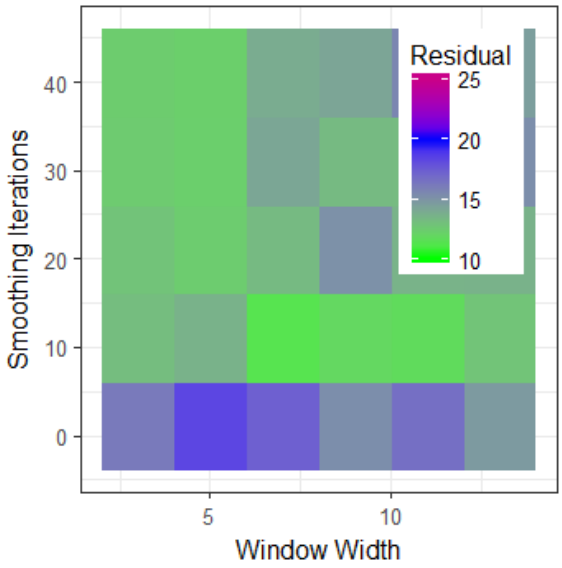

1200, 65, SG, (7, 11, 11.27)

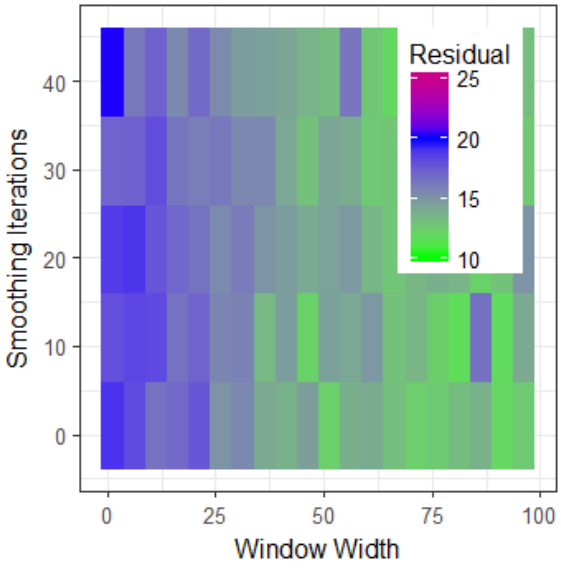

1200, 65, LO, (51, 41, 7.96)

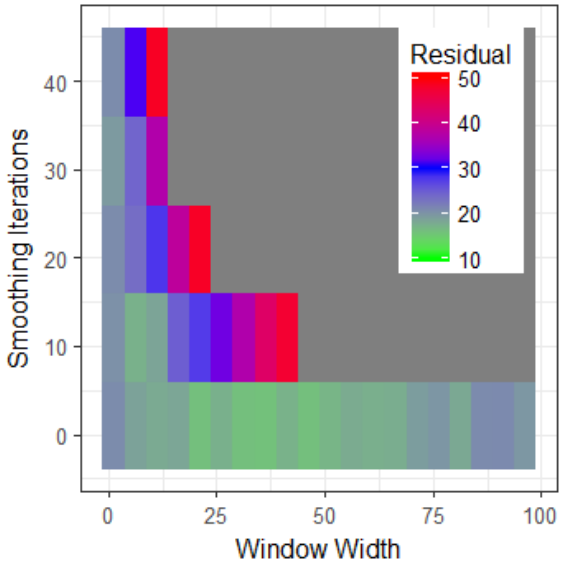

900,65, MA, (36, 1, 14.83)

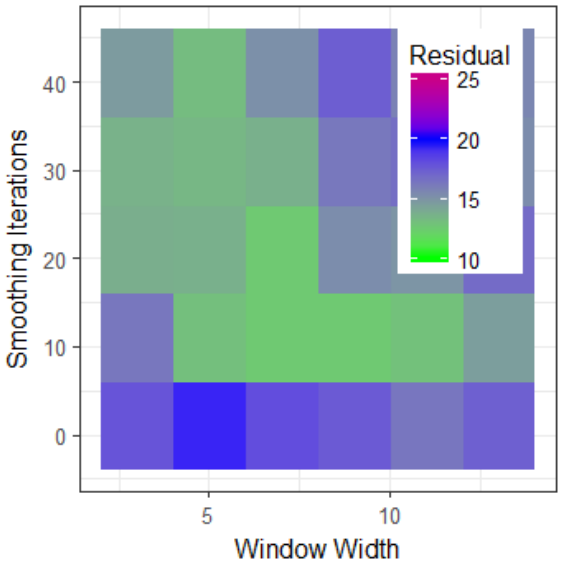

900, 65, SG, (5, 31, 11.62)

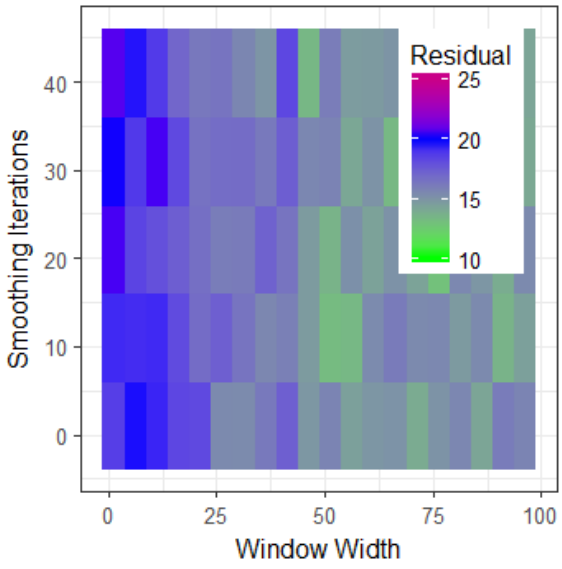

900,65, LO, (86, 1, 9.87)

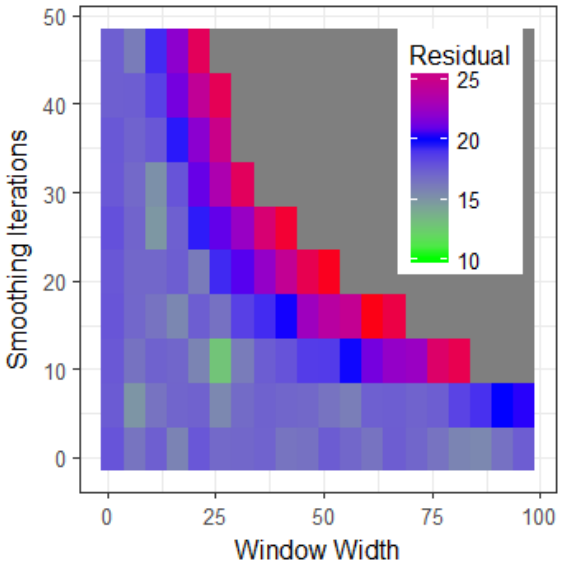

1500, 65, MA, (26, 11, 12.76)

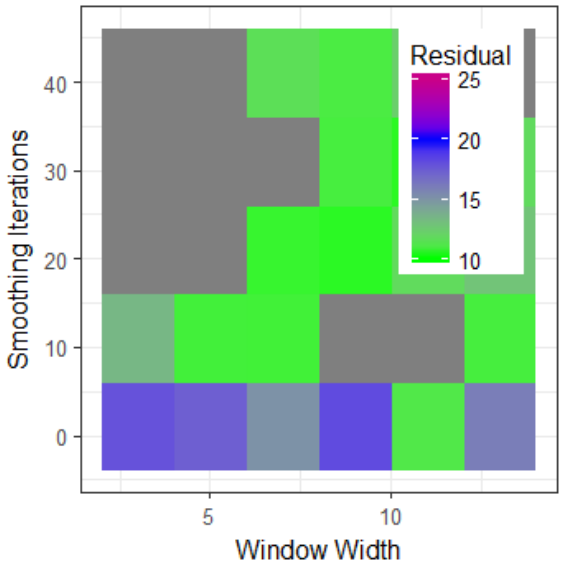

1500, 65, SG, (13, 41, 8.18)

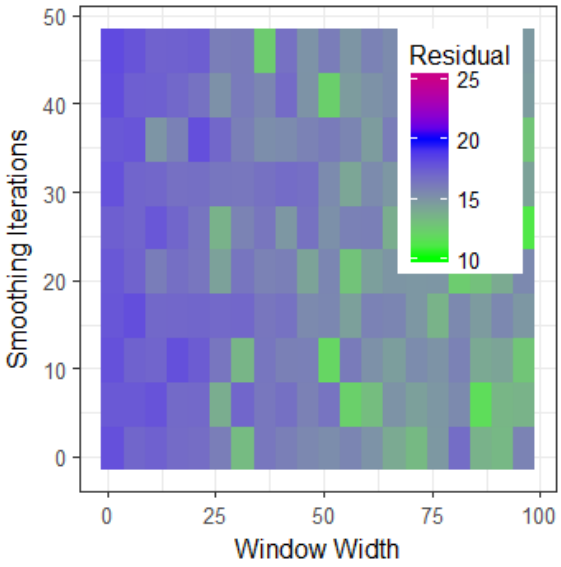

1500, 65, Lo, (96, 26, 11.04)

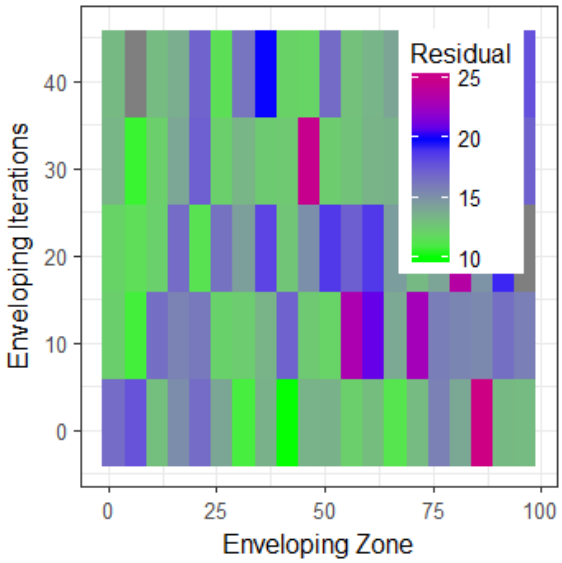

1500, 65, Env, (6, 41, 9.66)

Appendix B

Supplementary materials in the development of eco-driving metric

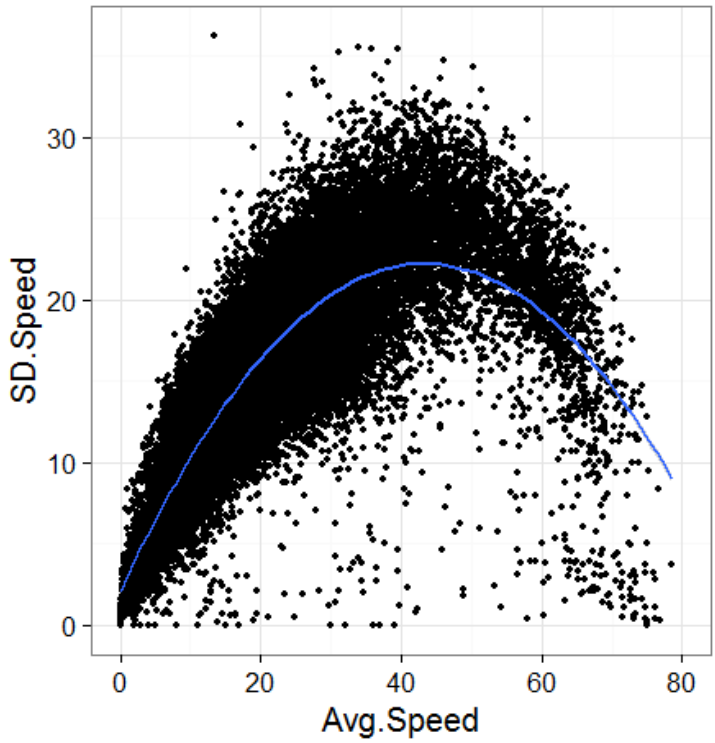

Figure B1. Variability of speed at different trip average speeds

Input Data Requirement

Two types of data required to estimate FES

a. 1 Hz instantaneous vehicle speed (mph)
b. 1 Hz estimated fuel consumption (gram/second) for a standardized vehicle[4]

Development of Historic Trip Fuel Use Percentiles

Step 1: Data filtering

- Only the trips over 1 mile length and 1 minute duration are selected for computing the FES (must meet BOTH)
- Two driver IDs (ID = 69033, ID = 107722) were randomly chosen and their trip data was not used to develop historic trip percentiles

[4] Estimated instantaneous fuel consumption for standard vehicle is based on vehicle specific power (VSP) computed at 1 Hz resolution with parameters of a standard light-duty gasoline vehicle.

Step 2: Calculating trip average speed

$$Average\ Speed, \bar{v} = \frac{\sum Instantenous\ Speed}{Total\ \#\ of\ Speed\ Observations}$$

(Equivalent to Distance/ Travel Time)

Step 3: Factoring the trips into trip average speed bins (*i*)

- 10 mph bin sizes were selected
- The lowest bin contains all trips over 0 mph average speed and below 10 mph average speed ($0 \leq \underline{v} < 10$)
- The highest bin contains all trips over 70 mph average speed and below 80 mph average speed ($70 \leq \underline{v} < 80$)

Step 4: Calculating the trip fuel usage based on standardized vehicle

a. Calculating total trip fuel usage ($TF = \sum Instantaneous\ Fuel\ Consumption$)
b. Calculating trip length ($L = \sum Instantaneous\ Speed$)
c. Calculating trip miles per gallon[5]

$$f = \frac{L\ in\ miles}{TFin\ Gallons}$$

Step 5: Calculating frequency distribution of trip mpg values (*f*) at different speed bins (*i*)

Step 6: Getting 10th percentile (l_i) and 90th percentile (u_i) trip mpgs for each speed bin (i)

[5] A conversion factor of 1 gallon = 2,800 grams is used in the calculation

Table B1. Trip Fuel Use Percentiles

Speed Bin (i) (mph)	10th Percentile mpg (l_i)	90th Percentile mpg (u_i)
[0,10]	10.3	14.9
(10,20]	15.7	20.9
(20,30]	20.4	25.1
(30,40]	24.2	27.8
(40,50]	26.2	29.2
(50,60]	27.3	30.3
(60,70]	28.4	30.6
(70,80]	28.5	30.3

Implementation Algorithm

Step 1: Calculate trip length (L)

Step 2: Calculate trip average speed ($\underline{v}$)

Step 3: Determine trip average speed bin i

Step 4: Calculate trip miles per gallon (f)

Step 5: Calculate Fuel Efficiency score for an individual trip

$$FES_i = 20 + \frac{f - l_i}{u_i - l_i} * (100 - 20)$$

If the reported trip mpg is either lower than 10 percentile, or higher than the 90th percentile, set it to either boundary.

Step 6: Determine FES for all the trips made in time duration T ($7\ days\ or\ more$), assume k trips were made during this period.

- FES for collection of trips weighted by trip length in time period T

$$\frac{\sum_1^k Trip\ Length_k * FES}{total\ distance\ traveled\ in\ \tau}$$

Step 7: Determine FES for each of the trips made in time duration T (7 $days\ or\ more$), assume J trips were made during this period. [j = 1, 2, ……, J]

- FES for collection of trips weighted by trip length in time period T

$$FES = \frac{\sum_{j=1}^{J} FES_j * L_j}{\sum_{j=1}^{J} L_j}$$

Step 8: The driving style grade can be found from the table below. The table is derived in a way that approximately 20% of the drivers remain in each of the 5 discrete grades (Fig.B2).

FES	**Grade**
<=55.2	E
>55.2 - <=62.1	D
>62.1 - <= 66.7	C
>66.7 - <=71.9	B
> 71.9	A

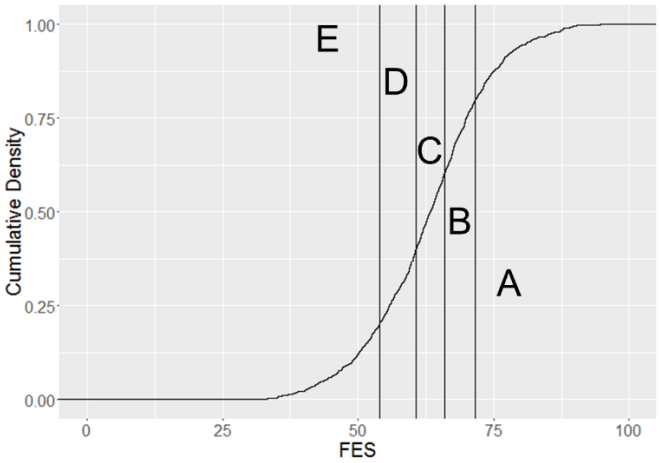

Figure B2. Cumulative density of weekly aggregates FES across all trips in the database

Example
A driver made 4 trips during a chosen time duration of 7 days.

Trip Number	Trip Avg Speed (mph), $\underline{v}$	Trip Fuel Use (mpg), f	Trip Distance (mile), L	*FES*
1	12	17	8	40
2	35	26	6	61
3	65	29	5	41
4	75	30	3	86

The driver's combined FES for 7 days would be = $\frac{(40*8) + (61*6) + (41*5) + (86*3)}{8+ 6+ 5 + 3}$= 52.3
Therefore, the grade of this driver in this time period is: E

Validation
FES for the intermediate quantile values were generated to verify the spread of scores across different trips. The following tables show trip standardized MPG and corresponding FES values.

Table B2. Trip standardized MPG values

	10%	20%	30%	40%	50%	60%	70%	80%	90%
[0,10]	10.3	11.6	12.2	12.7	13.1	13.5	13.8	14.2	14.9
(10,20]	15.7	16.5	17.2	17.8	18.3	18.8	19.4	20.0	20.9
(20,30]	20.4	21.2	21.8	22.3	22.8	23.3	23.8	24.3	25.1
(30,40]	24.2	24.8	25.2	25.6	26.0	26.3	26.7	27.1	27.8
(40,50]	26.2	26.6	27.0	27.3	27.7	28.0	28.3	28.7	29.2
(50,60]	27.3	27.9	28.3	28.6	28.9	29.1	29.4	29.8	30.3
(60,70]	28.4	28.8	29.1	29.4	29.6	29.8	30.0	30.2	30.6
(70,80]	28.5	28.7	28.9	29.1	29.3	29.4	29.6	30.0	30.3

Table B3. Corresponding FES

	10%	20%	30%	40%	50%	60%	70%	80%	90%
[0,10]	20	42	53	61	69	76	82	88	100
(10,20]	20	33	44	52	61	69	77	87	100
(20,30]	20	34	44	53	61	69	77	87	100
(30,40]	20	34	44	52	60	68	76	86	100
(40,50]	20	32	42	50	59	68	76	86	100
(50,60]	20	36	46	55	62	69	75	86	100
(60,70]	20	33	46	54	62	69	75	83	100
(70,80]	20	29	38	48	54	62	68	87	100

The two driver IDs (69033 and 107722) initially left to validate developed FES were used to generate 90th and 10th percentile values and compared with the percentile values for the rest of the trips. Figure B3 shows cumulative distribution for the trips made by IDs 69033 and 107722.

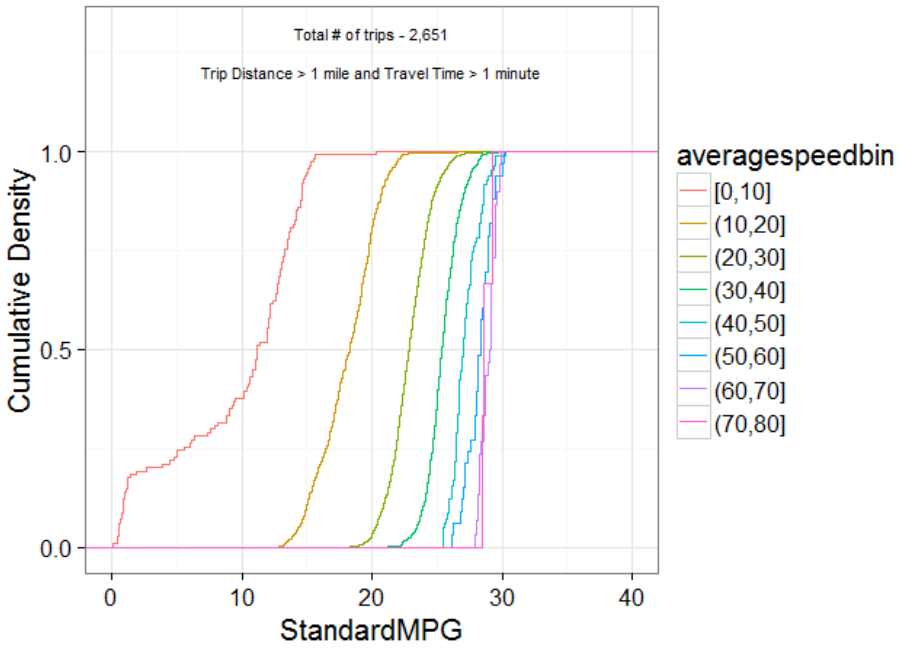

Figure B3. Cumulative densities of standard MPG at different trip average speeds for driver ID 69033 and 107722.

Table B4. Difference of percentiles for different speed bins between developed FES and validation set

Speed Bin (i) (mph)	10th Percentile MPG for 2 Drivers	10th Percentile MPG for Rest	Difference	90th Percentile MPG for 2 Drivers	90th Percentile MPG for Rest	Difference
[0,10]	0.86	10.3	-92%	14.6	14.9	-2%
(10,20]	14.9	15.7	-5%	20.7	20.9	-1%
(20,30]	20.8	20.4	2%	24.8	25.1	-1%
(30,40]	23.9	24.2	-1%	27.1	27.8	-3%
(40,50]	25.9	26.2	-1%	28.6	29.2	-2%
(50,60]	27.0	27.3	-1%	29.4	30.3	-3%
(60,70]	28.2	28.4	-1%	29.6	30.6	-3%
(70,80]	28.5	28.5	0%	29.1	30.3	-4%

Eco-driving pilot experiment result

We started providing monetary incentives to four drivers in the NC State University fleet starting April 24, 2017. The initial incentive rate was 1 grade point = 10 ¢. The before e.g. baseline experiment was in place from October 2016 to March 2017. Only weeks with at least 7 qualified trips (minimum 1 mile length and 1 minute duration) were considered in analysis. The FES distributions for the 4 incentivized drivers in before and after conditions are shown in Figure B4.

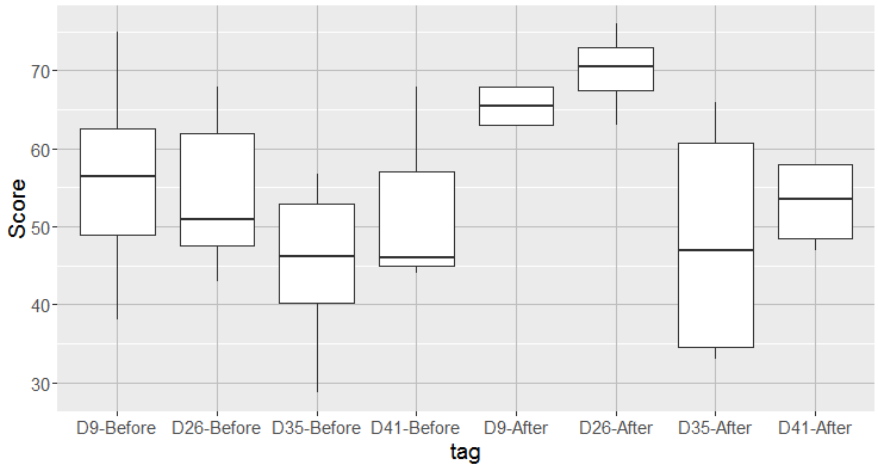

Figure B4. Results from the pilot study. The before after weekly FES distribution.

The regression equation for trip FES vs FUD is as follows

$$FUD=7.17-0.13*FES \quad \textbf{(1)}$$

For FES and FUD measured in before and after cases, from equation 1

$$\Delta(FUD)=-0.13*\Delta(FES) \quad \textbf{(2)}$$

The pilot study provides an estimated average $\Delta(FES)$ of 7.46 at the trip level. Using this relationship of Equation 2, a shift of 0.97 (= 0.13 * 7.46) is estimated in the FUD distribution.
Therefore, the incentivized FUD distribution is estimated to be $N(-0.97,2.2)$

Implementation of pilot experiment results in system model

The total fuel use for a single trip can be obtained by the following formula:

$$FC_{i,j} = FC_{Moves,i}\left(1+\frac{FUD_j}{100}\right) \quad \textbf{(3)}$$

Where

$FC_{i,j}$ = Trip Fuel Consumption for Trip i made by Agent or Driver j
$FC_{Moves,i}$ = Estimated Trip Fuel Consumption by the Moves Lite model for Trip i
FUD_j = Fuel Use Difference for Driver j $\sim N(0,2.2)$ (percent)

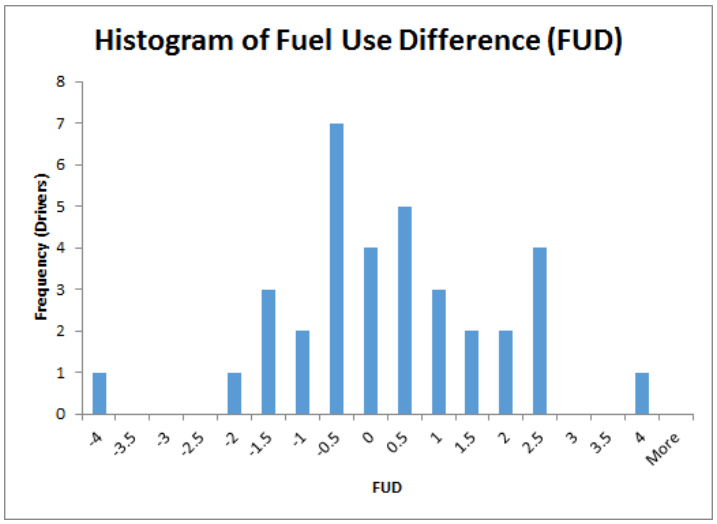

Figure B5. Baseline Distribution of FUD for Implementation in System Model

The FUD is distributed according to a normal distribution with a mean of 0 and standard deviation of 2.2. When the driver agent is created in the system model, FUD can be randomly assigned from the distribution and used for the trip in which they are a driver. This distribution applies solely to passenger cars at this point as there are no data on differences in fuel use due to driver behavior for heavy vehicles, buses, or subway/rail. The FUD is also not used for any passengers or non-driving carpoolers in the system as they have no impact on behavior-based fuel use. Of course, the share of energy use by traveler can be estimated

knowing the vehicle occupancy, and equally dividing the energy use among all travelers in a single vehicle.

Algorithm

Step 1: Generate the agent randomly with either non-incentivized (B) or incentivized (I) using the baseline information about the percentage of drivers in a particular O-D pair with access to eco-driving monetary incentives.

Step 2: Find FUD_j randomly for agent/driver j from a distribution ~ $N(0,2.2)$ if the agent is non-incentivized (B) and from a distribution $N(-0.97,2.2)$ if the agent is found incentivized (I) in step 1.

Step 3: Estimate the fuel consumption $FC_{Moves,i}$ made by agent j for trip i

Step 4: Apply equation 3 ($FC_{i,j} = FC_{Moves,i}\left(1 + \frac{FUD_j}{100}\right)$) to find out the estimated fuel consumption for trip i considering whether the agent is of type B or type I.

Figure B6 shows how the FUD distribution varies between the two groups.

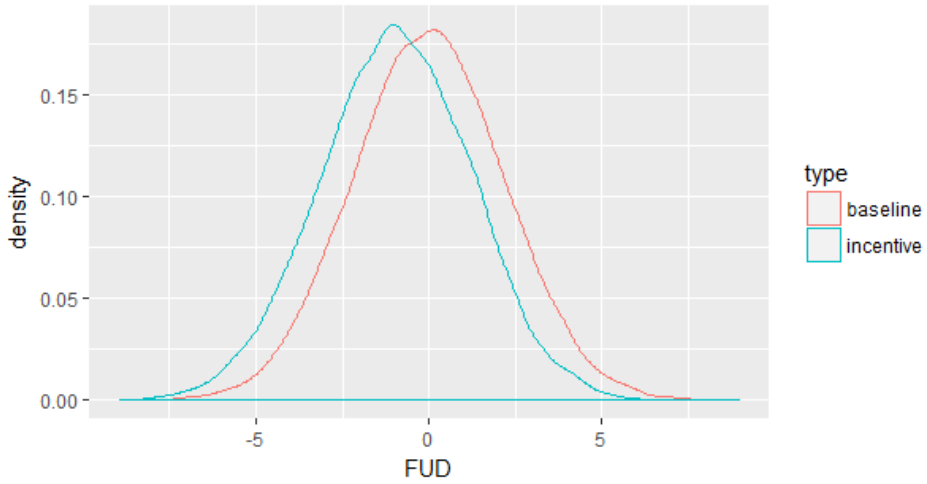

Figure B6. Recommended FUD distribution for baseline and incentive groups